공학박사 학위논문

Advanced Process Design and Operation in a Natural Gas Supply Chain using Superstructure Optimization and Multi-modular Approach

천연가스 공급망 내 초구조 최적화 및 다중모듈방식을 이용한 공정설계 및 운전

2019년 2월

서울대학교 대학원

화학생물공학부

이 용 석

Abstract

Advanced Process Design and Operation in a Natural Gas Supply Chain using Superstructure Optimization and Multi-modular Approach

Yongseok Lee
School of Chemical & Biological Engineering
The Graduate School of Seoul National University

Recently in the field of process systems engineering in natural gas processing, various researches trying to make changes in the existing framework of process design and operation have been studied with the emerging need of sustainability and safety in the chemical processes. These two considerations of sustainability and safety either result in a totally new solution for a certain decision making or require far different methods or technologies for it.

Especially for a natural gas supply chain broadly from drilling of the gas/oil reservoirs to distributing the product gas to end-users like households or offices, new frameworks of process design and operation critically influence the way of producing desired products and supplying them to the users in the associated industries. Then it determines the structure, operating conditions, and operation

procedures of chemical processes which are economically powerful and good in operability. Recently, as the natural gas sources becomes unconventional varying from mid-to-small size reservoirs or shale gases, this change makes the offshore natural gas plants emerge as an alternative and vital site of producing LNG (liquefied natural gas) with strict requirements of safety. It also makes additional processing units like a cryogenic nitrogen recovery be necessary for sustainable production of LNG with leaner feed natural gases.

Among various processes in the overall natural gas supply chain, this thesis dealt with largely three parts including gas pre-treatment, liquefaction, and distribution to the end-users, attempting to design new processes or develop new methods of decision making in the context of the new framework considering sustainability and safety in process systems engineering. In this thesis, I will discuss the process synthesis, intensification, and optimization for sequential units, multi-objective optimization for economic feasibility and inherent safety, and multi-modular approach for interactive simulation of dynamic process and 3D-CFD (computational fluid dynamics) accident models.

First of all, for designing a sustainable process of producing LNG from feed natural gases with high amounts of nitrogen, two cryogenic nitrogen recovery processes integrated with LNG production and NGL (natural gas liquid) recovery were designed and optimized based on the structural analysis of components separation: one for integrated nitrogen recovery unit and the other for standalone one. The difference of each process is the way the nitrogen is removed from the natural gas. The former recovers nitrogen in the integrated heat and mass transfer

structure with natural gas liquefaction while the latter separates the nitrogen recovery unit into an independent structure apart from the liquefaction section. These sophisticated nitrogen recovery solutions follow the recent demand of highly efficient electric motors as alternative compressor drivers which require less or no fuel gas, the major sink of nitrogen in the feed gas.

These two processes were compared with each other in terms of specific power (kWH/kg_LNG), which is equivalent to the overall process efficiency, with respect to the nitrogen content in the feed gas from 0mol% to 20mol%. Consequently, as the nitrogen content in the feed gas increases, the specific power of each process also increases while the standalone solution has a priority over the other until around 17mol% of nitrogen and after that point the integrated solution becomes relatively more efficient. It should be noted that all of the optimization results of each configuration were improved with the reduced specific power by up 38.6% compared to those from previous studies which have similar configurations. The way this study aimed could be reasonable guidelines for other chemical process designs as well as nitrogen recovery in natural gas processing.

Secondly, for designing a safer process of natural gas processing, two different systematic approaches were newly proposed in this study: one for risk reduction method based on rigorous QRA (quantitative risk assessment) results through process design modification of an existing plant which already finished up to the detailed design stage, and the other for deciding an optimal process design through multi-objective optimization for minimizing both the TAC (total annual cost) and the risk (fatality frequency) at the preliminary design stage. This latter approach

could largely lower the cost required for finalizing the design as it doesn't need to follow the general QRA procedure where the recursive loop is recycled until the risk is reduced to an acceptable level. But before this approach starts to be applied, the suitability of its method should be verified as it has to make some assumptions in assessing the safety level of the process with limited information. Also the computation load would be higher as it needs to simultaneously consider the economic feasibility and inherent safety in designing a process. Despite the differences these two approaches have each other, however, they are essentially in the same context in that they share the same purpose of deciding a process design which is safer and/or even cheaper than the existing processes.

Consequently, for the former approach of which the target process is the GTU (gas treatment unit) of an existing GOSP (gas oil separation plant) for processing associated natural gas, the modified design with different operation conditions reduced the total risk integrals by 27% at the expense of only the additional $50,000 for capital cost. In addition, sensitivity analysis of total risk with respect to probability of success for safety barriers was carried out in order to show the preferences of process design modification, this study proposed, over the improvement of safety systems. Meanwhile, the latter approach of superstructure formulation and multi-objective optimization for designing an optimal heat transfer structure and operating conditions was applied to the natural gas liquefaction processes, deciding that the SMR (single-stage mixed refrigerant process) structure with the TAC of 626.6MM$/yr and fatality frequency of 1.28E-03/yr has the highest priority over all possible solutions.

Finally, with the aim of safely operating a chemical plant, a new operator training module which mainly targets the interactive cooperation of control room operators and field operators was developed through using multi-modular approach with advanced simulations and data processing technologies. This interactive simulation modeling delivers the online simulation results of process operation to the operators and induces them to take proper actions in case of a random accidental situation among pre-identified scenarios in a chemical plant. Developed model integrates the real-time process dynamic simulations with the off-line database of 3D-CFD accident simulation results in a designed interface using OLE (Object Linking and Embedding) technology so that it could convey the online information of the accident to trainees which is not available in existing operator training systems. The model encompasses the whole process of data transfer till the end of the training at which trainees complete an emergency shutdown system in a programmed model.

The developed module was applied to a natural gas pressure regulating station where the high pressure gas is depressurized and distributed to the end-users like households or offices. An overall scenario is simulated in the interactive simulation model, which starts from an abnormal increase of the discharge (2^{nd}) pressure of the main valve due to its malfunction, spreads to an accidental gas release through the crack of a pressure recorder, and ends with gas dispersion and explosion. Then the magnitude of the accident outcomes with respect to the lead time of each trainee's emergency response is analyzed. Consequently, the module could improve the effectiveness of operator training system through interactively linking the trainee actions with the model interface so that the associated accident situations would

vary with respect to each trainee's competence facing an accident.

Keyword : Process Intensification; Optimization; Computational Fluid Dynamics; Multi-modular Approach; Dynamic Simulation; Inherent Safety; Natural Gas Processing.

Student Number : 2013-23169

Table of Contents

List of Figures

List of Tables

CHAPTER 1. Introduction

1.1. Research motivation

Recently in the field of process systems engineering in natural gas processing, various researches trying to make changes in the existing framework of process design and operation have been studied with the emerging need of sustainability and safety in the chemical processes. These two considerations of sustainability and safety either result in a totally new solution for a certain decision making or require far different methods or technologies for it.

Especially for a natural gas supply chain (Figure 1-1) broadly from drilling of the gas/oil reservoirs to distributing the product gas to end-users like households or offices, new frameworks of process design and operation critically influence the way of producing desired products and supplying them to the users in the associated industries. Then it determines the structure, operating conditions, and operation procedures of chemical processes which are economically powerful and good in operability.

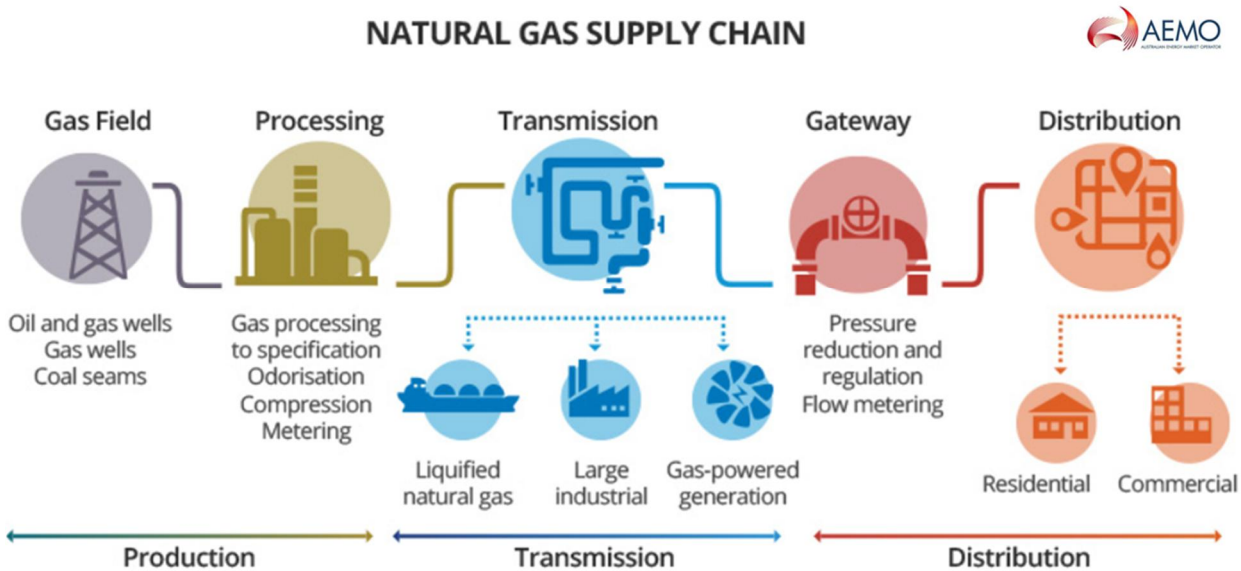

Figure 1-1. Natural gas supply chain

Recently, as the natural gas sources becomes unconventional varying from mid-to-small size reservoirs or shale gases, this change makes the offshore natural gas plants emerge as an alternative and vital site of producing LNG with strict requirements of safety. It also makes additional processing units like a cryogenic nitrogen recovery be necessary for sustainable production of LNG with leaner feed natural gases.

Therefore, it is critical to establish various methods for design and operation of chemical process with different requirements from those of the past through considering sustainability and safety. Furthermore, their application to the natural gas industry is also significant.

1.2. Research objectives

In this thesis, I will discuss the advanced process design and operation of a natural gas supply chain using superstructure optimization and multi-modular approach. Among various processes in the overall natural gas supply chain, this thesis dealt with largely three parts including gas pre-treatment, liquefaction, and distribution to the end-users, attempting to design new processes or develop new methods of decision making in the context of the new framework of process systems engineering. For addressing these objectives, several technologies including process synthesis and intensification for sequential units, superstructure formulation and multi-objective optimization of economic feasibility and inherent safety, and multi-modular approach for interactive simulation of dynamic process and accident models for safer operation are developed.

For the process synthesis and intensification for sustainably producing LNG from feed natural gases of high amounts of nitrogen, two different cryogenic nitrogen recovery processes integrated with LNG production and NGL recovery are designed and optimized based on the structural analysis of components separation and exergy analysis. And for designing a safer process of natural gas processing, two different methods are newly proposed: one for risk reduction through process design modification of an existing GOSP plant based on the QRA results, and the other for deciding an optimal design of LNG processes through superstructure formulation and multi-objective optimization for minimizing both the total annual cost and the risk at the preliminary design stage. Finally, with the aim of safely operating a chemical plant, a new operator training module which mainly targets the interactive

cooperation of control room operators and field operators is developed through multi-modular approach using advanced simulation and data processing technologies. This interactive simulation modeling delivers the online simulation results to the field operators and induces them to take proper actions in case of a random accidental situation among pre-identified scenarios in a chemical plant. And the effectiveness of the developed module is evaluated with two trainees with different operating proficiency via the demo version of training program.

1.3. Outline of the thesis

From modeling and technical perspectives, the contribution of the thesis is to solve a variety of problems in process systems engineering following the recent need of new technologies from oil and gas industries.

Chapter 2 addressed the problem occurring as two new trends emerged in the natural gas processing industries. One is the enlarged portion of unconventional natural gas sources like small-to-midsize reservoirs or shale gases recently, and the other is the switching of compressor drivers from steam turbines to highly efficient aero-derivative gas turbines or electric motors. The former requires sophisticated nitrogen recovery units in conventional LNG processes as the feed gases from unconventional sources are generally leaner containing higher amount of nitrogen. The latter makes the LNG processes completely recover the methane to product LNG almost not producing the fuel gas as the new drivers consume less or no fuel gas. Following these trends and associated needs of new technologies, the chapter aimed at designing new cryogenic nitrogen recovery processes integrated with LNG production and NGL recovery through structural expansion and pinch-exergy integration. Also, the proposed solutions were compared with each other in terms of thermodynamic efficiency with respect to the nitrogen content in the feed gases so that the study could give reasonable guidelines to deciding the optimal solution based on the order of design priority at certain feed gases.

Chapter 3 tried to solve the problem of how to manage the plant risk fundamentally in the context of general procedures of process design (top figure of Figure 1-2).

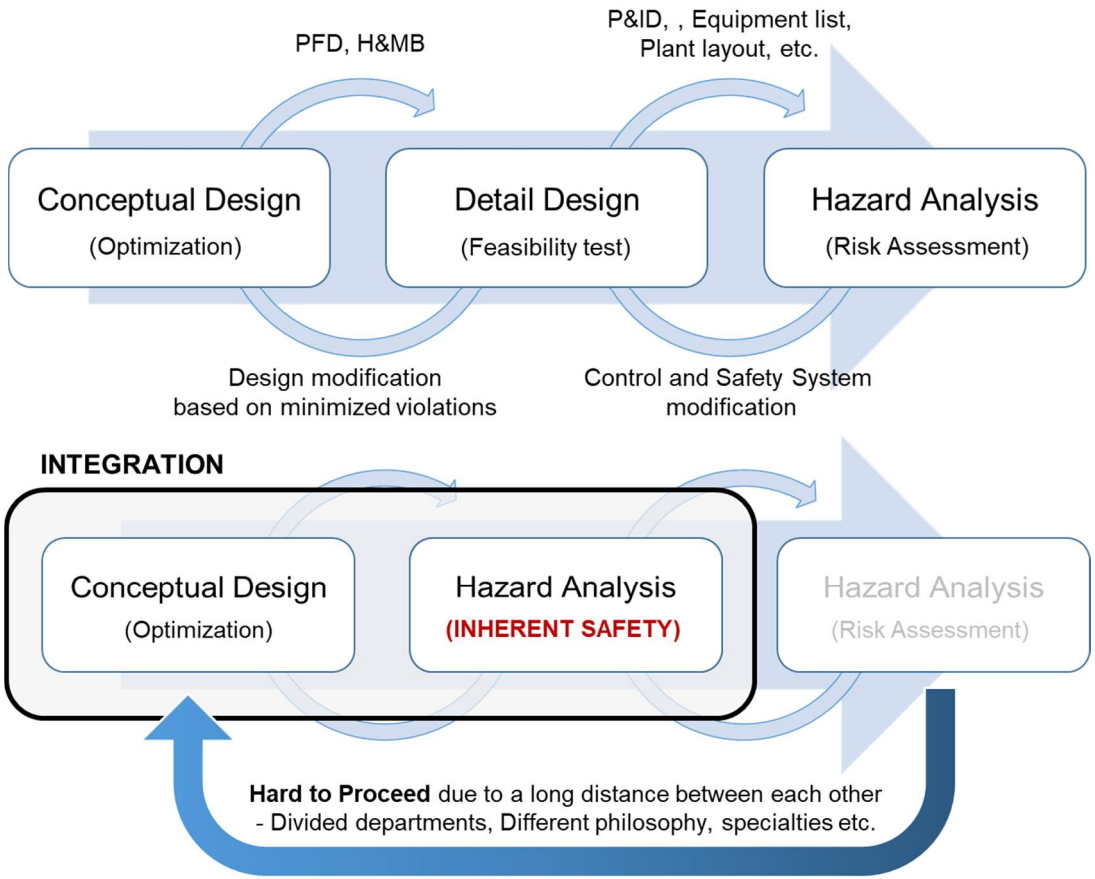

Figure 1-2. General Procedures of Process Design (top) and Inherent Safety (bottom)

Briefly, the process design proceeds from conceptual design to detail design to hazard analysis, and each stage is recursively performed in a sequential manner until the desired process is completed satisfying lots of requirements before construction. Conceptual design stage mainly performs unit operations and optimization study making PFDs (process flow diagram) and H&MB (heat and material balances) sheets. Then at detail design stage, feasibility tests for practical operation of the plant is performed based on the results of conceptual design, and discussions for the design modification proceeds with conceptual designers based on minimized violations. If the P&ID (piping and instrumentation diagram), equipment lists, and plant layout etc. are completed, they go on to the hazard analysis stage where risk assessments like HAZOP (hazard and operability) study or QRA are finally performed. If the assessed risk is unacceptable the associated control and safety systems should be modified in the detail design stage.

With the aim of designing a safer process in the context of these design procedures, Chapter 3 newly proposed two systematic approaches. One tried to reduce the risk through design modification of an existing GOSP plant based on the QRA results following the general design procedures. Meanwhile, the other integrated the conceptual design and hazard analysis by introducing inherent safety concept at the preliminary design stage (bottom figure of Figure 1-2), and decided an optimal process design through superstructure formulation and multi-objective optimization for minimizing both the TAC and the risk. This latter approach could largely lower the cost required for finalizing the design as it doesn't need to follow the general procedure where the recursive loop is recycled until the risk is reduced to an

acceptable level. But before this approach starts to be applied, the suitability of its method should be verified as it has to make some assumptions in assessing the safety level of the process as there are limited information. Also the computation load would be higher as it needs to simultaneously consider the economic feasibility and safety in designing a process. Despite the differences these two approaches have each other, however, they are essentially in the same context in that they share the same purpose of deciding a process design which is safer and/or even cheaper than the existing processes.

Chapter 4 addressed the problem incurred by the weak interactions between control room operators and field operators in operating a certain plant. Even though the real accident occurs in the plant site and the cooperation of operators is crucial for stably and safely operating a plant in unwanted situations, problems of information gap between each other has been hardly dealt with due to the different nature of each part. In this chapter, a new interactive operator training module covering the whole process from normal operation to accident situations was developed through multi-modular approach using advanced simulation and data processing technologies. This interactive simulation modeling delivers the online simulation results to the control room and field operators and induces them to take proper actions in case of a random accidental situation among pre-identified scenarios in a chemical plant. Developed model integrates the real-time process dynamic simulation with the off-line database of 3D-CFD accident simulation results in a designed interface using OLE technology so that it could convey the online information of the accident to trainees which is not available in existing

operator training systems. The model encompasses the whole process of data transfer till the end of the training at which trainees complete an emergency shutdown system in a programmed model. Consequently, the module could improve the effectiveness of operator training system through interactively linking the trainee actions with the model interface so that the associated accident situations would vary with respect to each trainee′s competence facing an accident.

1.4. Associated publications

The works presented in Chapter 2 and Chapter 3.2 are introduced in [1] and [2] respectively, and that in Chapter 3.3 has been submitted to *Industrial & Engineering Chemistry Research*. The work presented in Chapter 4 is introduced in [3].

CHAPTER 2. Process Intensification

Recently in natural gas processing, with various feed gases from small to mid-size gas reservoirs or shale gases and new compressor drivers of high efficiency that require less or no fuel gas, there has been a growing need of sophisticated nitrogen recovery solutions. In this study two cryogenic nitrogen recovery processes integrated with LNG production and NGL recovery are designed and optimized based on the structural analysis of components separation. The difference of each process is the way the nitrogen is removed from the natural gas: Integrated nitrogen recovery unit and standalone one. The former recovers nitrogen in the integrated heat and mass transfer structure with natural gas liquefaction while the latter separates the nitrogen recovery unit into an independent structure apart from the liquefaction section. These two processes are compared with each other in terms of specific power (kWH/kg_LNG), which is equivalent to the overall process efficiency, with respect to the nitrogen content in the feed gas from 0mol% to 20mol%. Consequently, as the nitrogen content in the feed gas increases, the specific power of each process also increases while the standalone solution has a priority over the other until around 17mol% of nitrogen and after that point the integrated solution becomes relatively more efficient. It should be noted that all of the optimization results of each configuration are improved with the reduced specific power by up 38.6% compared to those from previous studies which have the similar configuration. We believe that the way this study aimed is reasonable

guidelines for other chemical process designs as well as nitrogen recovery in natural gas processing.

2.1. Introduction

In recent small to mid-size onshore LNG plants and some shale gas export projects, nitrogen recovery in natural gas processing has been of great importance as nitrogen content in the pipeline feed gas varies over time and location. Traditionally the nitrogen removal has been relatively easy as the nitrogen content is low and the fuel containing nitrogen is going to boilers for steam turbines or large gas turbines. Several modern LNG plants, however, require sophisticated nitrogen removal schemes due to increasing amount of nitrogen in the feed gas, lower auto-consumption of fuels and/or lower tolerance for nitrogen content in the fuel inlet stream [1].

When it comes to nitrogen recovery, possible nitrogen sinks in a natural gas process are the product LNG (N_2 less than 1mol% for preventing tank roll-over phenomenon), fuel gas, and/or nitrogen purge gas (hydrocarbons less than 1mol% for vented safely to the atmosphere). Among these three sinks, the demand of fuel gas which is generated from an end-flash drum in the natural gas liquefaction process decreases recently as compressor drivers are gradually switched from steam turbines to aero-derivative gas turbines or electric motors which require less or no fuel gas for energy source in a plant [2]. Then the rest of nitrogen should be vented to atmosphere while meeting the environmental regulations which limit the hydrocarbon content less than 1mol% in vent gas. These two major trends in recent

LNG projects of varying feed composition and low plant fuel demand make it necessary to completely recover nitrogen from methane as the conventional LNG process would generate too large fuel gas exceeding the plant demand losing much methane to it.

This study aims at designing an optimal process of nitrogen recovery integrated with natural gas liquefaction and NGL recovery, following these trends assuming almost no fuel demand required for the mid-scale LNG plants of 1.5mtpa with complete recovery of nitrogen from natural gas for venting it to the atmosphere.

Researches for optimal process designs of the natural gas liquefaction process have been studied for decades. Remeljej et al. [3] performed an optimization of small-scale natural gas liquefaction process based on pinch technology with exergy analysis, and Guido et al. [4] compared the performances of different types of refrigeration cycles in low-temperature distillation processes for purifying natural gas.

In recovering NGL from treated feed gas before LNG production, Mehrpooya et al. [5] introduced a novel configuration with a self-refrigeration system for minimum energy requirement, and Vatani et al. [6] and He et al. [7] proposed and optimized an integrated process configuration for co-production of NGL and LNG with high liquefaction efficiency and high ethane recovery. Mehrpooya et al. [8] compared three process configurations for LNG and NGL co-production using C3-MR, DMR, and MFC refrigeration cycles respectively in terms of thermodynamic efficiency, and Ansarinasab et al. [9] evaluated these three configurations using advanced

exergoeconomic analysis aiming at reducing exergy destruction cost in the process components.

With the emerging need of nitrogen recovery, researches dealing with single nitrogen removal units or integrated configurations with NGL and LNG production have been studied recently. Rufford et al. [10] reviewed conventional and emerging technologies for CO2 and nitrogen removal from using cryogenic distillation to using pressure swing adsorption, and Kuo et al [11] focused on the selection and design criteria considered for the design of optimum nitrogen removal solutions. Hamedi et al. [12] designed optimal standalone nitrogen rejection units of single-column and multi-column systems with respect to nitrogen content in the natural gas.

Based on several solutions reviewed before, Ghorbani et al. [13-16] developed complex integrated processes of natural gas liquefaction, NGL recovery, and nitrogen rejection using C3MR, DMR, and MFC refrigeration systems with maximizing process efficiency in producing LNG. Based on the integrated configuration proposed in above researches, Mehrpooya et al. [17] investigated the process by advanced exergoeconomic analysis as they applied it to the NGL and LNG co-production processes before.

Above researches, however, have some limits in maximizing process efficiency in that possible separation structures are not fully considered as they only change the refrigeration cycles from C3MR to MFC with the same nitrogen removal scheme, and the interaction between optimization and exergy analysis is week as the results of exergy analysis do not affect the direction of optimization.

In order to improve the previous works, this study designed largely two different cryogenic nitrogen recovery processes which are integrated with LNG production and NGL recovery following the procedures below. Firstly, for the conceptual design of nitrogen recovery, possible process configurations are investigated and selected based on the structural analysis of components separation. With the selected configurations of integrated one and standalone ones for nitrogen recovery unit, each process is newly designed through structural modifications from a reference base case with optimization based on the exergy analysis. Then each optimal process is compared with each other in terms of specific power [kWH/kg_LNG], which is equivalent to the overall process efficiency, with respect to the nitrogen content in the feed gas from 0mol% to 20mol%. The results may give directions to the process design of nitrogen recovery with the order of priority for proposed design solutions at each nitrogen content.

2.2. Conceptual Design of the Nitrogen Recovery

For a process producing LNG and NGL with some fuel gas and/or purge nitrogen from a treated feed gas containing hydrocarbons(C1~C4), nitrogen, and few CO2, a possible separation structure could be described like Figure 2-1. Each product is produced at a node (blue, red, green, or yellow) with a separating ratio ($\alpha_i, \beta_i, \gamma_i, \delta_i$) for i component respectively. NGL containing C2+ components is firstly recovered from the feed gas at yellow node and the remaining gas of mainly methane and nitrogen is separated at blue and/or red node producing LNG, fuel gas, and purge nitrogen vented to the atmosphere.

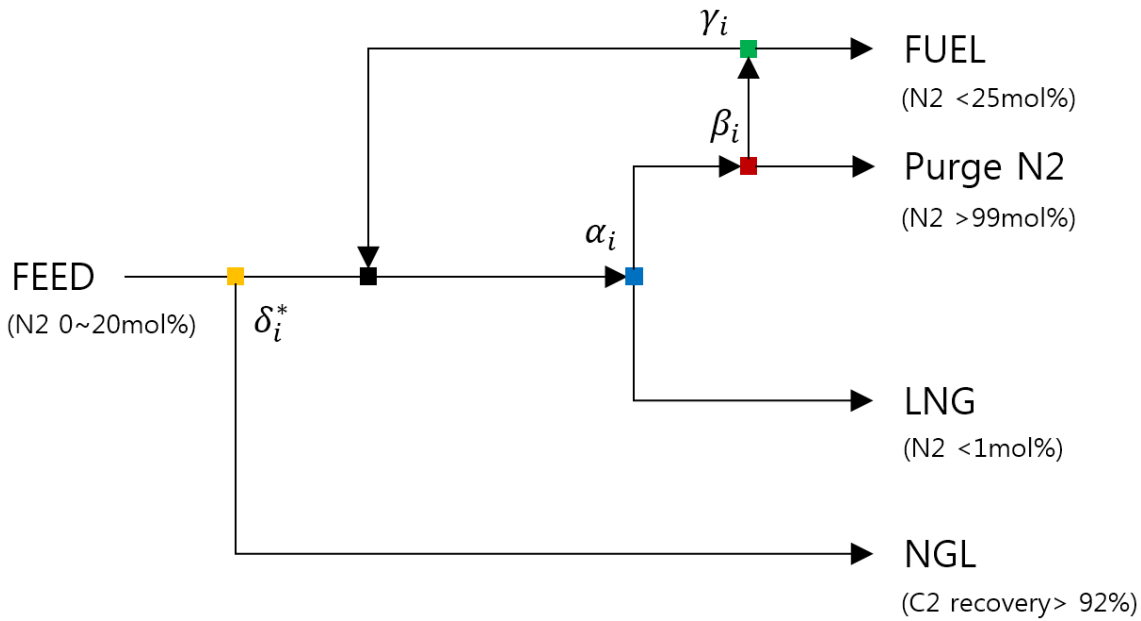

Figure 2-1. Separation structure from feed gas to products

In conventional LNG processes with a feed gas containing low nitrogen, only a single end-flash drum after the liquefaction section is located at blue node producing LNG and some fuel gas without separating the nitrogen via red node, $(\beta_i, \gamma_i) = (1, 0)$.

For recent nitrogen recovery processes with larger amount of nitrogen, however, the red node should be activated for venting nitrogen to the atmosphere via purge nitrogen stream. If complete nitrogen removal and LNG production occur at the single blue node simultaneously, other nodes of red and green could be omitted ($\beta_i = 0$, γ_i: none) resulting in a simple but delicate structure which would be called an integrated NRU later in this section. Otherwise, the separation proceeds by two stages at blue and red nodes with a non-zero value of β_i, and an off-spec stream containing methane and unseparated nitrogen from red node is recycled to the main liquefaction process via green node for complete recovery of methane and nitrogen, $(\beta_i, \gamma_i \neq 0)$. At the same time, the fuel gas is also produced at green node to the other direction with the extent meeting the plant fuel demand. This process scheme would be called a standalone NRU later.

When it comes to each product specification, nitrogen content in the product LNG should be less than 1mol% to prevent “roll-over” phenomenon which could cause a huge vapor flash-off leading to containment loss in the storage tank. Fuel gas also needs to meet the nitrogen content specification as it is supplied to the gas turbine as a compressor driver. For the aero-derivative gas turbine, the fuel gas must contain less than 25mol% nitrogen to meet the heating value specification. This high effective compressor driver with low tolerance for nitrogen content in the fuel has low auto-consumption in the plants decreasing the fuel demand. Purge nitrogen

should contain hydrocarbons less than 1mol% in order for directly vented to the atmosphere safely. Ethane recovery in producing NGL is set higher than 92%.

From the design standpoint a separation structure is selected according to how much material is separated at each node as it determines the structure having different equipment and energy for the separation. For example, a 'cryogenic' 'distillation column' at blue node is necessary if the process needs complete separation of nitrogen. For yellow node, the separation ratio (δ_i^*) is fixed by the NGL product specification ($\delta_{C2}^* = 0.92$) so that it could be ignored in designing an optimal structure.

When we focus on the nitrogen component material balance, as the specifications of nitrogen content in all sinks except fuel gas are defined with one recycle stream, degree of freedom in this structure is three. It means that when the plant fuel demand (e.g. 20MW) is estimated based on the product capacity (e.g. 1.5mtpa LNG), thermodynamic equilibriums at both of blue and red node need to be selected in defining all the material balance in the separation structure. This study chooses three possible nitrogen recovery options by determining α_i and β_i with full recycle (γ_i=1) assuming that there is no fuel demand in the target LNG plant as all the compressors could be driven by electric motors not by gas turbines.

1. Integrated NRU (Nitrogen Recovery Unit, $\beta_i = 0$) in Figure 2-2(a) - Methane and nitrogen are completely separated at blue node producing LNG (1atm, 109K) and venting nitrogen (1atm, 293K) to the atmosphere without producing fuel gas. All the cryogenic heat necessary in the separation is provided from the refrigeration system as is for that of the liquefaction.

2. Standalone NRU ($\beta_i \neq 0$) in Figure 2-2(b) - Methane and nitrogen are separated by two stages at blue and red nodes with full recycle and no fuel gas. LNG is produced at blue node and the remaining vapor is routed to red node of standalone NRU section at which the purge nitrogen is completely separated and vented. Off-spec column bottom stream is recycled to the main liquefaction process via green node. Possible two options are selected as below (A, B) according to how much methane is recovered at blue node.

   A. End-flash drum at blue node ($\alpha_{N2} > 0.9,\ \alpha_{C1}$: high) – An end-flash drum could simply separate methane and nitrogen meeting product specifications when nitrogen content in the feed gas is low enough, but it would carryover too much methane through the vapor stream with high α_{C1} when the nitrogen content increases as it is limited to a single equilibrium. This would cause large separation load to the NRU section.

   B. Stripping column at blue node ($\alpha_{N2} > 0.9,\ \alpha_{C1}$: low) – As a stripping column separates methane and nitrogen more strictly than the end-flash drum, methane carryover to the vapor is reduced with relatively lower α_{C1} so that separation load to the standalone NRU also decreases with less recycle.

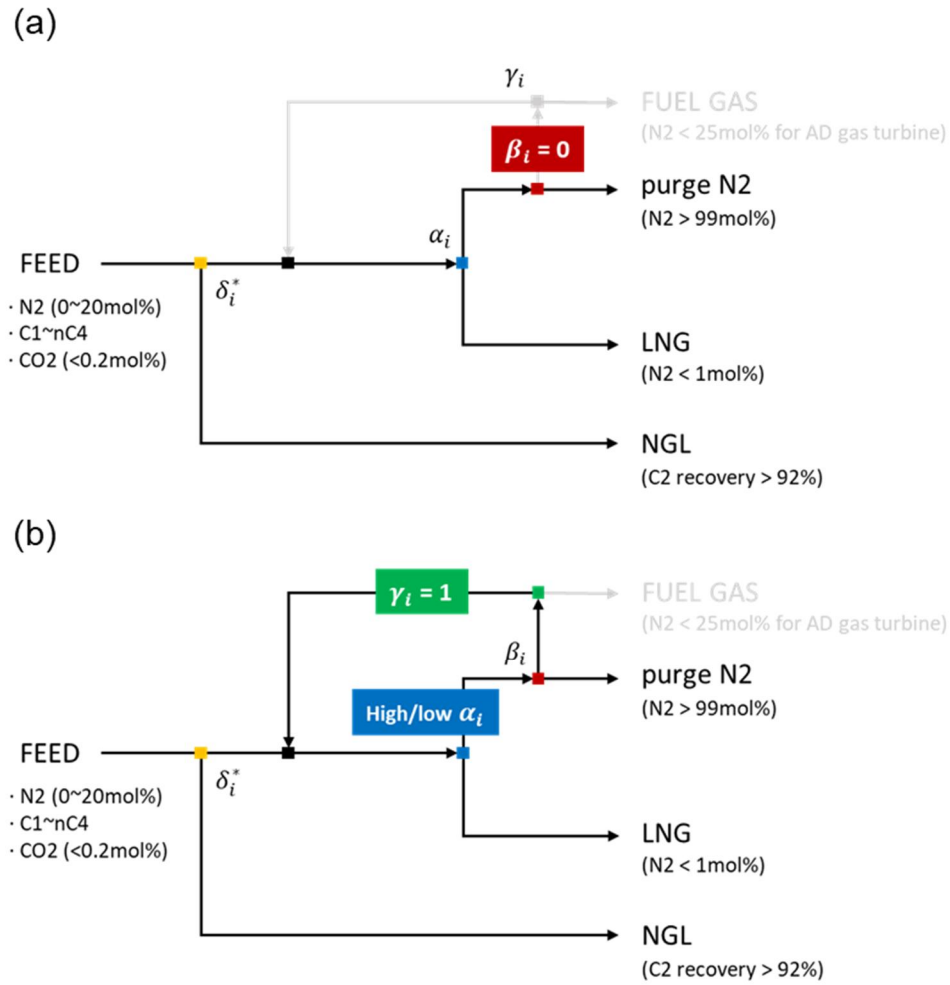

Figure 2-2. Separation structures of (a) integrated NRU and (b) standalone NRU

For a treated feed gas containing nitrogen, methane, ethane, propane, n-butane, and CO2 with the mole fraction of 0.05, 0.83, 0.06, 0.04, and 0.02 respectively, separation ratios of each design option meeting all the product specifications could be simply calculated as Table 2-1.

Table 2-1. Separation ratios for each design option when nitrogen content in the feed gas is 5mol%

Separation Ratio		α_i		β_i		γ_i		δ_i	
	i	N2	C1	N2	C1	N2	C1	C1	C2
Integrated		0.85	0.00	0.00	0.00	-	-	0.00	0.92
Standalone	End-flash	0.92	0.30	0.50	1.00	1.00	1.00	0.00	0.92
	Stripping	0.90	0.10	0.36	1.00	1.00	1.00	0.00	0.92

It can be seen that the integrated NRU completely separate nitrogen at single blue node with the α_{N2} value of 0.85 which is equivalent to the overall nitrogen recovery rate. For standalone NRU, stripping option recovers more methane to product LNG at blue node than the end-flash one (α_{C1}= 0.10 for stripping, 0.30 for end-flash) with less recycle at green node lowering the main process capacity (β_{N2}=0.36 for stripping, 0.50 for end-flash).

These three nitrogen recovery options selected through the structural analysis are designed and optimized with respect to the nitrogen content in the feed gas from 0 to 20mol%. As each process requires cryogenic heat transfer for the separation, a complex heat and mass transfer structure is developed maximizing process efficiency with minimal exergy destruction via optimization. Then the results are compared with each other for the design priority of nitrogen recovery.

2.3. Design Improvement and Optimization

2.3.1. Integrated Nitrogen Recovery Unit (NRU)

Integrated nitrogen recovery solution simplified in Figure 2-3 removes nitrogen from a high pressure feed gas between NGL recovery and natural gas liquefaction sections. Overhead stream of a binary mixture of methane and nitrogen from NGL recovery column at 25bar is expanded at a throttling valve, partially condensed by a refrigerant at MSHEs (Multi Stream Heat Exchangers), and then routed to the NRU column operating in a lower pressure at around 14bar. Methane rich bottom stream from the NRU column is sub-cooled to around 108K in the liquefaction section and depressurized to 1bar to be the product LNG at 1bar 109K.

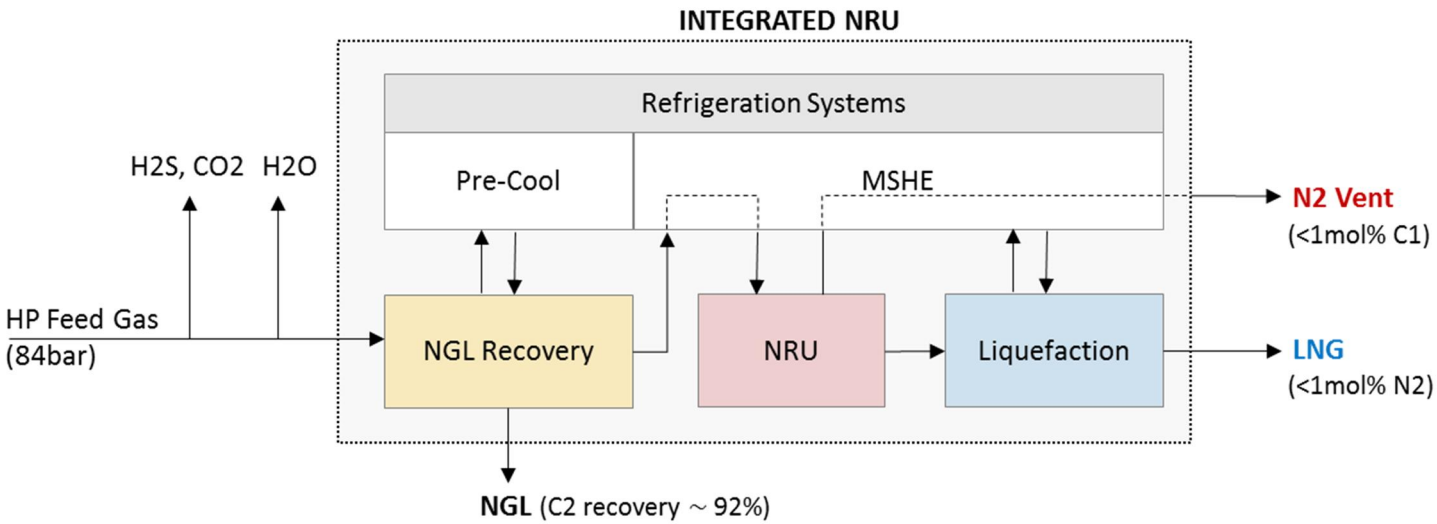

Figure 2-3. Block flow diagram of integrated NRU

In a base case designed by Ghorbani et al. [14] illustrated in Figure 2-4, this bottom stream departing from D6 as a liquid – "LNG stream" in orange – is fully vaporized at HX4, compressed at C4, and re-condensed at the same heat exchanger of HX4 for improving heat transfer efficiency. Refrigeration system in this case is propane precooled mixed refrigerant cycle (C3MR) which is a conventional and reliable option in LNG plants, where a pure propane cycle pre-chills natural gas by three stages ahead of NGL section and a mixed refrigerant one mainly liquefies and sub-cools the natural gas. NGL recovery in this study uses GSP (Gas Subcooled Process) configuration where some portion of vapors from the feed stream splitted in SP03 is subcooled in HX4 and routed to the top of NGL recovery column, T100, giving cold energy to it as a reflux. NRU column has a similar configuration with that of a conventional distillation column except that utility streams are not necessary as the heat transfer necessary in a condenser and a reboiler is fully integrated with the refrigeration system at HX4 and HX5.

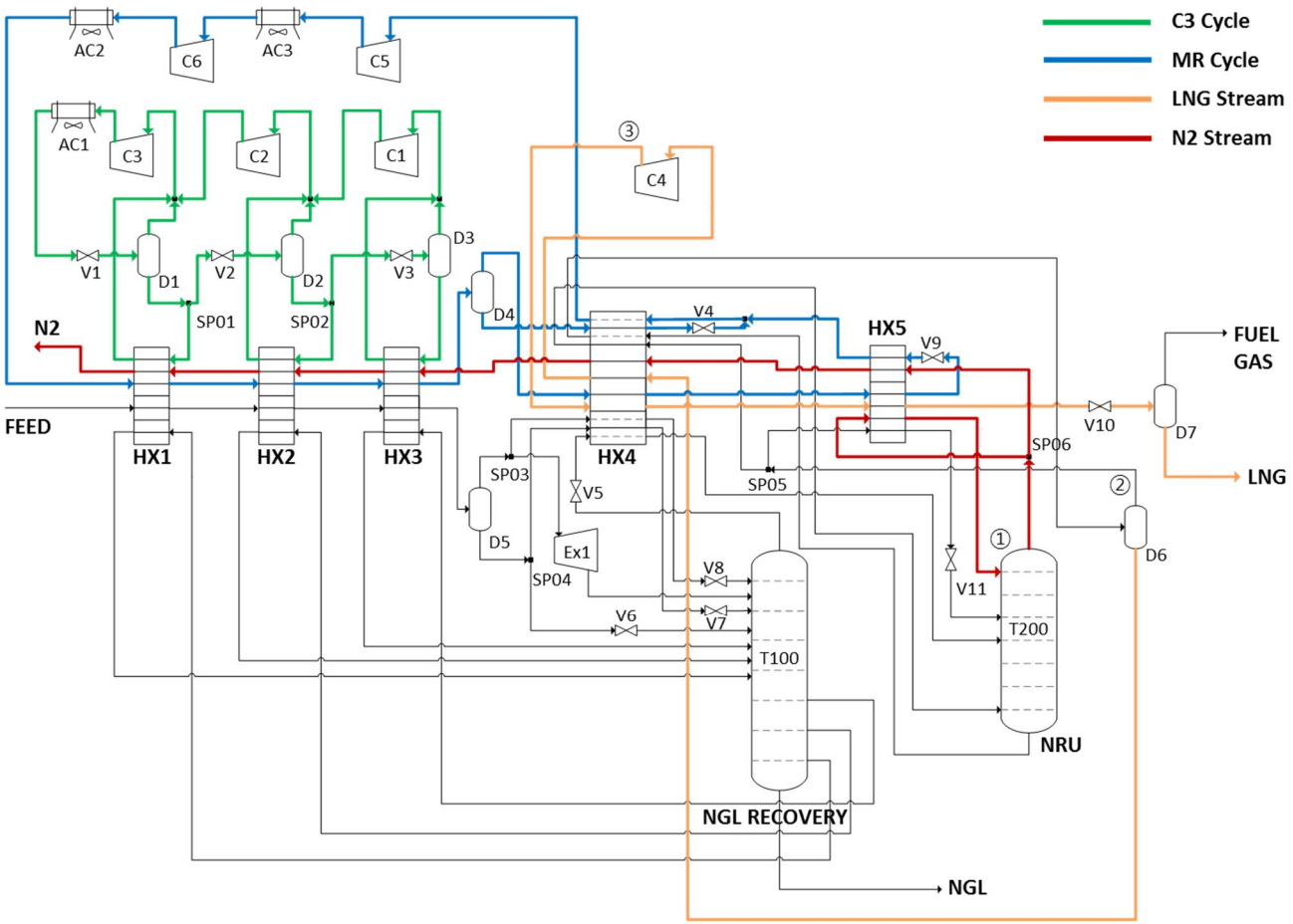

Figure 2-4. Process flow diagram of the reference base case of integrated NRU

Main stream data of the base case are summarized in Table 2-2, and other specifications for unit operations are omitted in this paper as they are described in the Ghorbani's previous work in detail. As this study would propose an improved design compared to the base case, in the following section is this base case optimized meeting the constraints newly set in this study and then structural modifications for reducing exergy destructions and re-optimization with adjusted control variables are applied to that optimized base case for clear comparison.

Table 2-2. Base case main stream data

		FEED	C3	MR	NGL	LNG	N2
Pressure [bar]		63.09	14.30	38.00	25.00	1.00	1.00
Temperature [K]		310.15	308.15	311.15	298.95	109.15	293.15
Molar Flow [kmol/h]		14,000	25,000	37,000	1,611	11,737	652
Molar composition	N2	0.055	0.000	0.257	0.000	0.010	0.990
	C1	0.825	0.000	0.334	0.000	0.984	0.010
	C2	0.058	0.000	0.239	0.463	0.006	0.000
	C3	0.037	1.000	0.170	0.315	0.000	0.000
	nC4	0.024	0.000	0.000	0.208	0.000	0.000
	CO2	0.002	0.000	0.000	0.014	0.001	0.000

2.3.2. Optimization of the Base Case

As described in above structural analysis section, the main goal of optimization is to design a process producing specified amount and quality of products – LNG, NGL, purge N2 – from a certain feed stream with a minimal power consumption meeting the thermodynamic feasibility in heat and mass transfer. Thermodynamic feasibility could be verified solving the balance equations in each unit operation via gProms simulator with an additional custom model developed in this study. This custom model is for the analysis of internal heat transfer in multi-stream heat exchangers, which gives a minimum temperature across in each heat exchanger to prevent violating 2nd law of thermodynamics. As the gProms simulator solves all the process model simultaneously in an equation-oriented manner unlike the sequential-oriented one of other commercial software, it could effectively employ a sequential quadratic programming (SQP) for the optimal solution of a complex non-linear programming (NLP) problem.

Optimization information is summarized in Table 2-3. Objective function is to minimize a specific power [kWH/kg_LNG], the amount of energy necessary in producing 1kg LNG same as previous works, and inequality constraints are for satisfying the product specifications of NGL, LNG, and purge N2 and for feasible heat exchanger designs which have the minimum temperature across over 3K for all multi-stream heat exchangers. Control variables are selected based on their sensitivity to the objective function and exergy efficiencies of process components and then are classified in each subsection of NGL recovery, LNG production, NRU, and two cycles in the refrigeration system.

Table 2-3. Optimization summary of base case

Optimization Summary		Descriptions	Annotations
Objective Function		Specific Power [kWH/kg_LNG]	
Control variables			
NGL Recovery		Cold reflux temperature Cold reflux flowratio T100 side stream molar flowrate	SP03_HX4_outlet_T SP03_flowratio T100_side_F
LNG Production		HP LNG stream pressure LNG Temperature	C4_outlet_P V10_inlet_T
NRU		T200 feed temperature T200 bottom pressure T200 reboiling flow ratio T200 reboiling temperature T200 reflux flow ratio T200 reflux temperature	V5_HX4_outlet_T T200_btms_P SP05_flowratio D6_inlet_T SP06_flowratio SP06_HX5_outlet_T
Refrigeration System	C3 Cycle	Molar flowrate $1^{st}/2^{nd}$ stage split ratio $1^{st}/2^{nd}/3^{rd}$ stage pressure	C3_cycle_F SP01/SP02_flowratio V1/V2/V3_outlet_P
	MR Cycle	Molar flowrate, Composition Pressure($1^{st}/2^{nd}$) Temperature	MR_F_N2/C1/C2/C3 C6/V4_outlet_P MR_HX4/HX5_outlet_T
Constraints		C1 recovery in NGL recovery > 0.999 C2 recovery in NGL recovery > 0.920 C1 recovery in NRU > 0.999 N2 molar content in LNG < 0.01 C1 molar content in purge N2 < 0.01 All heat exchangers MTA(Minimum Temperature Across) > 3K	

The optimization results of these variables are listed in Table 2-4. Each control variable is optimized from the initial value of base case between lower and upper bounds. Optimal value of each variable is not that far from the initial value but these results satisfy all the constraints set in this study so that they could be a new base case which would be clearly compared to other design proposals in this study.

As the exergy analysis for the whole process will play an important role in proposing new NRU designs in the rest of this study, the method of it and the definitions of exergy parameters are described after the Table 3-4 ahead of the discussion about design proposals.

Table 2-4. Optimization results of base case of integrated NRU

Subsections	Control Variables	Optimal value	Initial value	Lower bound	Upper bound
NGL Recovery	SP03_HX4_outlet_T	179.33	181.15	175.00	185.00
	SP03_flowratio	0.67	0.60	0.50	0.70
	T100_side_F	2730	2700	2500	3000
LNG Production	C4_outlet_P	36.09	25.00	15.00	40.00
	V10_inlet_T	105.18	105.00	100.00	110.00
NRU	V5_HX4_outlet_T	152.23	161.15	150.00	165.00
	T200_btms_P	12.03	14.00	12.00	16.00
	SP05_flowratio	0.328	0.369	0.200	0.500
	D6_inlet_T	151.68	155.15	145.00	160.00
	SP06_flowratio	0.0002	0.02	1.0E-6	0.05
	SP06_HX5_outelt_T	106.70	103.15	90.00	110.00
C3 Cycle	C3_cycle_F	25561	27000	20000	30000
	SP01_flowratio	0.27	0.35	0.20	0.40
	SP02_flowratio	0.64	0.63	0.5	0.7
	V1_outlet_P	5.02	5.00	4.50	5.50
	V2_outlet_P	2.50	2.50	2.00	3.00
	V3_outlet_P	0.94	1.00	0.50	1.50
MR Cycle	MR_F_N2	10214	10264	5000	15000
	MR_F_C1	13888	13364	8000	15000
	MR_F_C2	9025	9560	5000	15000
	MR_F_C3	7144	6812	1000	10000
	C6_outlet_P	38.2	38.0	30.0	55.0
	V4_outlet_P	2.88	2.00	1.00	3.00
	MR_HX4_outlet_T	139.57	142.53	135.00	150.00
	MR_HX5_outlet_T	106.80	104.15	90.00	110.00

Exergy Analysis

In order for a comprehensive analysis of the optimization results compared to the base case, exergy could be a suitable parameter for evaluating the thermodynamic efficiency of an overall process or process components. The maximum theoretically useful work achievable in a process that brings the system into the reference state is called exergy. Exergy analysis is based on the second law of thermodynamics to implicitly evaluate a system, which yields the efficiency that is a measure of how close the actual performance approaches the ideal and identifies the causes and locations of thermodynamic losses more clearly than energy analysis [18]. Exergy analysis in this study is implemented in a set of external routines integrated with the flowsheeting simulator calculating exergies of material streams and exergy destructions and efficiencies of unit operations in process components along with mass and energy balance equations. Complete exergy analysis has a role of a diagnostic tool for judging chemical processes which could suggest or indicate the ways to reduce the irreversibility.

Stream Exergy

Assuming a system is rest with the environment, neglecting the effects of kinetic, potential, and nuclear energies, the total exergy contained in a material stream could be divided into chemical and physical exergy as expressed in Eq. (2-1).

$$exergy = \dot{m}(e^{CH} + e^{PH}) \quad (2\text{-}1)$$

where $\dot{m}$ =molar/mass flowrate [kg(mol)/s]; e^{CH} , e^{PH} =molar/mass specific chemical or physical exergy respectively [kJ/kg(mol)].

Chemical exergy is the maximum theoretical useful work obtainable as the system passes from the restricted dead state to the dead state where it is in complete equilibrium with the environment [18]. Calculation of standard chemical exergy of a material stream proposed by Moran and Shapiro [19] considers the material stream as a fuel which is combusted according to Eq. (2-2) and the mathematical expression for the molar chemical exergy of a mixture with its component j could be illustrated in Eq. (2-3) and (2-4) [20, 21].

$$C_aH_bO_c + \left(a + \frac{b}{4} - \frac{c}{2}\right)O_2 \rightarrow \mathrm{a}CO_2 + \frac{b}{2}H_2O \tag{2-2}$$

$$\bar{e}_j^{\,CH} = \left[\bar{g}_f + \left(a + \frac{b}{4} - \frac{c}{2}\right)\bar{g}_{O_2} - a\bar{g}_{CO_2} - \frac{b}{2}\bar{g}_{H_2O(g)}\right]_{T_0,p_0} + RT_0 \ln\left[\frac{\left(x_{O_2}^{air}\right)^{a+\frac{b}{4}-\frac{c}{2}}}{\left(x_{CO_2}^{air}\right)^{a}\left(x_{H_2O}^{air}\right)^{\frac{b}{4}}}\right] \tag{2-3}$$

$$\bar{e}_M^{\,CH} = \sum_j x_j \bar{e}_j^{CH} + RT_0 \sum_j x_j \ln x_j \tag{2-4}$$

where $\bar{e}_j^{\,CH}$ =molar chemical exergy of a single compounds j [kJ/mol]; $\bar{e}_M^{\,CH}$=molar chemical exergy of a mixture [kJ/mol].

The second term of right hand side in Eq. (2-3) is the stoichiometric ratio of molar fractions of the combustion gases present in air which could come from the partial pressure ratio of these reference species evaluated at a mean atmospheric pressure of 99.31kPa according to Szargut et al. [22].

Physical exergy is the maximum theoretical useful work obtainable as the system passes from its actual state with temperature T and pressure p to the restricted

dead state with temperature T_0(=273.15K) and pressure p_0(=1bar) given by Eq. (2-5) below [23, 24].

$$e^{PH} = [h(T,p) - h(T_0,p_0)] - T_0[s(T,p) - s(T_0,p_0)] \quad (2\text{-}5)$$

where h=molar specific enthalpy of a mixture [kJ/mol]; s=molar specific entropy of a mixture [kJ/mol_K]

Process Component Exergy

Exergy destruction and efficiency in each process component like compressors could be estimated by applying the exergy balance on each component at the steady state given by following equation, Eq. (2-6) [25].

$$Ex_i + Ex_{Qi} = Ex_o + Ex_{Qo} + W_{sh} + I \quad (2\text{-}6)$$

where $Ex_i, Ex_o, Ex_{Qi}, Ex_{Qo}$=exergy of inlet and outlet material and energy streams respectively; W_{sh}=shaft work; I=irreversibility or exergy destruction.

Based on this exergy balance, the definitions for irreversibility and exergy efficiency of each component are summarized in Table 2-5 [26-28].

Table 2-5. Definitions of exergy destruction and efficiency of process components

Components Exergy Destruction	Exergy Efficiency
Compressor/Expander/Pump $\mathrm{I} = Ex_i - Ex_o = \sum(\dot{m} \cdot e)_i + W - \sum(\dot{m} \cdot e)_o$	$\varepsilon = \frac{\sum(\dot{m} \cdot e)_i - \sum(\dot{m} \cdot e)_o}{W}$
Air cooler $\mathrm{I} = Ex_i - Ex_o = \sum(\dot{m} \cdot e)_i + e_{ai} + W - \sum(\dot{m} \cdot e)_o - e_{ao}$	$\varepsilon = \frac{\sum(\dot{m} \cdot e)_o + e_{ao}}{\sum(\dot{m} \cdot e)_i + W}$
Heat Exchanger $\mathrm{I} = Ex_i - Ex_o = \sum(\dot{m} \cdot e)_i - \sum(\dot{m} \cdot e)_o$	$\varepsilon = 1 - [\left\{\frac{\sum(m \cdot \Delta e)}{\sum(m \cdot \Delta h)}\right\}_h - \left\{\frac{\sum(m \cdot \Delta e)}{\sum(m \cdot \Delta h)}\right\}_c]$
Expansion Valve $\mathrm{I} = Ex_i - Ex_o = \sum(\dot{m} \cdot e)_i - \sum(\dot{m} \cdot e)_o$	$\varepsilon = \frac{e_o^{\Delta T} - e_i^{\Delta T}}{e_i^{\Delta P} - e_o^{\Delta P}}$
Column $W_{min} = Ex_i - Ex_o = \sum(\dot{m} \cdot e)_i - \sum(\dot{m} \cdot e)_o$ $\text{Lost Work(LW)} = T_o(\sum(\dot{m} \cdot s)_o - \sum(\dot{m} \cdot s)_i$	$\varepsilon = \frac{W_{min}}{LW + W_{min}}$
Process (Overall) $\mathrm{I} = Ex_o + Ex_{Qo} + W_{sh} - Ex_i + Ex_{Qi}$	$\varepsilon = 1 - \frac{Total\ irreversibility}{Total\ consumed\ power}$

2.3.3. Design Improvement

When the base case is optimized in a fixed structure of Figure 2-4 meeting constraints in Table 2-3, power consumption of each process component and resultant objective function value are summarized in the first two columns in Table 2-12. Specific power after optimization of the reference base case has a slightly lower value of 0.653kWH/kg_LNG than that of the reference case of 0.656kWH/kg_LNG. From these results which would be regarded as a new base case from this chapter, a retrofit design called improved case illustrated in Figure 2-5 is proposed through modifying the heat and mass transfer structure of the base case based on exergy analysis.

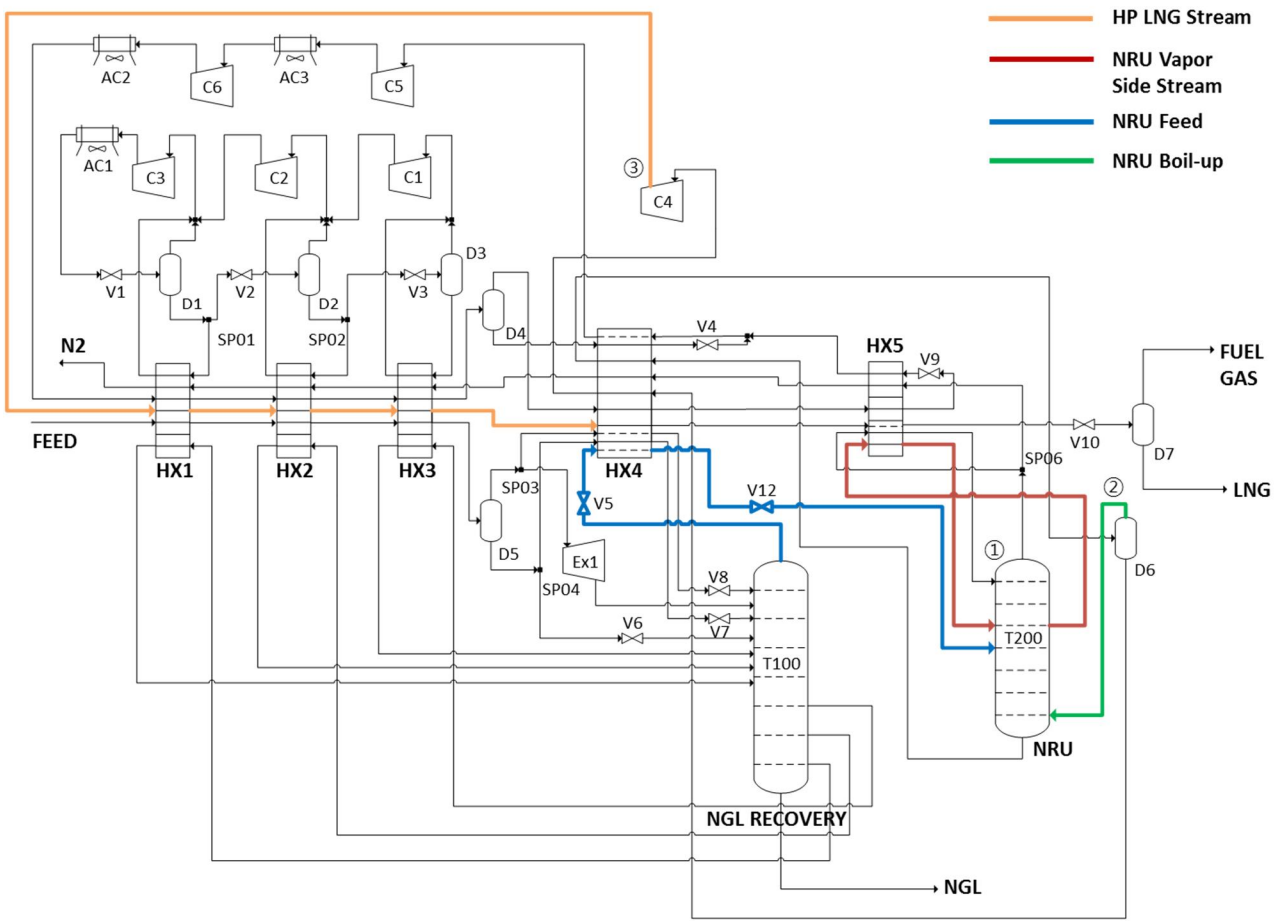

Figure 2-5. Process flow diagram of the improved case of integrated NRU

Structural Modification

From the grand composite curve of the base case in the left graph of Figure 2-7, it can be seen that a large gap between hot and cold stream curves exists in HX4 and HX5 due to the mismatches between horizontal lines of each curve which would come from the latent heat transfer of almost pure streams like column overhead or bottoms at different temperatures, resulting in large exergy losses. These mismatches of horizontal lines limit the minimization of exergy destructions in heat exchangers preventing two curves from closely approaching each other. In order to solve this limitation, two ways of structural modifications are applied to the base case improving the performance of heat and mass transfer.

1. Introducing vapor side stream in NRU column (T200)

Firstly, in the heat transfer in HX5 in left graph in Figure 2-7, only one horizontal line exists in the hot stream curve which comes from an almost pure reflux stream in NRU column (T200) consisting of 99mol% nitrogen. When the nitrogen content in the feed gas increases, this horizontal line becomes longer in length as larger quantity of reflux stream needs to be condensed for meeting the product quality, resulting in huge exergy destruction in HX5.

In order to decrease the flowrate of this pure nitrogen reflux stream, a non-pure vapor side stream is withdrawn at a certain stage in the rectifying section of NRU column and re-routed to the same location after partial condensation in HX5 as the red line (①) in Figure 2-5, providing complemental cold reflux to the rectifying section of the column. Then the original additional cold reflux stream (②) in Figure 2-4 from SP05 to HX5 to NRU column in the base case could be replaced by this side stream and unnecessary heat transfer of the streams departing from SP05 could be omitted as the green line (②) in Figure 2-5, resulting in a simpler heat and mass transfer network in both HX4, HX5, and NRU column.

Through this modification, hot and cold stream curves with much shorter horizontal line in HX5 could be tighten narrowly by controlling the mixed refrigerants in optimization.

2. Introducing a high pressure LNG stream in the main liquefaction section, and two-stage decompression between NGL recovery (T100) and NRU (T200) columns

Similar to previous modification, heat transfer in HX4 accounting for almost half of the total also has the point to be modified for minimizing exergy destruction in the base case. There are three horizontal heat transfer lines in HX4 section, two in the hot stream curve and the other in the cold stream one.

For the hot stream curve, one at around 155K comes from partial condensation of NGL recovery column overhead stream before it is routed to NRU column as a feed stream, and the other at around 185K comes from total condensation of the compressed LNG stream after C4 as the orange line (③) in Figure 2-4.

For cold stream one, the horizontal line at around 152K comes from partial vaporization of NRU column bottom stream for re-boiling and total vaporization of D6 liquid stream for compression at C4, even though it seems as if this line comes from a single stream as these two streams have almost the same pressure, temperature and composition originating from the same column bottoms.

One option for matching these four almost pure streams in HX4 is to eliminate the horizontal line at around 185K in hot stream curve which comes from C4 outlet stream and adhere the remaining lines lying in similar temperature to each other closely. As the horizontal line in the composite curve is generated while a pure stream passes two-phase region during condensation as the path of base case in Figure 2-6, one possible way to eliminate this line is increasing the outlet pressure of C4 until it enters the supercritical region over the critical point (a triangular point in the figure) to be maintained as a single phase during refrigeration to the

temperature at which the LNG stream exists as a single liquid phase even after expanded to 1bar as the path of improved case in Figure 2-6.

When the LNG stream is compressed over the critical pressure at C4, the temperature of C4 outlet stream is higher than the temperature ranges of heat transfer in HX4 so that it should be re-routed to HX1 not to HX4 like the orange line (③) in Figure 2-5.

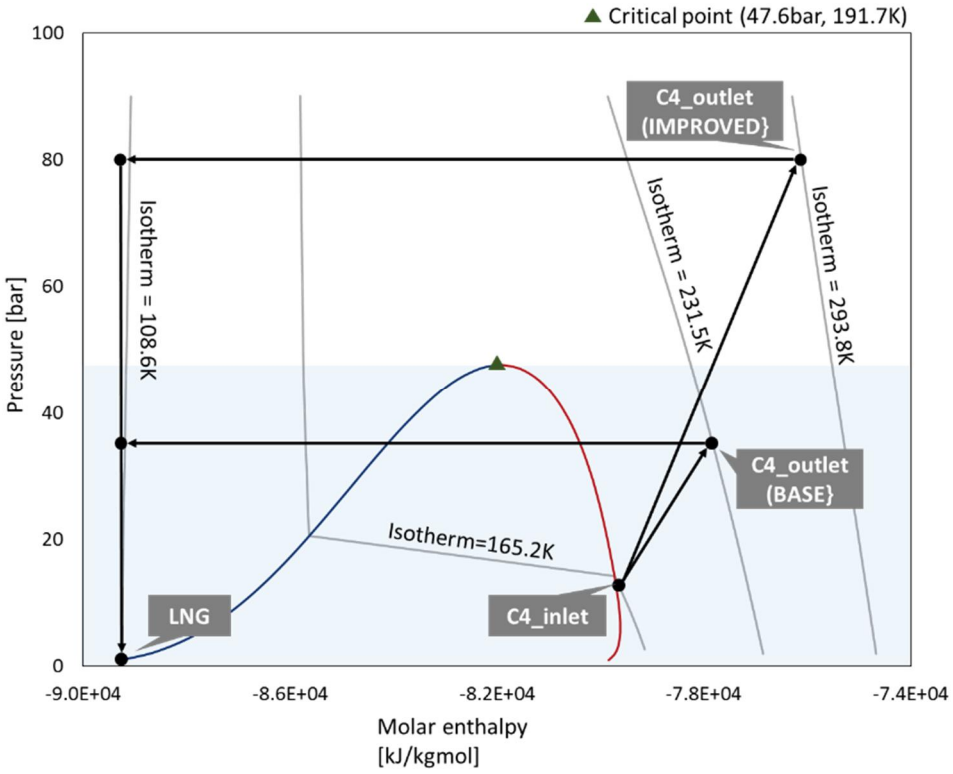

Figure 2-6. PH diagram of LNG stream from compression to refrigeration to expansion of the base and improved case of integrated NRU

The remaining two horizontal lines could be attached closely through optimization adjusting the temperature (height) and quantity of heat flow (length) of each line. As the temperature and heat flow of each line are determined mainly by the pressure at which the phase is changed, the overhead stream of NGL recovery column should be decompressed by two-stage unlike single-stage in the base case in order to control the pressure of condensation in HX4 as the blue line with additional throttling valve of V12 in Figure 2-5, and then this additional variable of pressure drop in V5 would be controlled with the bottom pressure of NRU column in optimization matching the horizontal lines in hot and cold stream curves.

As the refrigeration system in this study considers only the C3-MR cycle, structural modification for minimizing the irreversibility occurring in the pre-cooling section of HX1, HX2, and HX3 in Figure 2-7 is not considered here, but the variables like flowrate and pressure of each compression stage in the cycle are included in the control variables of optimization.

Optimization of Improved Case

Based on the structural modifications for lowering exergy destruction in the heat exchangers, optimization minimizing specific power could be solved with following changes in control variables in Table 2-6 from those of base case optimization in Table 2-3. Through modifications, V5 outlet pressure (V5_outlet_P) could be additionally controlled between the feed pressure of NRU column (13.72bar – default value of 5th tray) and the top pressure of NGL recovery column (25bar), and NRU column reboiling flow ratio (SP05_flowratio) would be omitted as the splitter SP05 is deleted after modification. For an added vapor side stream of NRU column, its flowrate and outlet temperature at HX5 would be also controlled in optimization.

The optimization results of all control variables are listed in 2-7. Especially the MR cycle flowrates largely decrease by 36.0% from 40271kmol/h of base case to 25764kmol/h of improved one, which would result in much less power consumption for cycle compressors and increase the thermodynamic efficiency of the process in producing same amount of products

Table 2-6. Changes in control variables in optimization of improved case

Control variables	Descriptions	Annotations	Status
NGL Recovery	T100 overhead pressure drop	V5_outlet_P	Add
NRU	T200 reboiling flow ratio	SP05_flowratio	Delete
	T200 vapor side stream molar flowrate	T200_side_F	Add
	T200 vapor side stream temperature	T200_side_outlet_T	Add

Table 2-7. Optimization results of improved case of integrated NRU

Subsections	Control Variables	Optimal value	Initial value	Lower bound	Upper bound
LNG Production	SP03_HX4_outlet_T	155.00	179.33	140.00	190.00
	SP03_flowratio	0.75	0.67	0.50	0.90
	T100_side_F	2716	2730	2650	2750
	V5_outlet_P	17.72	20.00	14.00	25.00
	C4_outlet_P	80.04	36.09	60.00	100.00
	V10_inlet_T	105.18	105.18	100.00	110.00
	V5_HX4_outlet_T	151.22	152.23	145.00	165.00
NRU	T200_btms_P	11.86	12.03	10.00	14.00
	T200_side_F	4706	3000	1E-6	6000
	T200_side_outlet_T	113.43	115.15	110.00	120.00
	D6_inlet_T	151.68	151.68	145.00	160.00
	SP06_flowratio	0.24	0.20	1.0E-6	0.5
	SP06_HX5_outlet_T	100.05	106.70	90.00	110.00
C3 Cycle	C3_cycle_F	22336	25561	20000	30000
	SP01_flowratio	0.34	0.27	0.20	0.40
	SP02_flowratio	0.61	0.64	0.5	0.7
	V1_outlet_P	5.02	5.00	4.50	5.50
	V2_outlet_P	2.49	2.50	2.00	3.00
	V3_outlet_P	0.94	1.00	0.50	1.50
MR Cycle	MR_F_N2	5071	10214	1000	15000
	MR_F_C1	8451	13888	5000	15000
	MR_F_C2	7204	9025	1000	15000
	MR_F_C3	5038	7144	1000	10000
	C6_outlet_P	41.95	38.2	30.0	50.0
	V4_outlet_P	3.39	2.88	1.50	5.00
	MR_HX4_outlet_T	151.55	139.57	130.00	160.00
	MR_HX5_outlet_T	100.45	106.80	90.00	110.00

The grand composite curves of heat transfer in base and improved case after optimization are compared in Figure 2-7, and the performance of heat exchangers are summarized in Table 2-8. As can be seen in Figure 2-7, hot and cold stream curve of improved case (right figure) adhere narrowly to each other with matched horizontal lines as intended by structural modifications described before. Consequently, total heat flow of improved case decreases by 11.6% from 260.4MW to 230.1MW and exergy destruction of heat exchangers also decreases dramatically by 46.5% from 27.1MW to 14.5MW mainly at the HX4 and HX5 both by over 50%, as summarized in Table 2-8.

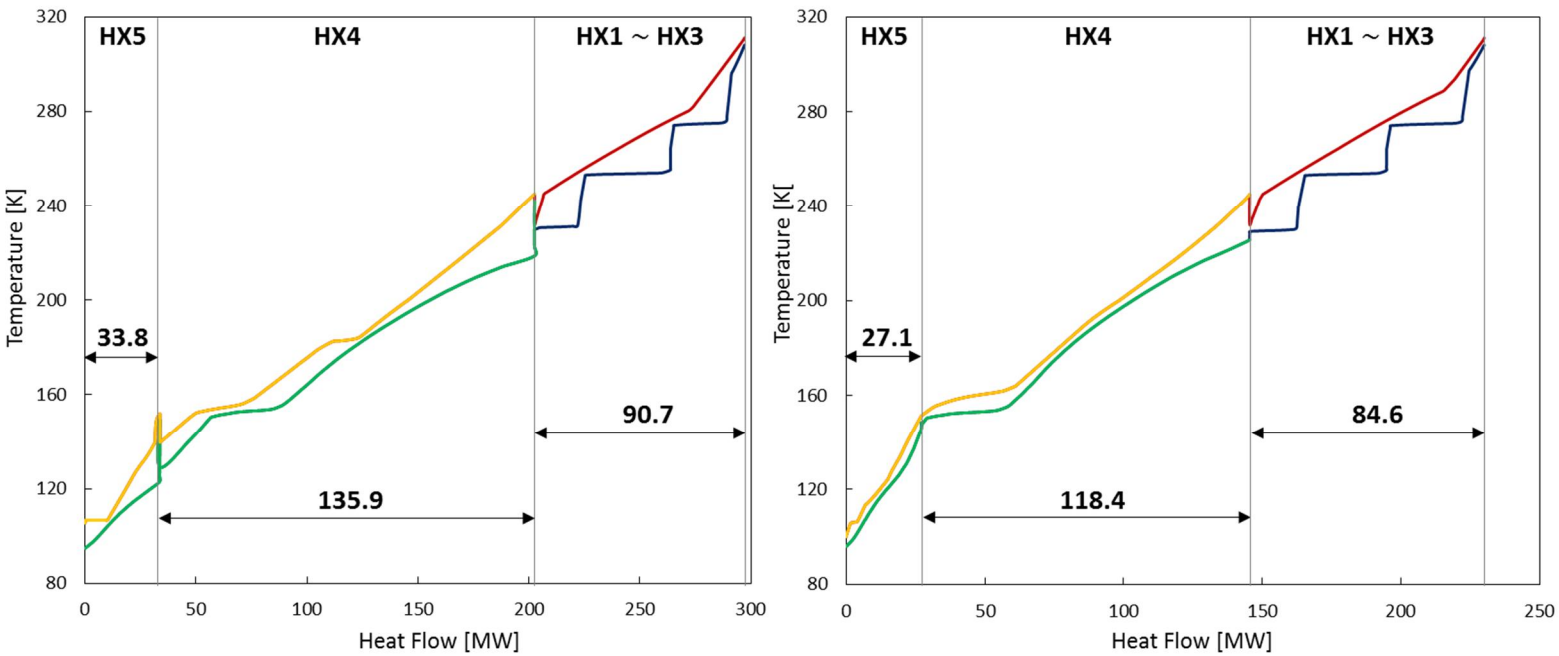

Figure 2-7. Grand composite curve of base (Left) and improved case (Right)

Table 2-8. Performance of heat exchangers in base and improved case

Parameter	Unit									
	HX1		HX2		HX3		HX4		HX5	
Case	B*	I*	B	I	B	I	B	I	B	I
LMTD [K] **	3.0	3.0	3.0	3.0	3.0	4.6	6.0	3.3	6.0	3.5
MTA [K]	3.0	3.0	3.0	3.0	3.0	3.0	3.0	3.0	3.0	3.0
Heat duty [MW]	32.0	33.9	39.8	30.8	18.9	19.9	135.9	118.4	33.8	27.1
ED [MW] ***	1.3	1.2	2.2	1.7	1.9	1.7	14.1	6.6	7.6	3.3
EE [%]***	95.9	96.3	94.5	94.6	91.9	91.6	91.6	94.4	77.6	87.8
Number of sides	5	5	5	5	5	5	11	10	6	6

* B; Base case; I: Improved case

** LMTD: Log mean temperature difference

*** ED: Exergy destruction, EE: Exergy Efficiency

The performances of other process components of compressors and expanders are summarized in Table 2-9, and the components exergy destructions and efficiencies of each case are compared in Figure 2-8. With less heat flow in overall heat transfer, all refrigerant compressors consume less power as can be seen in Table 2-9 especially for those of mixed refrigerant (C5, C6) in Figure 2-8. LNG stream compressor, C4, exceptionally requires more power consumption as it makes its discharge stream enter the supercritical region for eliminating the horizontal line occurring during refrigeration. But this increase occupies a small percentage of total power consumption of compressors.

Table 2-9. Performance of compressors and expanders in base and improved case

Unit	Pressure ratio		Eff [%] **		Power[MW]		E.D [MW]***		E.E [%]***	
	B*	I*	B	I	B	I	B	I	B	I
C1	2.65	2.65	76.42	76.35	3.35	2.68	0.96	0.87	70.8	70.9
C2	2.01	2.01	76.04	76.08	7.31	6.15	2.29	1.84	71.4	71.5
C3	2.85	2.85	76.76	76.71	22.92	19.56	6.38	5.59	72.9	72.9
C4	3.00	6.74	78.42	79.04	6.29	12.25	2.32	4.25	65.7	68.3
C5	6.94	7.37	78.98	78.99	61.61	41.18	15.90	12.54	70.9	71.7
C6	1.91	1.68	76.46	76.19	24.43	11.83	10.10	3.31	74.0	73.5
Ex1	0.41	0.41	73.59	73.59	-1.49	-1.68	0.88	0.99	47.1	47.1

* B; Base case; I: Improved case

** Polytropic efficiency (Adiabatic efficiency = 75%)

*** E.D: Exergy destruction, E.E: Exergy efficiency

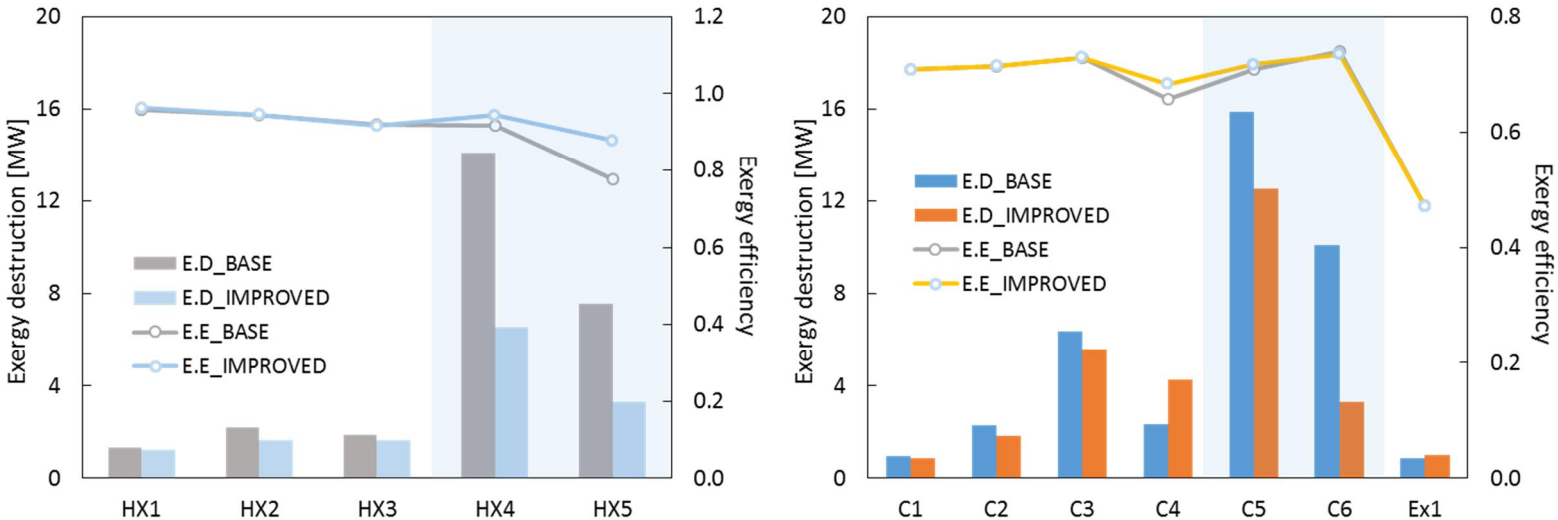

Figure 2-8. Component exergy destruction and exergy efficiency of base and improved case

(Left: Heat exchangers, Right: Compressors and an expander)

In the aspect of overall exergy destructions in Figure 2-9, the percentage of useful effect equivalent to the overall process/cycle exergy efficiency in Table 2-10 increases from 28.1% to 35.0% with a large decrease in exergy losses of heat exchangers from 20.2% to 14.7%. For compressors and valves in the pie graphs, however, the exergy destructions of improved case seem to slightly increase from base case, the absolute values of irreversibility decrease by 24.3% from 38.8MW to 29.39MW and by 21.1% from 15.22MW to 12.01MW respectively as the total irreversibility of process also decreases by 33.2% from 95.97MW to 64.09MW after improvement.

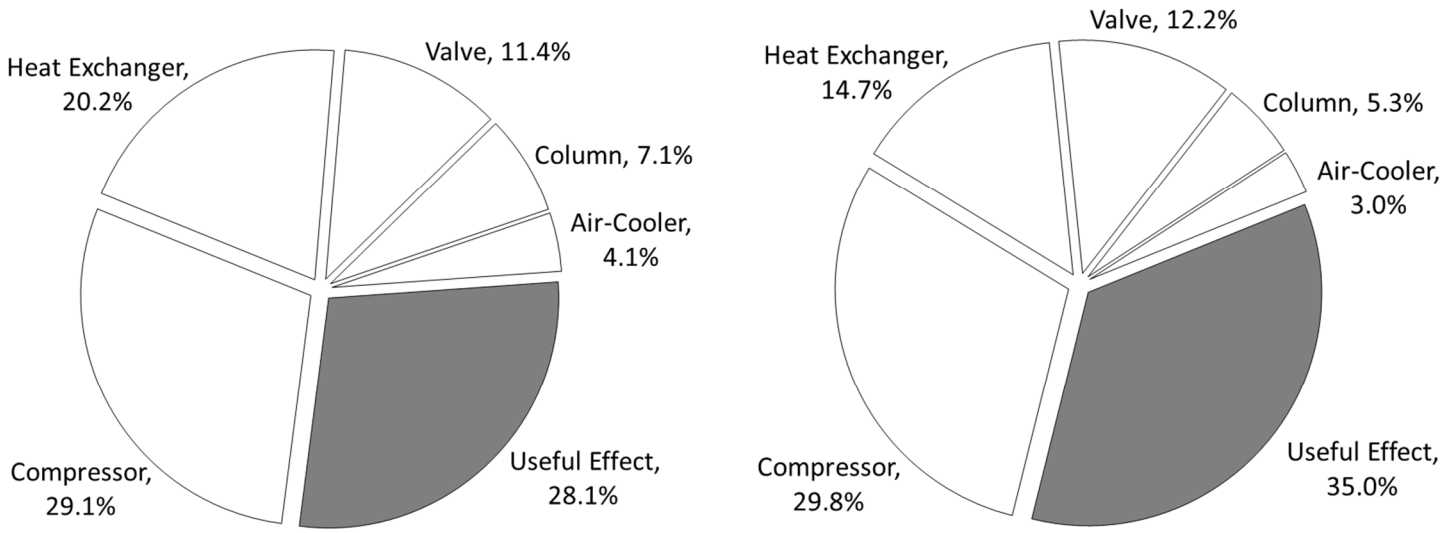

Figure 2-9. Overall exergy destruction of base (Left) and improved cases (Right)

Table 2-10. Component exergy destructions and power consumption in base and improved case

Unit	Exergy Destruction[MW]			Power Consumption[MW]			Exergy Efficiency	
	B*	I*	Δ[%]	B	I	Δ[%]	B	I
Air cooler	5.48	2.98	-45.5	0.39	0.32	-17.9		
Column	9.42	5.25	-44.3	-	-	-		
Compressor & Expander	38.82	29.39	-24.3	124.41	91.96	-26.1		
Heat exchanger	27.03	14.47	-46.5	-	-	-		
Valve	15.22	12.01	-21.1	-	-	-		
Total	95.97	64.09	-33.2	124.8	92.28	-26.1	0.281	0.350

* B; Base case; I: Improved case

Especially for the columns of which the irreversibility decreases largely by 44.3%, calculation of exergy destruction of each tray in NRU column, T200, is summarized and compared in Figure 2-10 and Table 2-11 for base and improved case where the tray number of feed location is five.

As the nitrogen is completely separated from the methane rich feed stream with less than 1mol% hydrocarbons in NRU column, the exergy destruction mainly occurs in the rectifying section as can be seen in Figure 2-10. The differences in the separation between two cases are the existence of vapor side stream in the rectifying section and the vapor fraction of feed stream after pressure drop and partial condensation of NGL column overhead, all of which are induced by structural modifications.

Through controlling the flowrate and temperature of the vapor side stream added to the rectifying section in optimization and lowering the vapor fraction of feed stream from 0.24 to 0.08 by two-stage depressurization of NGL column overhead, the separation efficiency of NRU column increases with less amount of reflux stream at the top and even thermodynamic equilibrium for each tray.

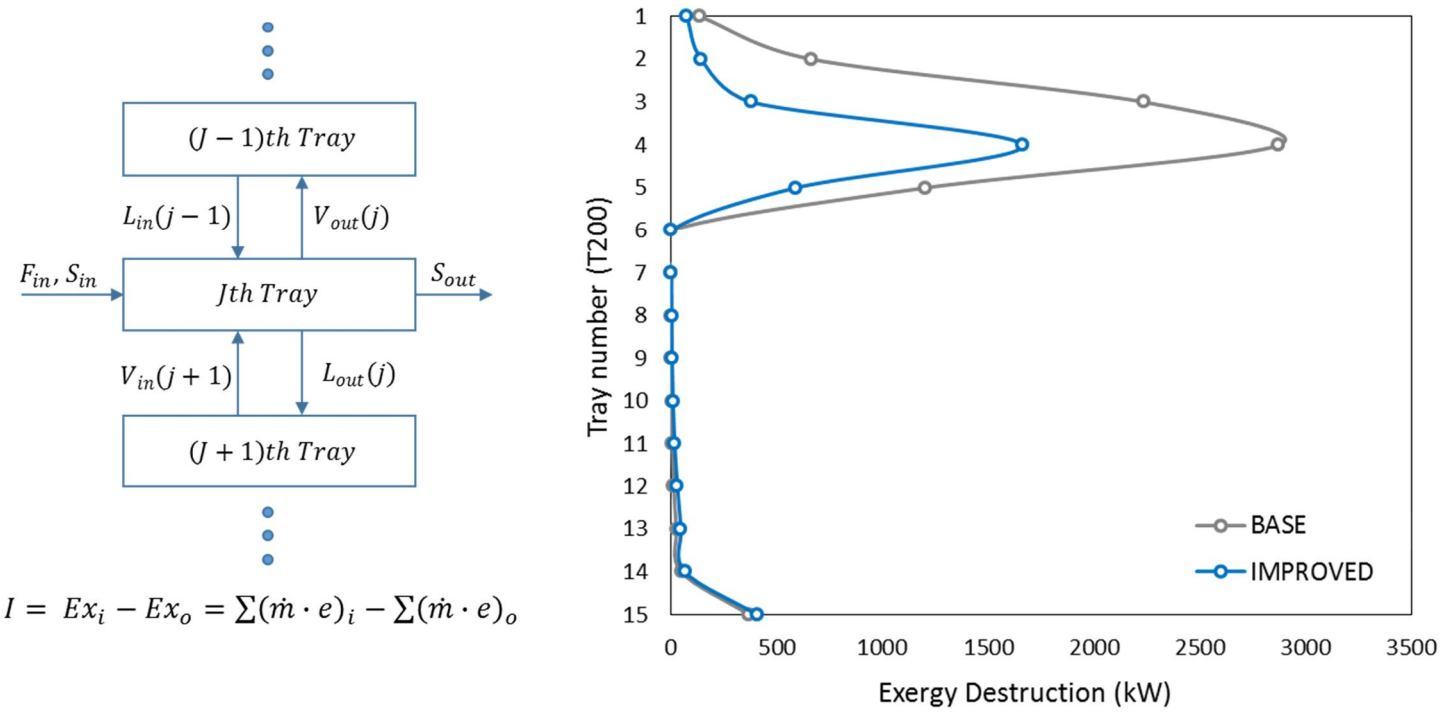

Figure 2-10. Exergy destruction in column T200 of base and improved case

Table 2-11. Column (T200) exergy destruction of each tray of base and improved case

Tray number	Exergy Destruction [kW]			Δ/BASE_TOTAL [%]
	BASE	IMPROVED	Δ	
1	137.35	76.19	-61.16	-0.80
2	666.72	144.78	-521.94	-6.86
3	2238.27	383.47	-1854.80	-24.39
4	2874.30	1663.36	-1210.95	-15.92
5	1203.14	590.96	-612.18	-8.05
6	2.45	3.13	0.68	0.01
7	2.53	3.68	1.16	0.01
8	2.74	4.48	1.74	0.02
9	3.27	6.56	3.29	0.04
10	4.57	11.36	6.79	0.09
11	7.61	18.85	11.25	0.15
12	14.20	31.81	17.60	0.23
13	27.20	48.99	21.80	0.29
14	50.33	67.35	17.03	0.22
15	371.25	408.12	36.87	0.48
Total	7605.93	3463.09	-4142.84	-54.47

Compared with two base cases, one for the reference case and the other for optimized one, the equipment power consumption and specific power of improved case are summarized in Table 2-12.

With same feed gas and products, improved case has lower power consumption especially in operating the MR cycle resulting in the specific power of 0.482kWH/kg_LNG lower by 26.2% than that of base case of 0.653kWH/kg_LNG. The small differences in product quantities come from slightly different products compositions like 0.990mol% N2 in purge N2 stream for improved case which is constrained in optimization and that of 0.997mol% for reference base case.

Table 2-12. Equipment power consumption and specific power of each case of integrated NRU

Component		Power Consumption [MW] BASE (Ghorbani [14])	BASE (OPTIM)	IMPROVED (OPTIM)
Compressors and Expanders	C1	2.44	3.35	2.68
	C2	9.05	7.31	6.15
	C3	21.08	22.92	19.55
	C4	3.00	6.29	12.25
	C5	72.15	61.61	41.18
	C6	18.66	24.43	11.83
	Ex1	-1.67	-1.49	-1.68
Air coolers	AC1	0.68	0.28	0.25
	AC2	0.04	0.04	0.04
	AC3	0.07	0.07	0.04
Mass flows [kg/h]	Feed	305227	305227	305227
	LNG	191449	191037	191291
	NGL	96082	95999	95746
	N2	17695	18190	18188
Specific power [kWH/kg_LNG]		0.656	0.653	0.482

2.4. Alternative Process Design and Optimization

2.4.1. Standalone NRU

In designing an optimal process aiming the lowest specific power with minimum power consumption producing specified products, the configuration of a standalone NRU simplified in Figure 2-11 where the nitrogen removal is located “after” the liquefaction section could be proposed as a competitive alternative design. As the heat transfer network for required nitrogen separation in that structure would be optimized independently apart from other sections of NGL recovery and NG liquefaction, it could possibly lead the optimization to a better point at the expense of the increased number of process components.

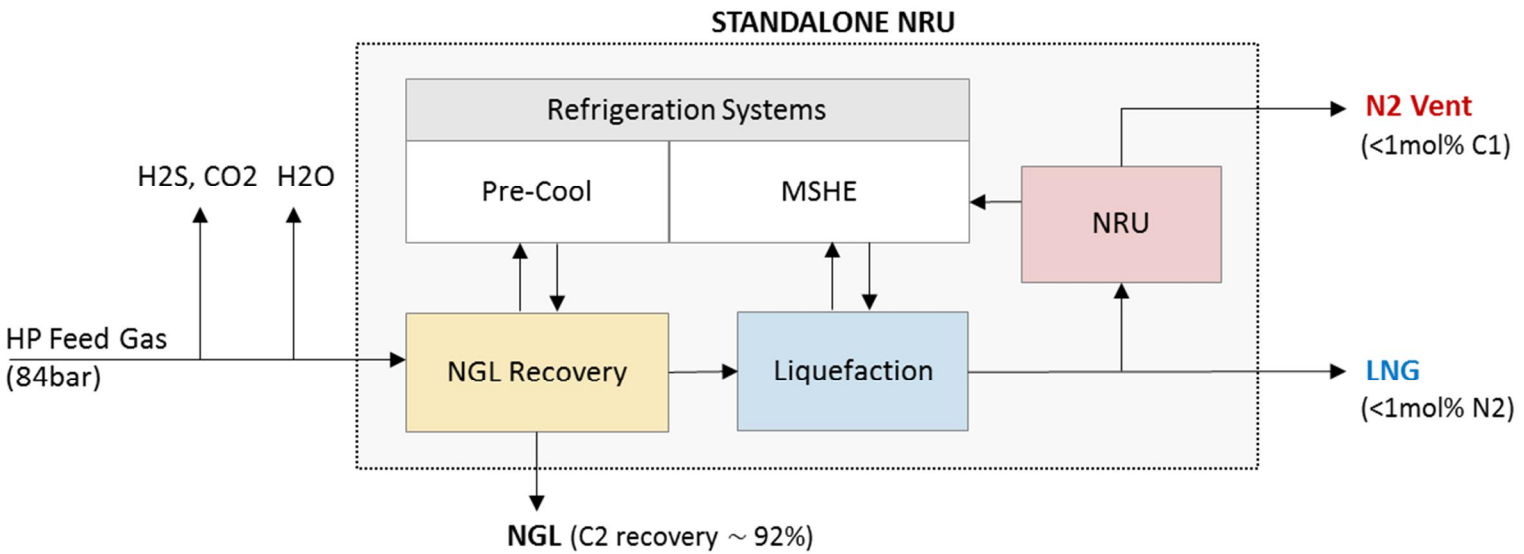

Figure 2-11. Block flow diagram of standalone NRU

Two possible configurations of the standalone NRU are shown in Figure 2-12, one for using an end-flash drum at blue node of separation structure ($\alpha_{N2} > 0.9,\ \alpha_{C1}$: high) in Figure 2-1 and the other for using a stripping column with higher methane recovery at the same node ($\alpha_{N2} > 0.9,\ \alpha_{C1}$: low).

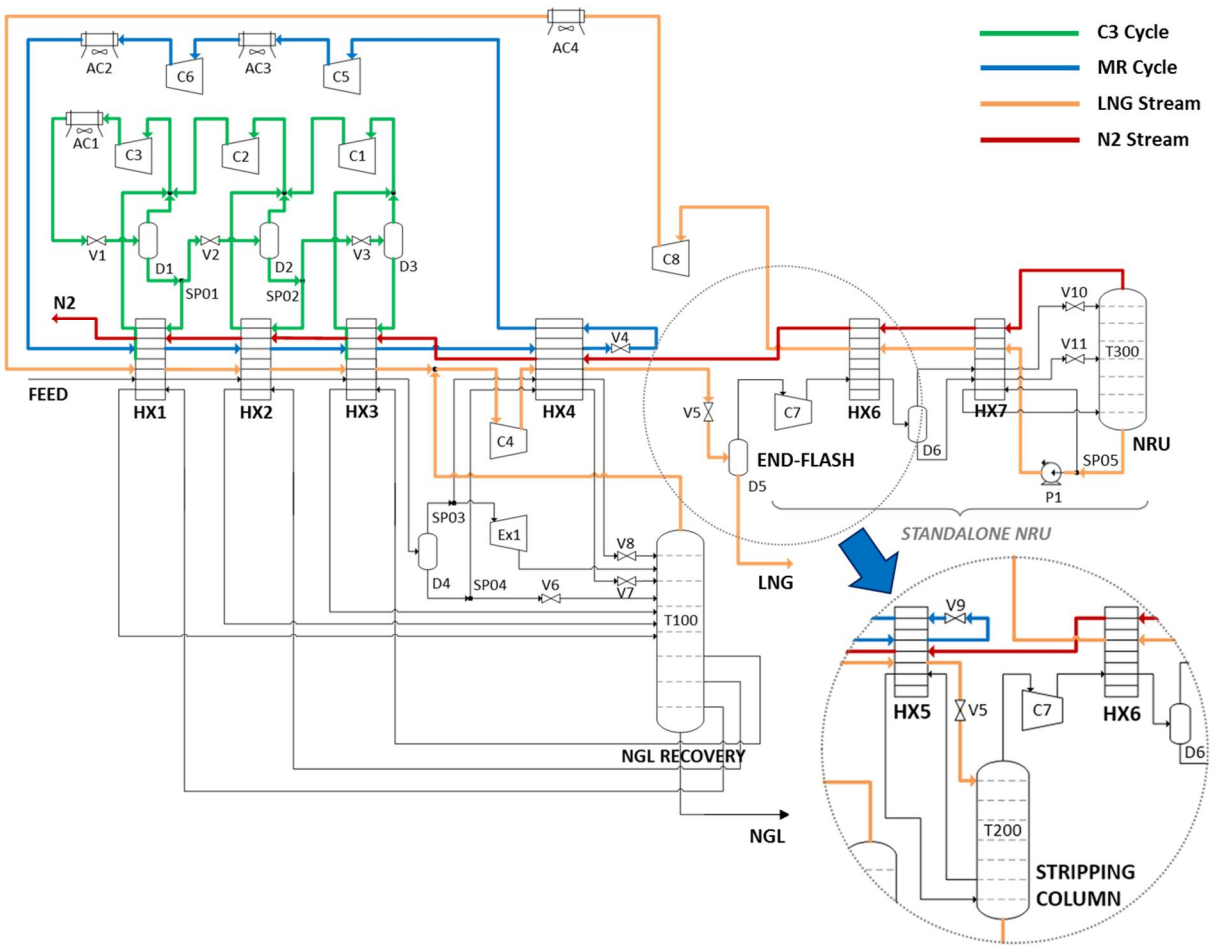

Figure 2-12. Process flow diagram of standalone NRU

Both options have similar process schemes to that of integrated one with a C3-MR cycle for the refrigeration system and the GSP unit in recovering NGL from feed gas.

For nitrogen removal, however, there are two significant differences in heat and mass transfer due to different structures. Firstly, the heat transfer networks of both standalone options are more intuitive as the cold heat necessary for cryogenic nitrogen separation could be supplied by itself in additional HX6 and HX7, not from the refrigeration system. Reminding that the main issue in optimization of integrated one was to match the horizontal lines at different temperatures in composite curves, this self-supply of cold heat could increase the thermodynamic efficiency of overall heat transfer as the feed and product streams of NRU column which have similar compositions transfer the latent heat with each other. Also as the mixed refrigerant could focus only on liquefying the LNG stream in HX4 and HX5, determining optimal conditions of the refrigerant could be easier.

Secondly, the requirement of separation in the NRU column differs from that of integrated one in that standalone option only needs to meet the minimum hydrocarbon content in purge nitrogen stream in the separation which is equivalent to the purity of nitrogen product. In integrated NRU, the NRU column should meet the specifications of not only the purity of purge nitrogen stream but also the nitrogen recovery higher than 85% as the separation of nitrogen should be completed at this single NRU column. Standalone NRU, however, could recycle the remaining hydrocarbons with unseparated nitrogen to the main process until it satisfies the required flowrate of purge nitrogen stream so that the NRU column does not need to recover nitrogen to a high level. This could make the heat and mass

transfer in NRU section simpler as shown in the process flowsheet of Figure 2-12 where the NRU column takes the form of a stripping column without reflux condensation, and also in the composite curves of that section and the exergy analysis of NRU column in Figure 2-13, all of which results from the optimization which will be described in the later section. The hot and cold stream curves in the composite curve at HX6 and HX7 adhere to each other as expected above.

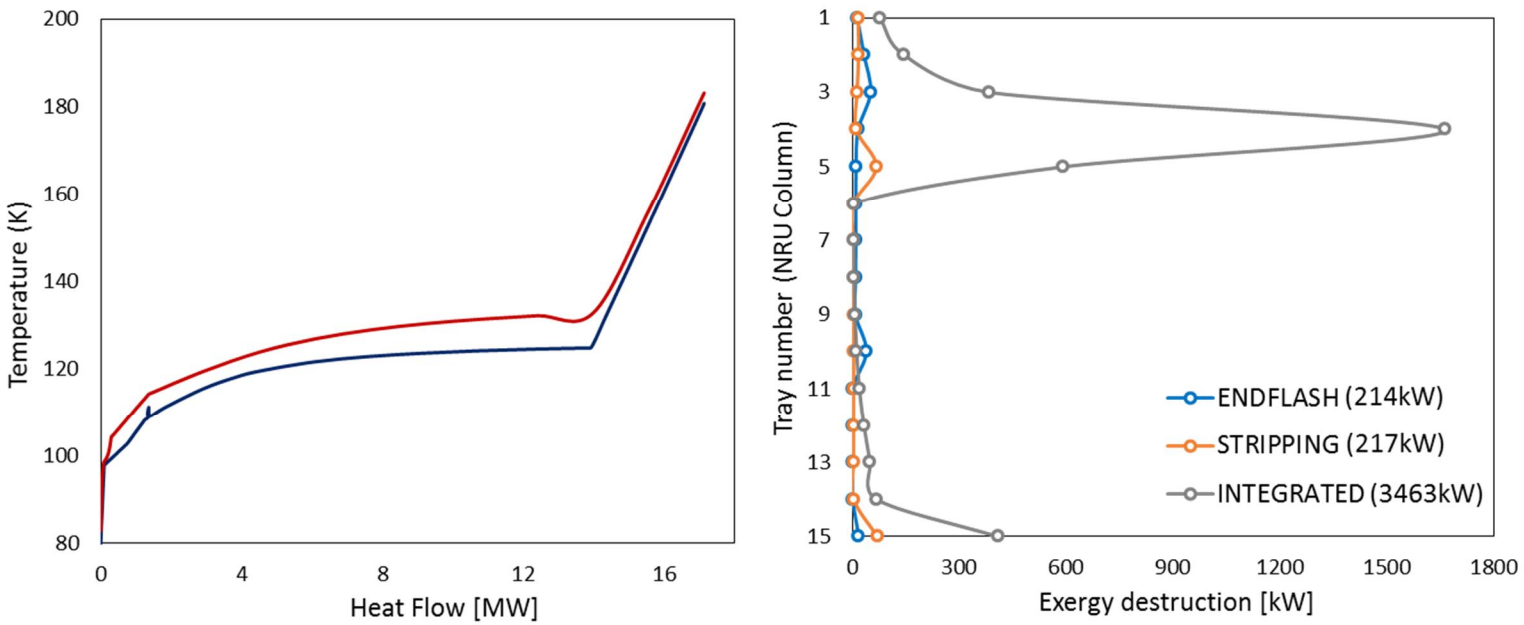

Figure 2-13. Composite curves in NRU section of standalone (end-flash) option (Left) and exergy destructions of each tray in NRU column for three different options (Right)

Additionally, for the natural gas liquefaction, the necessity of sub-cooling LNG stream in HX5 needs to be considered, which makes the liquefied LNG stream remain still as a liquid without producing fuel gas even after expanded to 1bar at V5. In the standalone NRU, however, as nitrogen is separated in two-stage and methane loss to vapor stream in the first separation node is inevitable, HX5 could be omitted like the end-flash option in Figure 2-12. Brief comparison for this consideration after optimization is summarized in Figure 2-14, which shows that the elimination of HX5 lowers the total heat flow in HX4 and HX5 by 28.0% from 120.2MW to 86.6MW and total irreversibility by 10.2% from 71.1MW to 63.8MW, resulting in lower specific power of 0.454kWH/kg_LNG which is 8.9% less than that with HX5 of 0.498kWH/kg_LNG in the standalone NRU using an end-flash drum. For stripping column option in Figure 2-12, however, HX5 should exist due to the necessary heat input to the bottom stage of the column for boiling up the nitrogen to the upper stages for purifying the product LNG.

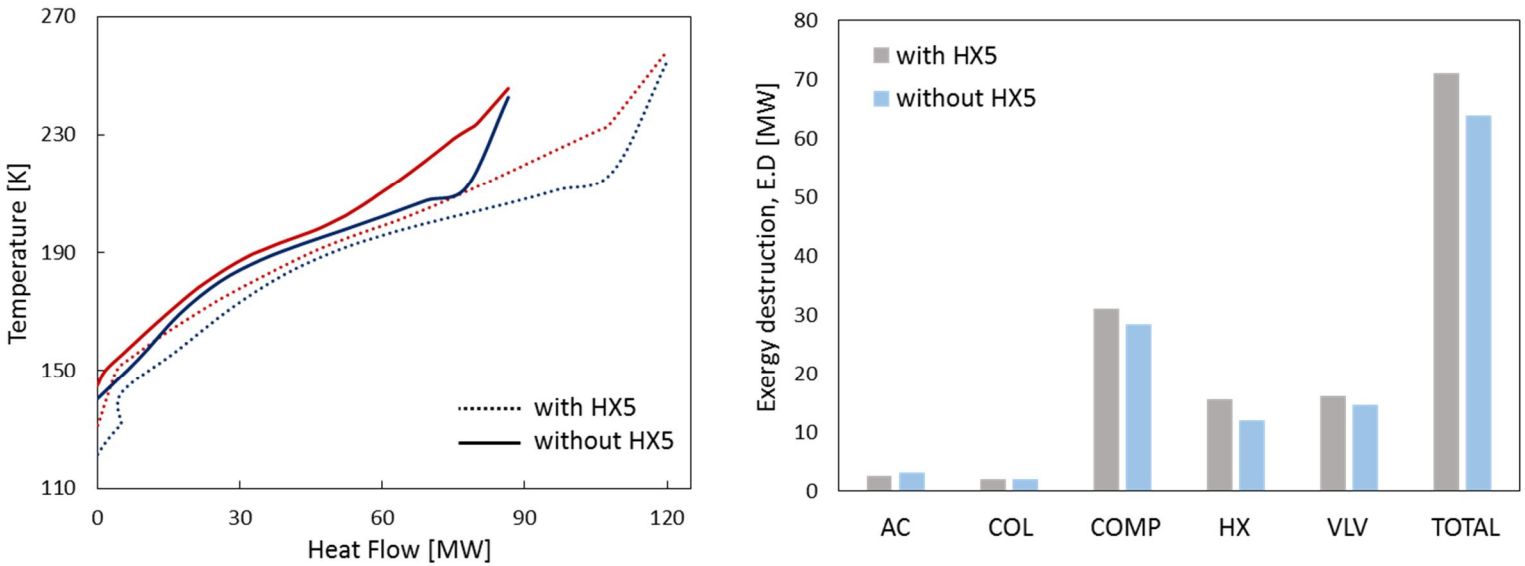

Figure 2-14. Comparison of composite curves (Left) and component exergy destructions (Right) with and without HX5 in end-flash drum option of standalone nitrogen recovery unit

2.4.2. Optimization of Standalone NRU

With different heat and mass transfer structures of standalone NRU schemes, control variables of each end-flash and stripping option are adjusted as given in Table 2-13 from those of base case optimization of integrated one in Table 2-3. All control variables related to the NRU section of integrated NRU are replaced by following variables in Table 2-13 with different nitrogen removal schemes.

For both end-flash and stripping options, outlet pressure at C7 (C7_outlet_P) from 1bar of LNG production pressure, degree of partial condensation of NRU feed at HX6 (D6_inlet_VF), chilling temperature at HX7 for cold reflux at the top of NRU column (V10_inlet_T), and degree of reboiling by SP05 split ratio (SP_05_flowratio) and outlet temperature at HX7 (NRU_reboil_HX7_VF) are controlled in optimization.

Especially for the stripping option, the liquid side stream flowrate in the stripping column (T200_side_F), and the degree of partial vaporization of that stream determined from the outlet temperature at HX5 (T200_side_outlet_T) are added with HX5 and T200 which do not exist in end-flash one. The optimization results of all control variables for each option are listed in Table 2-14 and Table 2-15.

Table 2-13. Changes in control variables in optimization of standalone NRU

Control variables		Annotations	ENDFLASH	STRIPPING
NRU	All variables of integrated NRU		Delete	Delete
	T200 liquid side flowrate	T200_side_F	-	Add
	T200 liquid side temperature	T200_side_outlet_T	-	Add
	C7 outlet pressure	C7_outlet_P	Add	Add
	T300 feed vapor fraction	D6_inlet_VF	Add	Add
	T300 cold reflux temperature	V10_inlet_T	Add	Add
	T300 reboiling ratio	SP05_flowratio	Add	Add
	T300 reboiling vapor fraction	NRU_reboil_HX7_VF	Add	Add
	P1 pressure ratio	P1_P_ratio	Add	Add

Table 2-14. Optimization results of end-flash option in standalone NRU

Subsections	Control Variables	Optimal value	Initial value	Lower bound	Upper bound
LNG Production	SP03_HX4_outlet_T	178.18	181.15	175.00	185.00
	SP03_flowratio	0.68	0.60	0.50	0.70
	T100_side_F	2713	2700	2650	2750
	C4_outlet_P	59.03	60.00	40.00	80.00
	V5_inlet_T	150.01	148.68	155.00	145.00
	C7_outlet_P	5.50	5.00	3.00	10.00
NRU	D6_inlet_VF	0.05	0.10	0.01	0.15
	V10_inlet_T	82.86	80.00	75.00	85.00
	SP05_flowratio	0.84	0.50	0.10	0.90
	NRU_reboil_HX7_VF	0.11	0.10	0.05	0.20
	P1_P_ratio	2.01	1.50	1.00	3.00
C3 Cycle	C3_cycle_F	22598	20000	15000	25000
	SP01_flowratio	0.30	0.20	0.10	0.50
	SP02_flowratio	0.58	0.63	0.30	0.80
	V1_outlet_P	5.02	5.00	4.50	5.50
	V2_outlet_P	2.50	2.50	2.00	3.00
	V3_outlet_P	0.94	1.00	0.50	1.50
MR Cycle	MR_F_N2	0.01	5000	1E-6	10000
	MR_F_C1	4456	10000	1000	15000
	MR_F_C2	9372	10000	1000	15000
	MR_F_C3	2677	5000	1E-6	10000
	C6_outlet_P	28.91	30.0	15.0	45.0
	V4_outlet_P	1.98	2.00	1.00	3.00
	MR_HX4_outlet_T	144.79	151.44	140.00	160.00

Table 2-15. Optimization results of stripping option in standalone NRU

Subsections	Control Variables	Optimal value	Initial value	Lower bound	Upper bound
LNG Production	SP03_HX4_outlet_T	174.99	181.15	170.00	190.00
	SP03_flowratio	0.69	0.60	0.50	0.75
	T100_side_F	2699	2700	2650	2750
	C4_outlet_P	51.57	60.00	40.00	80.00
	V5_inlet_T	119.18	115.00	105.00	130.00
	T200_side_F	1315	10000	1E-6	15000
	T200_side_outlet_T	111.19	109.27	105.00	115.00
NRU	C7_outlet_P	12.18	10.00	5.00	15.00
	D6_inlet_VF	0.04	0.05	0.01	0.10
	V10_inlet_T	82.86	80.00	75.00	85.00
	SP05_flowratio	0.65	0.60	0.40	0.80
	NRU_reboil_HX7_VF	0.25	0.20	0.10	0.40
C3 Cycle	P1_P_ratio	3.51	2.00	1.00	5.00
	C3_cycle_F	21250	27000	15000	35000
	SP01_flowratio	0.21	0.48	0.10	0.60
	SP02_flowratio	0.57	0.63	0.50.	0.70
	V1_outlet_P	5.02	5.00	4.50	5.50
	V2_outlet_P	2.50	2.50	2.00	3.00
	V3_outlet_P	0.94	1.00	0.50	1.50
MR Cycle	MR_F_N2	151	1000	1E-6	5000
	MR_F_C1	6661	10000	1000	15000
	MR_F_C2	9775	10000	1000	15000
	MR_F_C3	1999	3000	1E-6	5000
	C6_outlet_P	33.26	40.00	30.00	50.00
	V4_outlet_P	2.39	2.00	1.00	3.00
	MR_HX4_outlet_T	148.47	151.44	140.00	160.00
	MR_HX5_outlet_T	109.82	105.00	90.00	120.00

2.4.3. Comparison between End-flash and Stripping Options

Difference in Material Balances

After optimization of both solutions, the major stream data with product LNG and purge nitrogen stream are listed in Table 2-16. LIQUEFAC is the LNG stream between heat exchangers for liquefaction and the expansion valve of V5. NRU FEED is the feed stream to NRU section after the end-flash drum (D5) or stripping column (T200) before compression at C7. RECYCLE comes from NRU column (T300) bottoms which would be recycled to the main liquefaction process merging with NGL column (T100) overhead before compression at C4.

Table 2-16. Major stream data in standalone NRU

	ENDFLASH			STRIPPING			BOTH	
	LIQUEFAC	NRU FEED	RECYCLE	LIQUEFAC	NRU FEED	RECYCLE	LNG	N2
Pressure [bar]	59.03	1.00	25.00	51.57	1.00	25.00	1.00	1.08
Temperature [K]	150.01	108.83	335.70	119.18	105.17	340.33	108.83	293.15
Flowrate [kg/s]	84.73	31.64	26.59	66.84	13.75	8.69	53.10	5.05
Flowrate [kmol/h]	17880	6138	5486	14071	2329	1677	11742	652
Molar composition								
N2	0.0786	0.2099	0.1174	0.0802	0.4346	0.2190	0.0100	0.9900
C1	0.9169	0.7901	0.8826	0.9141	0.5654	0.7810	0.9832	0.0100
C2	0.0036	0.0000	0.0000	0.0045	0.0000	0.0000	0.0054	0.0000
C3	0.0002	0.0000	0.0000	0.0003	0.0000	0.0000	0.0003	0.0000
nC4	0.0000	0.0000	0.0000	0.0000	0.0000	0.0000	0.0000	0.0000
CO2	0.0006	0.0000	0.0000	0.0009	0.0000	0.0000	0.0011	0.0000

As can be seen in Table 2-16, flowrates of all three streams related to NRU section of stripping option are much lower than those of end-flash one as the stripping column recovers more methane to product LNG which would lower the loads for separation of nitrogen in NRU section with less NRU FEED and liquefaction of LNG stream with less RECYCLE. Also the methane content of 56.5mol% in NRU FEED is much lower than that of end-flash one of 79.0% resulting in different mass transfer in NRU column as summarized in Table 2-17 and associated exergy destructions in the right graph in Figure 2-13. With more nitrogen content in NRU FEED of stripping option, the feed stream is located in lower stage of 10 than that of end-flash one of 5 with higher nitrogen recovery at the top vapor product and larger reboiling duty in producing same amount of purge nitrogen stream. But this amount of heat in reboiling is far less than that of feed condensation so that it's effect to the overall heat transfer in NRU section could be ignored. The temperature of LIQUEFAC stream of stripping option is around 30 degree below than that of end-flash one as the former sub-cools that stream at HX5 not existing in the latter, which lowers the irreversibility occurring in isenthalpic expansion from high pressure of 50~60 bar to 1bar at V5.

Table 2-17. Performance of NRU column in standalone NRU

NRU Column	Unit	ENDFLASH	STRIPPING
Number of stages		15	15
Feed stage		5	10
Top/bottom pressure	bar	1.08/1.50	1.08/1.50
Feed outlet pressure at C7	bar	5.50	10.33
Feed vapor fraction	mol/mol	0.038	0.034
Overhead to feed ratio	mol/mol	0.090	0.202
Bottoms to feed ratio	mol/mol	0.910	0.798
N2 recovery at the top		0.456	0.534
C1 recovey at the bottoms		0.999	0.997
Reboiling ratio	mol/mol	0.012	0.065
Reboiling duty	kW	202.82	374.41

Difference in Exergy Balance

In the composite curves of main liquefaction section before NRU in Figure 2-15, total heat flow of stripping option is slightly less than that of end-flash one even with a broader temperature range from 311.15K to 106.72K due to additional heat transfer at HX5. This is caused by less refrigeration load in the pre-cooling section with less RECYCLE in stripping option.

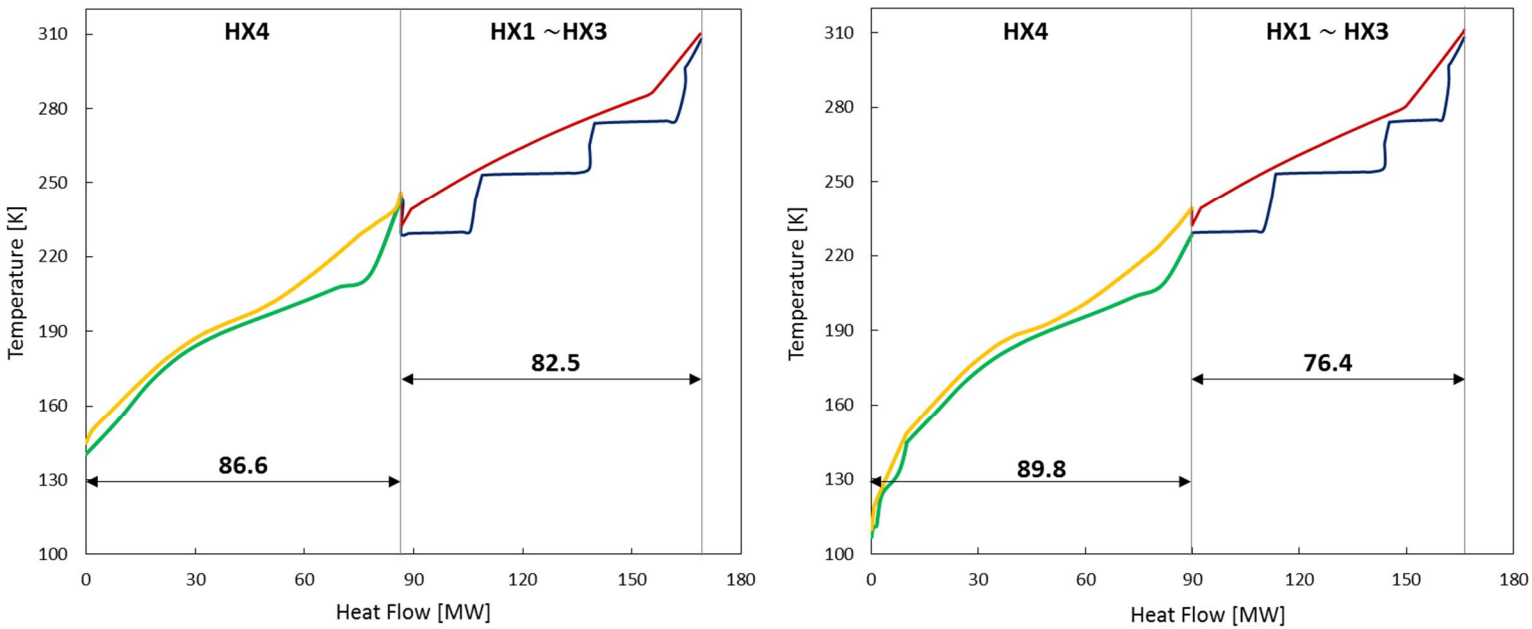

Figure 2-15. Composite curves without NRU section in end-flash (Left) and stripping options (Right)

Unlike this liquefaction section, a large difference in the amount of heat flow occurs in NRU section as can be shown in Figure 2-16. With less NRU FEED of 13.75kg/s in stripping option than that in end-flash option of 31.64kg/s, total heat flow of the former (6.6MW) is less than half of the latter (17.2MW). Especially at HX6, for similar degree of partial condensation of NRU FEED (vapor fractions of around 0.03 for both options) stripping one transfers heat (5.4MW) as much as one third of the end-flash one (15.8MW) at twice higher pressure at C7 of 10.33bar than that of the other of 5.50bar, the value determined in optimization. With higher pressure, less amount of latent heat is required for the same degree of condensation.

The performance of all heat exchangers are summarized in Table 2-18.

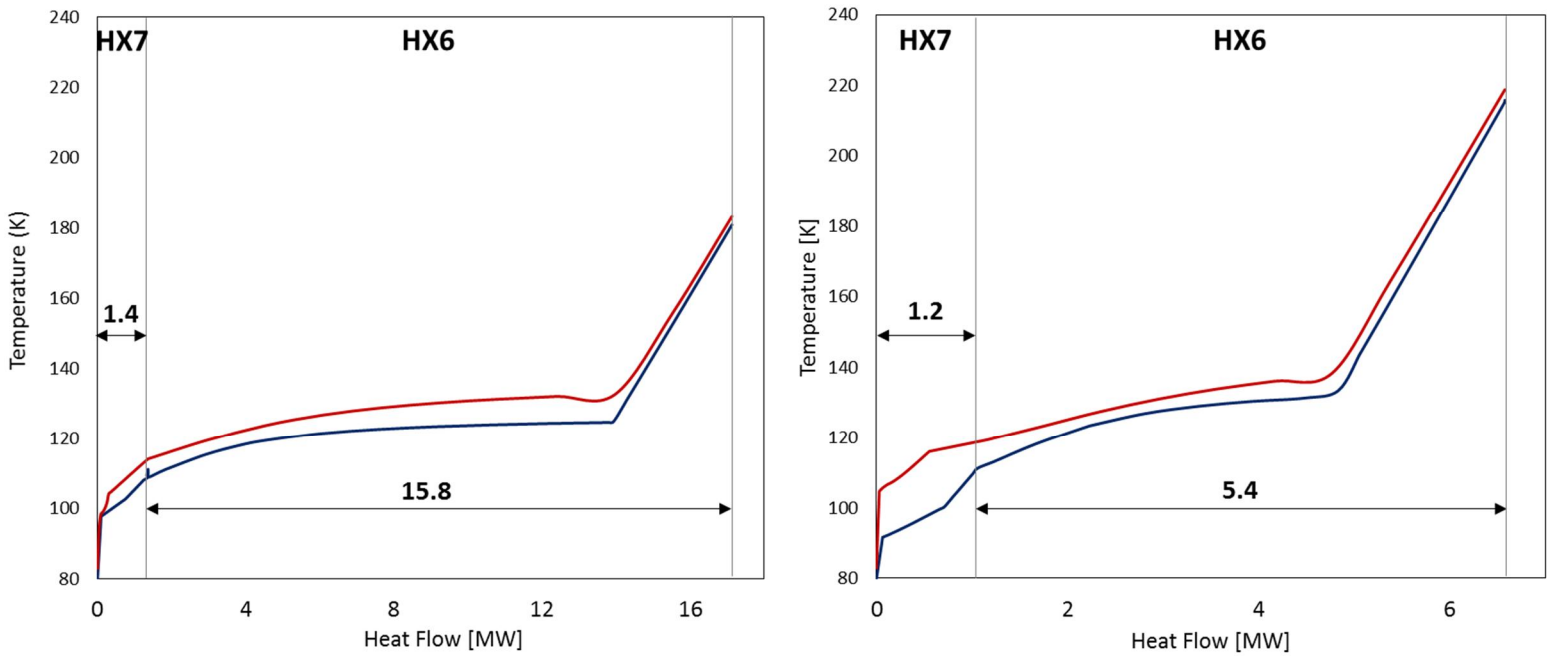

Figure 2-16. Composite curves of NRU section in end-flash (Left) and stripping options (Right)

Table 2-18. Performance of heat exchangers in end-flash and stripping options

Parameter	Unit													
	HX1		HX2		HX3		HX4		HX5		HX6		HX7	
Case	END*	STR*	END	STR	END	STR	END	STR	END	STR	END	STR	END	STR
LMTD [K] **	3.0	3.0	3.0	3.0	3.0	3.0	3.7	6.6	-	3.6	3.6	4.6	3.0	4.6
MTA [K]	3.0	3.0	3.0	3.0	3.0	3.0	3.0	3.0	-	3.0	3.0	3.0	3.0	3.0
Heat duty [MW]	29.3	21.0	30.9	31.9	22.3	23.5	86.6	80.0	-	9.8	1.4	5.4	15.8	1.2
ED [MW] ***	1.1	0.8	1.7	1.7	1.7	1.9	4.8	4.5	-	1.1	1.6	0.6	0.2	0.2
EE [%]***	96.2	96.0	94.5	94.5	92.2	91.8	94.4	94.4	-	88.5	90.0	89.6	87.0	61.6
Number of sides	5	5	5	5	5	5	6	6	-	4	3	3	5	5

* END: End-flash; STR: Stripping

** LMTD: Log mean temperature difference

*** ED: Exergy destruction, EE: Exergy Efficiency

From an overall exergy analysis in Figure 2-17 and Table 2-19, stripping option has less total irreversibility of 48.8MW than that of the other of 58.4MW consuming less total power of 81.4MW than 92.1MW resulting in higher exergy efficiency of 40.0% than 36.5%.

The performances of main components of compressors and valves occupying the majority of total exergy destructions are summarized in Table 2-20 and Table 2-21. In comparing each component of valves and compressors which largely differ in irreversibility for each option as in Table 2-19, exergy destruction of V5 which expands the LIQUEFAC stream to 1bar for producing LNG is lower for stripping option as much as one third of the value for end-flash one, which stands out remarkably in Figure 2-18. For compressors, NRU section components of C7 and C8 in stripping option have much lower irreversibility than that of end-flash one with less amount of NRU FEED.

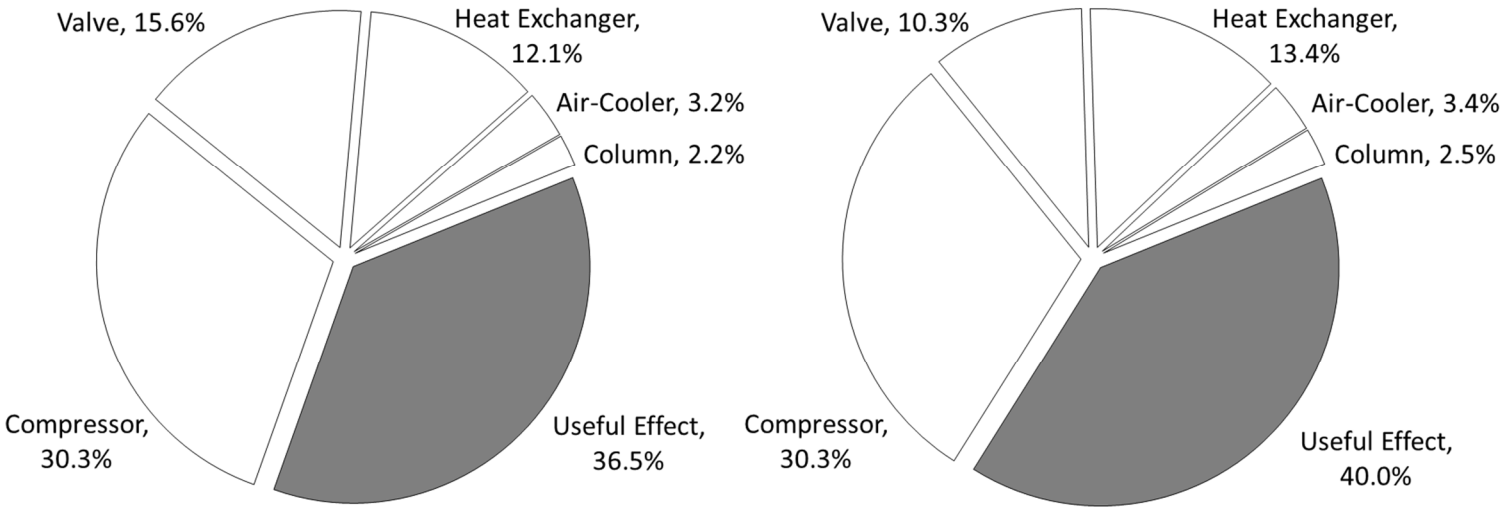

Figure 2-17. Overall exergy destruction of end-flash (Left) and stripping options (Right)

Table 2-19. Component exergy destructions and power consumption in end-flash and stripping options

Unit	Exergy Destruction[MW]			Power Consumption[MW]			Exergy Efficiency	
	END*	STR*	Δ[%]	END	STR	Δ[%]	END	STR
Air cooler	2.96	2.75	-7.1	0.31	0.30	-3.2		
Column	1.98	2.07	4.5	-	-	-		
Compressor & Expander	27.95	24.62	-11.9	91.78	81.07	-11.7		
Heat exchanger	11.15	10.94	-1.9	-	-	-		
Valve	14.40	8.41	-41.6	-	-	-		
Pump	0.01	0.01	0.0	0.01	0.01	0.0		
Total	58.44	48.79	-16.5	92.11	81.39	-11.6	0.37	0.40

* END: End-flash; STR: Stripping

Table 2-20. Performance of compressors and expanders in end-flash and stripping options

Unit	Pressure ratio		Eff [%] **		Power[MW]		E.D [MW]***		E.E [%]***	
	END*	STR*	END	STR	END	STR	END	STR	END	STR
C1	2.65	2.65	76.42	76.46	3.29	3.45	1.006	0.730	70.1	70.1
C2	2.01	2.01	76.07	76.08	6.53	6.81	1.950	2.728	71.1	71.1
C3	2.85	2.85	76.75	76.76	19.45	18.15	5.592	5.295	72.7	72.7
C4	2.36	2.06	77.69	77.36	7.81	4.48	2.708	1.621	67.5	66.1
C5	7.56	7.95	78.56	78.92	28.57	31.38	8.460	9.483	72.4	71.9
C6	1.93	1.75	76.35	76.23	9.71	9.24	2.705	2.580	73.5	73.5
C7	5.50	10.33	79.86	81.40	4.25	2.37	1.920	1.030	58.3	60.4
C8	8.33	4.76	80.25	79.08	8.31	2.07	2.719	0.643	70.0	71.2
Ex1	0.41	0.41	73.59	73.59	-1.52	-1.55	0.891	0.910	47.1	47.1

* END: End-flash; STR: Stripping

** Polytropic efficiency (Adiabatic efficiency = 75%)

*** E.D: Exergy destruction, E.E: Exergy efficiency

Table 2-21. Performance of valves in end-flash and stripping options

Unit	Pressure drop [bar]		E.D [MW]**		E.E [%]**	
	END*	STR*	END	STR	END	STR
V1	9.30	9.30	2.22	2.09	0.760	0.760
V2	2.50	2.50	0.44	0.47	0.917	0.917
V3	1.55	1.55	0.22	0.24	0.922	0.922
V4	26.92	30.87	1.42	1.34	0.950	0.943
V5	58.03	50.57	9.23	2.97	0.811	0.920
V6	37.59	37.59	0.20	0.20	0.538	0.538
V7	38.09	38.09	0.06	0.06	0.679	0.676
V8	38.09	38.09	0.41	0.37	0.821	0.830
V9	-	30.87	-	0.42	-	0.946
V10	4.42	9.25	0.00	0.00	0.982	0.975
V11	4.00	8.83	0.20	0.25	0.963	0.917

* END: End-flash; STR: Stripping

** E.D: Exergy destruction, E.E: Exergy efficiency

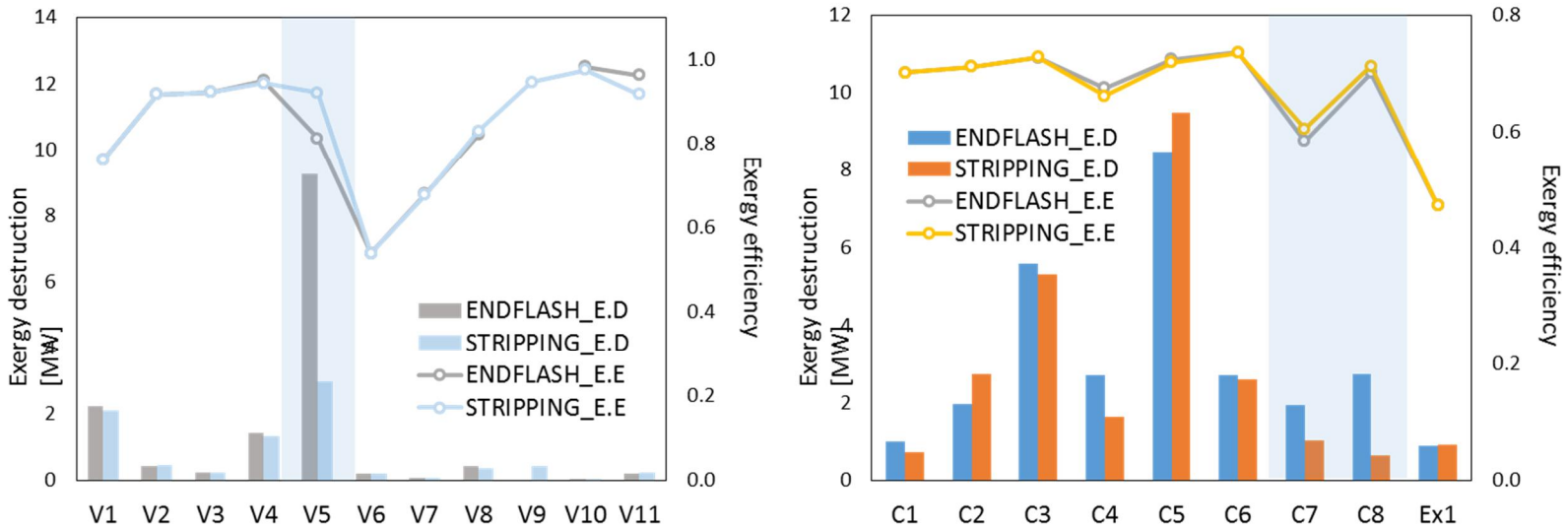

Figure 2-18. Component exergy destruction and exergy efficiency of end-flash and stripping options

(Left: Valves, Right: Compressors and an expander)

From base case improvement of integrated NRU to alternative design of standalone NRU, three NRU schemes proposed in this study are compared in Table 2-22 with respect to the performance of overall process in producing the same amount of products. Even the integrated NRU has been improved through structural modifications and optimization, the standalone solutions especially for the stripping option which uses a stripping column at the first nitrogen separation are better in thermodynamic efficiency with higher exergy efficiency and lower specific power.

Table 2-22. Equipment power consumption and specific power of each option of standalone NRU

Component		Power Consumption [MW]		
		INTEGRATED NRU	STANDALONE NRU	
		IMPROVED	END-FLASH	STRIPPING
Compressors and Expanders	C1	2.68	3.29	3.45
	C2	6.15	6.53	6.81
	C3	19.55	19.45	18.15
	C4	12.25	7.81	4.48
	C5	41.18	28.57	31.38
	C6	11.83	9.71	9.24
	C7	-	4.25	2.37
	C8	-	8.31	2.07
	Ex1	-1.68	-1.52	-1.55
Air coolers	AC1	0.25	0.25	0.24
	AC2	0.04	0.03	0.03
	AC3	0.04	0.03	0.03
	AC4	-	0.00	0.00
Mass flows [kg/h]	Feed	305227	305227	305227
	LNG	191291	191114	191147
	NGL	95746	95923	95891
	N2	18188	18190	18189
Process/cycle exergy efficiency [%]		35.0	36.5	40.0
Specific power [kWH/kg_LNG]		0.482	0.454	0.401

2.5. Varying Feed Composition and Optimization

In proposing several nitrogen recovery solutions including an improved design of integrated NRU and two alternative designs of standalone NRU, the nitrogen content in the feed gas has been set to be 5mol% according to the research of Ghorbani et al. [14]. At that feed composition, the stripping option of standalone NRU has the highest priority over other nitrogen recovery solutions in terms of overall process efficiency.

Feed gases routed from unconventional natural gas sources like several small-to-mid scale gas reservoirs or shale gas, however, are diverse in the component compositions especially for the nitrogen content. A comparative study would be performed in this chapter with respect to the nitrogen content in the feed gas from 5mol% to 20mol% for a conventional LNG process with all nitrogen solutions proposed before. The conventional LNG process selected in this study is the general co-production process of LNG and NGL without nitrogen recovery as is simplified in Figure 2-19, which has the form of standalone NRU configuration using an end-flash drum in Figure 2-12 minus the “standalone NRU” section. Performances of the conventional LNG process after optimization with respect to the nitrogen content are summarized in Table 2-23 and associated methane recovery and specific power are plotted in Figure 2-20.

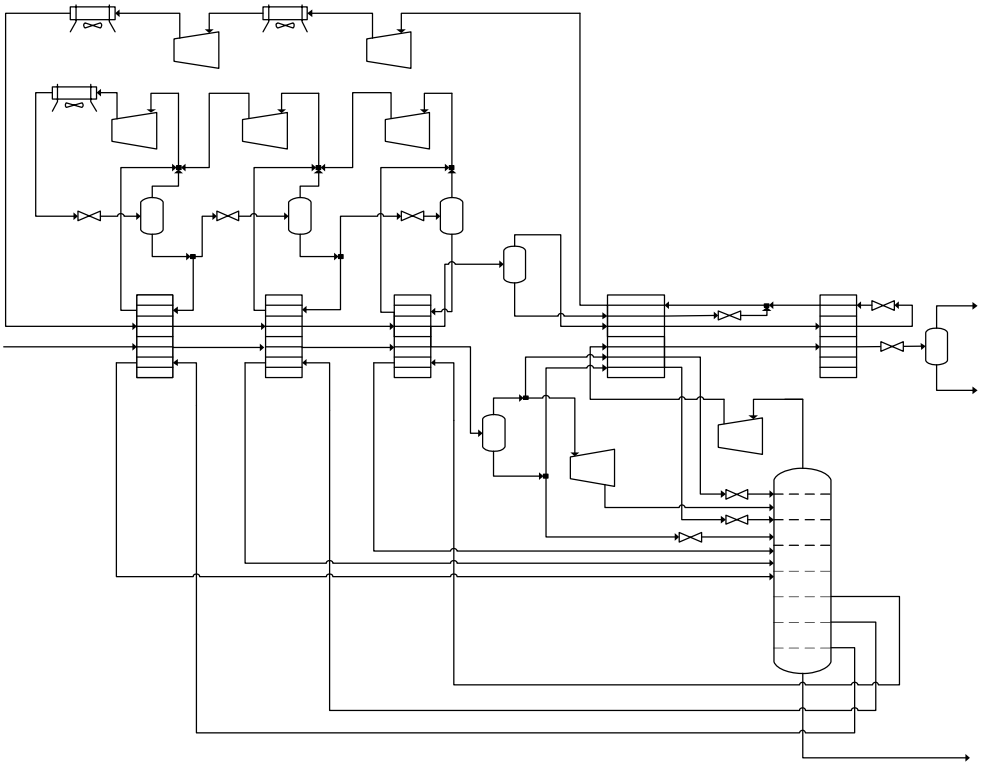

Figure 2-19. Simplified diagram of a conventional LNG process

Table 2-23. Performance of conventional LNG process without nitrogen recovery with respect to N2 content in feed gas

Conventional LNG process without NRU	N2 Content in feed gas [mol%]				
	0	5	10	15	20
LNG flowrate [kg/s]	52.14	41.66	29.33	15.04	4.35
C1 Recovery [%]	100	78.3	54.7	27.4	7.1
Power consumption [MW]	69.6	59.03	50.94	40.1	29.19
Specific power [kWH/kg_LNG]	0.371	0.394	0.482	0.740	1.863
Exergy destruction [MW]	40.58	39.26	42.74	45.39	45.86
Exergy efficiency [%]	41.7	33.5	16.1	-13.2	-57.1

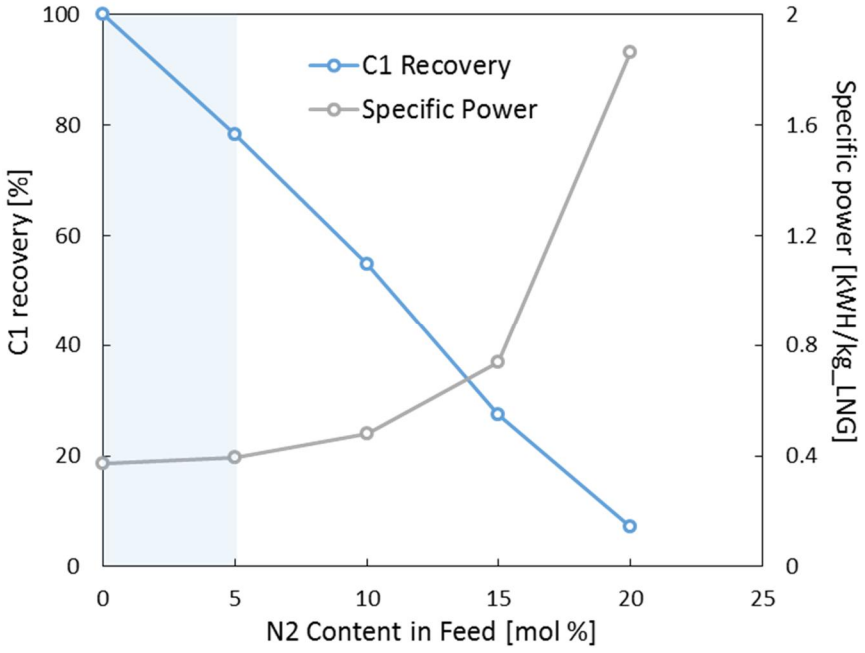

Figure 2-20. Specific power of conventional LNG process with respect to N2 content in feed gas

As the nitrogen content increases from 0mol% to 20mol%, the methane recovery decreases dramatically from 100% to 7.1% as only a single end-flash drum has to recover methane at 1bar, 108.8K in producing LNG where a large amount of methane is carried over with nitrogen to the fuel gas. Specific power until 5mol% of nitrogen (the blue region in Figure 2-20) has similar values with reasonable methane recovery of higher than 80% but it increases sharply after 5mol% with poor methane recovery due to much less amount of product LNG even with less power consumption from less amount of mixed refrigerants. Especially after 15mol% of nitrogen, the exergy efficiency has a negative value as the total exergy destruction value exceeds that of power consumption, which means the process after that point becomes unreasonable in the process/cycle exergy definition. These trends verify the need of nitrogen recovery in LNG production processes.

The performance of each nitrogen recovery solution is compared with each other in Table 2-24 and those values of specific power, irreversibility and exergy efficiency are plotted in Figure 2-21 and Figure 2-22. Methane recovery at each nitrogen content for all nitrogen recovery solutions is over 99.9%, and the product specifications like flowrate and composition are almost the same with each other as they are constrained in optimization. Only the flowrate of purge nitrogen differs with each nitrogen content in the feed gas.

In Figure 2-21, as the specific power of integrated NRU changes relatively more slowly with respect to nitrogen content than other solutions, there exist two intersection points between 5~10mol% and 15~20mol% where the design priority of nitrogen recovery switches.

Exergy destruction and efficiency in Figure 2-22 also have similar trends with that of specific power as these three parameters are all related to the thermodynamic efficiency of the overall process.

Table 2-24. Performance of each nitrogen recovery solution with respect to N2 content in feed gas

N2 [mol%]	Specific power [kWH/kg_LNG]			Exergy destruction [MW]			Exergy efficiency [%]		
	INTEGRATED	STANDALONE		INTEGRATED	STANDALONE		INTEGRATED	STANDALONE	
		END*	STR*		END	STR		END	STR
5	0.482	0.454	0.401	64.09	58.44	48.79	35.0	36.5	40.0
10	0.498	0.592	0.417	70.43	90.69	56.9	34.7	28.2	37.6
15	0.525	0.841	0.498	72.88	139.47	73.72	34.6	21.1	31.3
20	0.550	1.156	0.572	79.76	202.18	87.86	31.7	16.1	26.9

*END: End-flash, STR: Stripping option

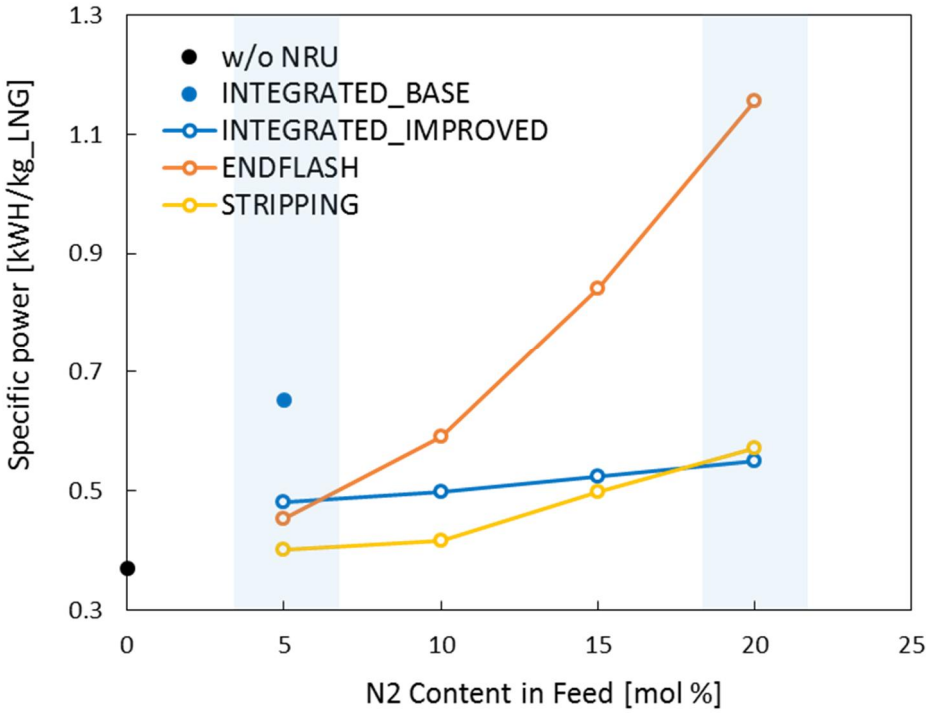

Figure 2-21. Specific power of each nitrogen recovery with respect to N2 content in the feed gas

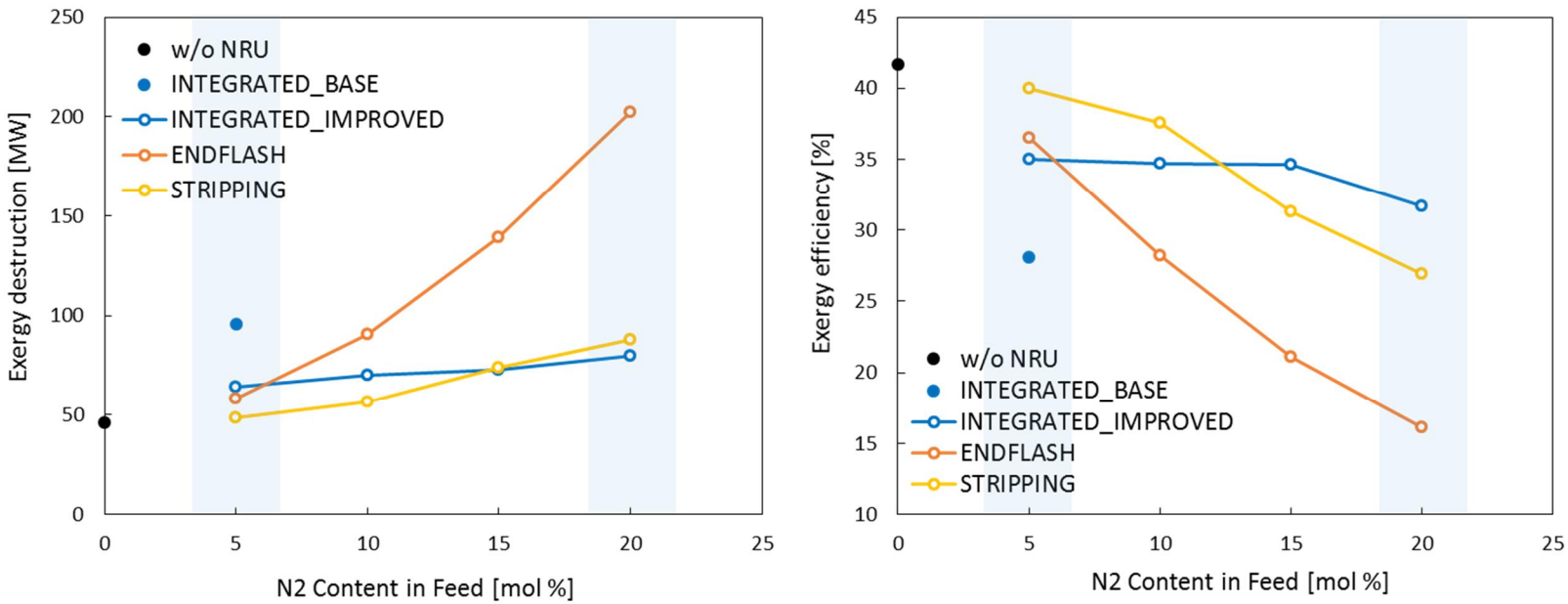

Figure 2-22. Exergy destruction and efficiency of each process with respect to N2 content in feed gas

(Left: Exergy destruction, Right: Exergy efficiency)

Based on these trends, the preferential configuration of nitrogen recovery process could be selected with respect to nitrogen content in the feed gas. In each blue region in Figure 2-21 and Figure 2-22, the order of priority is stripping option, end-flash one, and integrated one for 5mol% of nitrogen, and integrated one, stripping one, and end-flash one for 20mol%.

The reason for the difference in the rate of increase for each parameter between the integrated solution and standalone ones would be the different heat and mass transfer structure of each solution. The former option could absorb the separation load incurred by the increased amount of nitrogen through completely separating that component in a single distillation column of which the required cryogenic heat could be provided by the mixed refrigerant cycle. This large refrigeration system then acts as a buffer for relatively small increase of cryogenic heat necessary in condensing overhead nitrogen in the NRU column so that the overall process efficiency decreases only slightly.

For the latter option, however, the standalone NRU section should directly bear the increased load of separation consuming more power at the compressors in this section with larger NRU feed, and also the increased amount of recycle stream to the main liquefaction section for complete recovery of products would increase the total capacity of the process. This makes the overall process efficiency deteriorate more than the former option. Then the optimization would proceed in the direction of deciding how much this increased load should be distributed to each section. Distributed configuration of the standalone solution could have strengths in optimization by applying it to each distributed section independently but at the same time must be fragile to the increased amount of nitrogen.

2.6. Concluding Remarks

This chapter achieved the sustainability in the process design through proposing optimal nitrogen recovery processes in natural gas processing where the LNG and NGL are produced and the nitrogen is completely separated from natural gas to be vented to the atmosphere.

Based on the structural analysis of components separation, two nitrogen recovery solutions (integrated NRU and standalone one) were studied. The latter solution includes two process configurations of using an end-flash drum in producing LNG or using a stripping column at the same position.

For integrated solution, the heat and mass transfer structure of the reference base case from a previous research by Ghorbani et al. [14] was improved in the direction of minimizing exergy destruction costs. Then the new configuration for integrated one was optimized in terms of a specific power equivalent to the overall process efficiency through controlling major variables related to the heat and mass transfer satisfying product specifications. The improved design has higher process efficiency with the specific power of 0.482kWH/kg_LNG which is lower by 26.2% than that of base case of 0.653kWH/kg_LNG.

Standalone solutions consisting of end-flash option and stripping one which were newly designed in this study as design alternatives were optimized resulting in lower specific powers than that of integrated one for both options of 0.454kWH/kg_LNG and 0.401 kWH/kg_LNG, respectively. Consequently, each option reduced the specific power by 30.5% and 38.6% respectively than that of the reference base case.

All of these results are for the feed gas containing 5mol% of nitrogen. In order for evaluating the process efficiency with varying feed gas composition from various natural gas sources, each solution was optimized and compared with respect to the nitrogen content in the feed gas from 5mol% to 20mol%. As a result, from 5mol% to around 17mol% the standalone NRU using a stripping column has the priority over other options and after that point the integrated NRU leads the standalone solutions in terms of process efficiency. These results could give the reasonable guidelines to the process designers of nitrogen recovery with various feed gases. In addition, the method this study used in design improvement and optimization may be applied to other chemical process designs.

CHAPTER 3. Safer Process Design

First, a new methodology for the feasible integration of process design and risk assessment is proposed using commercial simulators with the goal of carrying out risk-based process safety management of an existing gas oil separation plant (GOSP). For integration of these two different natures, the concept of static inventory was deduced in order to adjust the dynamic behavior of the fluid in process simulation to accident simulation, considering the flow rate and release duration of the fluid in case of an accident. Particularly for the gas treatment unit (GTU) among the various subsections of the GOSP process, this methodology attempts to assess the potential risk at the preliminary design stage and modify the process design of the existing process to alleviate the major hazard recursively identified during rigorous quantitative risk assessment (QRA). Consequently, the modified design with different operation conditions reduces the total risk integrals by 27% at the expense of the additional $50,000 for capital cost. In addition, sensitivity analysis of total risk with respect to probability of success for the isolation process is carried out in order to give insight for a safer and more reliable process design.

Second, inherent safety approach is the systematic strategy to achieve safety in the chemical plant by avoiding or reducing hazards through designing a safer process at the preliminary design stage. In this study, a new decision making scheme of inherently safer process design will be proposed aiming at simultaneously considering the economic feasibility and process safety through

multi-objective optimization via gProms Process builder v.1.1. The optimization employs a sequential quadratic programming (SQP) for the optimal solution of complex non-linear programming (NLP) problem. The proposed method uses an inherent safety index of process route index (PRI) as the second objective function which could reflect the accidental situations and assesses the risk of fatality frequency [1/yr] at the optimal points by post-calculation using commercial quantitative risk assessment (QRA) software of SAFETI v.7.2. It is implemented to the natural gas liquefaction processes which clearly show the trade-off relation between two objective functions so that the effectiveness of the proposed method could be verified. Finally, the single-stage mixed refrigerant (SMR) process with TAC of 627MM$/yr and fatality frequency of 1.28E-03/yr is determined as the final optimal solution among other possible liquefaction processes. Consequently, this proposed approach and associated results could give reasonable guidelines to the designer who wants to decide not only the optimal design conditions but the structure of heat transfer also.

3.1. Introduction

Quantitative risk assessment (QRA) makes it possible to quantify the existing risks of an installation as data for determining whether they are acceptable, as well as assisting in the prioritization of decisions to reduce unacceptable ones [1].

From the advent of discussions on the issues related to nuclear safety by Rasmussen in 1975 [2], extensive researches to quantify the potential risks of chemical plants have been conducted for about 40 years. Although past and present researches have focused mainly on the general methodology for QRA integrated with loss-prevention technologies [3-5], future research would concentrate further on the practicality, reliability, and accuracy of risk assessment methods. The majority of these researches consist of hazard identification integrated with the use of fuzzy relations or Bayesian networks in process facilities to reflect human error or domino effects [6], improved computational fluid dynamics (CFD) calculations for modeling three-dimensional fire and explosion or toxic releases scenarios [7-10], and real-time risk analysis based on advanced process control.

Among these emerging topics, however, there are relatively few studies on the methodology for integrating QRA with both process and accident simulations. Domenico et al. [11] implemented a process simulation for the risk assessment in an early design stage of a future plant using a limited amount of information, and delimited safe regions for the operation. Nam et al. [12] studied a methodology for

evaluating the life cycle cost of an offshore natural gas liquefaction process in relation to the risk expenditure at the conceptual design stage. However, the former study just considered a simulation case study of the normal and worst-case operations, and the latter compared the existing two liquefaction processes in economic point of view. Thus, the results could not provide fundamental guidelines for designing safer processes.

From this standpoint, risk-based process safety management which integrates the QRA methodology with process simulation is very important for chemical plant safety in that it can evaluate the resilience of the process with respect to possible disturbances from the safety perspectives [13], but also can consider risk-reduction steps involving the modification of the existing process design or the construction of inherently safe designs [14-17] for new processes. Resulting design would have safer structures for plant-wide unit operation and optimal operating conditions with better economic efficiency and safety.

In this study, two different methods to design a chemical process considering safety are newly proposed in the following section: one in chapter 3.2 for risk reduction through process design modification of an existing plant based on the QRA results after a detailed design is finalized, and the other in chapter 3.3 for deciding an optimal process design through multi-objective optimization for minimizing both the total annual cost and the risk at the preliminary design stage.

These two approaches have totally different sequence in that the former targets the detailed design where the process information of plant layout and equipment list with its dimension etc. are available and suggests a modified design that could lower the risk but would not deteriorate the economic feasibility of the base case

following the general QRA procedure. Meanwhile the latter integrates the inherent safety with the process design at the preliminary design stage where the detailed information about the process is not yet determined. This approach could largely lower the cost required for finalizing the design as it doesn't need to follow the general QRA procedure where the recursive loop is recycled until the risk is reduced to an acceptable level. But before this approach starts to be applied, the suitability of its method should be verified as it has to make some assumptions in assessing the safety level of the process as there are limited information. Also the computation load would be higher as it needs to simultaneously consider the economic feasibility and safety in designing a process.

Despite the differences these two approaches have each other, however, they are essentially in the same context in that they share the same purpose of deciding a process design which is safer and/or even cheaper than the base case. This chapter will discuss both the proposed methods for different target process and try to give reasonable guidelines to the process designers who want to design a practical and reasonable process considering safety.

3.2 Risk Reduction through Design Modification

In this chapter, a risk-based process safety management which consists of the QRA and the risk reduction loop would be carried out for an existing gas oil separation plant (GOSP), particularly the gas treating unit (GTU) among the various subsections of the GOSP. A new approach for reducing the unacceptable risk in the process is proposed through integrating the process design (flowsheeting simulation) and accident modeling (fire & explosion, toxic dispersion simulation) using commercial simulators. This method firstly assesses the potential risk in the existing process through the general QRA and tries to reduce the risk through modifying its design by proposing several alternatives, in order to design a safer and more reliable plant.

This chapter includes the QRA simulation using commercial software, SAFETI™, based on the detailed information of the target process following its general procedure. While performing this, the static inventory concept is introduced which estimates the mass inventory of hydrocarbons in the process component like a pipeline or vessel based on its dimension, mass flowrate, and isolation time. After assessing the risk quantitatively, severe accident scenarios that account for the majority of the total risk are identified to be preferentially targeted for the modification. Then two risk reduction methods are to be discussed: one for modifying the process design, and the other for improving the safety barriers by altering the failure frequency of them. The comparison between each other would

show the superiority of the former method in reducing risk.

3.2.1. Risk Assessment for the Target Process

General Procedure of QRA

The potential risks of a chemical plant can be quantified through QRA. This makes it possible to determine the acceptability of a process and route unacceptable processes to the risk reduction procedures. Generally, QRA is composed of six steps as shown in Figure 3-1. After the system and objective are defined, the major hazards are identified and their consequences and frequencies are analyzed. Usually, the frequencies are obtained from historical data such as the UK's Health and Safety Executive (HSE) or Oil and Gas Producers (OGP). The total risk is assessed quantitatively considering both the consequences and frequencies of major hazards. If the overall risk level is judged to be tolerable, the QRA process ends and that of the system is ready to be managed. Otherwise, the process should go through the risk reduction step and define the system recursively (feed-back loop).

There are two standards for the tolerability criteria of associated risk – Individual Risk (IR) and Societal Risk (SR). IR is the annual risk of death or serious injury to which a person at the specified position is exposed. Thus it cannot reflect the overall risk of the plant with various population density. In contrast, SR considers the population density so that it is used as a measure of the risk to a group exposed to the effects of an accident [18]. In this study, SR is used as the standard for tolerability criterion as it can more reliably reflect the real plant safety. SR is

expressed in terms of the frequency distribution of multiple casualty events, which is called an F-N curve. This F-N curve is divided into three sectors: “Negligible”, “As Low As Reasonably Practicable (ALARP)”, and “Intolerable”. According to HSE’s publication [19], an individual risk of less than 1.0E-06 (per year) is considered negligible, while it is intolerable when it is above 1.0E-04 (per year) for the public and above 1.0E-03 (per year) for workers. As the number of people affected by an accident increases, its fatality probability unconditionally decreases. The ALARP region is located between these two areas, negligible and intolerable, and the total risk curve of a process should belong to the ALARP or tolerable region in order to be acceptable.

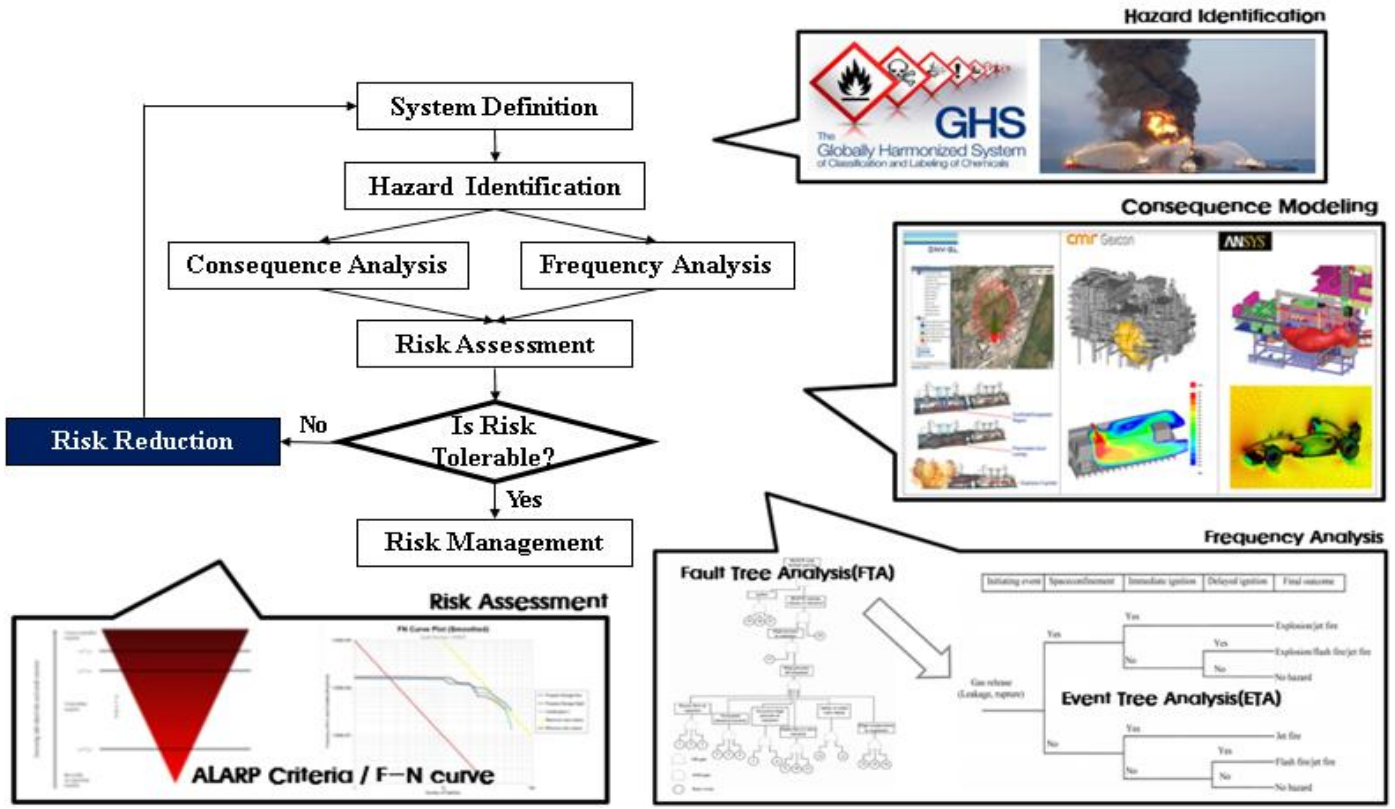

Figure 3-1. The general procedure of QRA

System Definition (GTU Process in GOSP)

The target process of this study is a Gas Treatment Unit (GTU) of a Gas Oil Separation Plant (GOSP) with a target production rate of 230 kbopd and a block flow diagram shown in Figure 3-2 [20]. The well fluid from the gathering system station enters the 1st stage separator, in which the free gas and water are separated from the crude oil. The oil is heated in the crude heater and depressurized prior to entering the 2nd stage separator for further separation. Approximately 44.9 MMSCFD of the free gas from the two-stage separator is routed to the GTU, and the remainder heads for Integrated Gas Process Plant (IGPP), where power generation, dry gas production, and LPG production are operated.

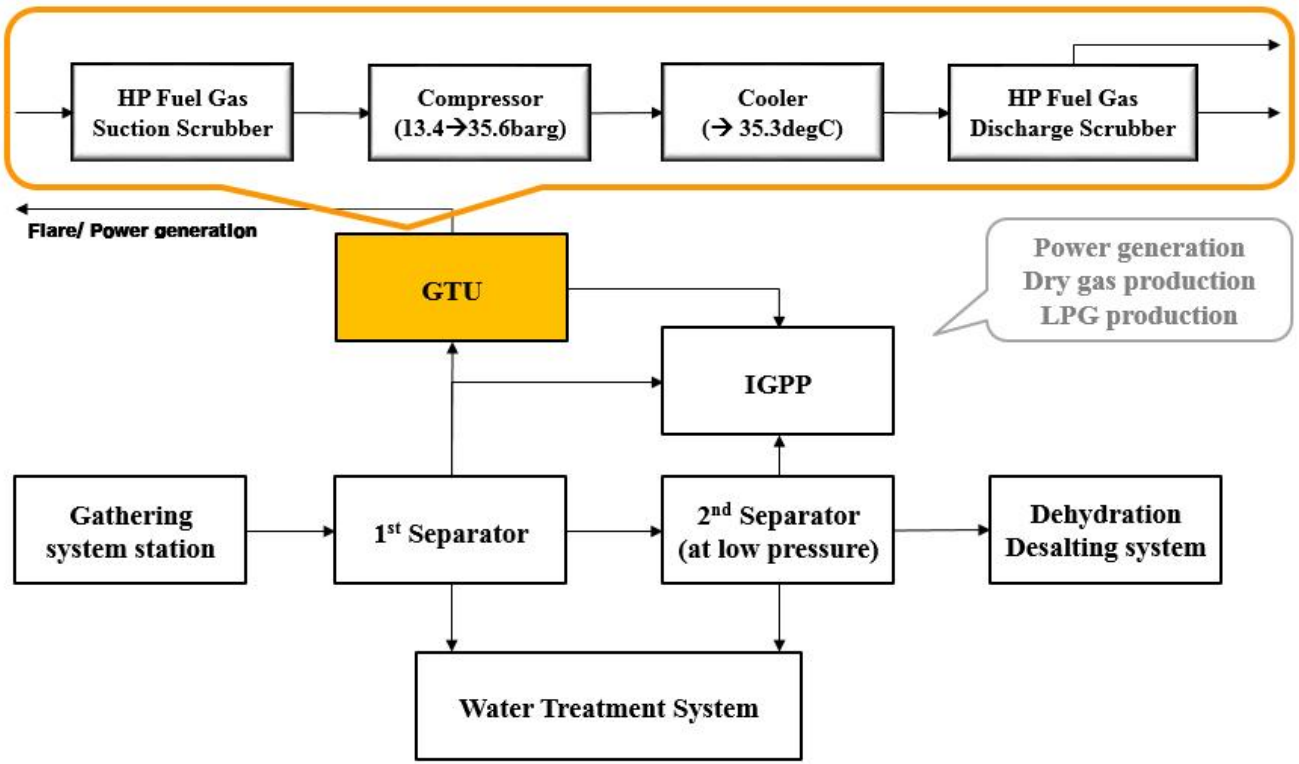

Figure 3-2. Block flow diagram of GOSP

In the GTU process of which the process flow diagram (PFD) is shown in Figure 3-3, the combined feed gas is routed through a pipeline (P_01) at 13.4barg to the high-pressure (HP) fuel gas suction scrubber (V_01, V_03) for liquid knock-out prior to being compressed to 35.8barg (P_02, P_03) by the HP fuel gas compressor. Compressed gas then enters the HP fuel gas discharge cooler (air cooling) to cool down to 60°C and is further chilled to 35°C in the chiller package. The refrigerated gas is then routed to the HP fuel gas discharge scrubber (V_02, V_04) for heavy hydrocarbon and water knock-out. The liquid (P_05 (1) & (2)) is separated into hydrocarbon liquid, water, and vapor in the three-phase separator (V_05), and the hydrocarbon liquid (P_06 (1) & (2)) is fed back to the upper process at 5.5barg. Fuel gas from the discharge scrubber is superheated to 80°C by the HP fuel gas discharge super-heater and finally sent to the power plant. Model of the GTU is simulated using Aspen HYSYS V8.4 based on PFD.

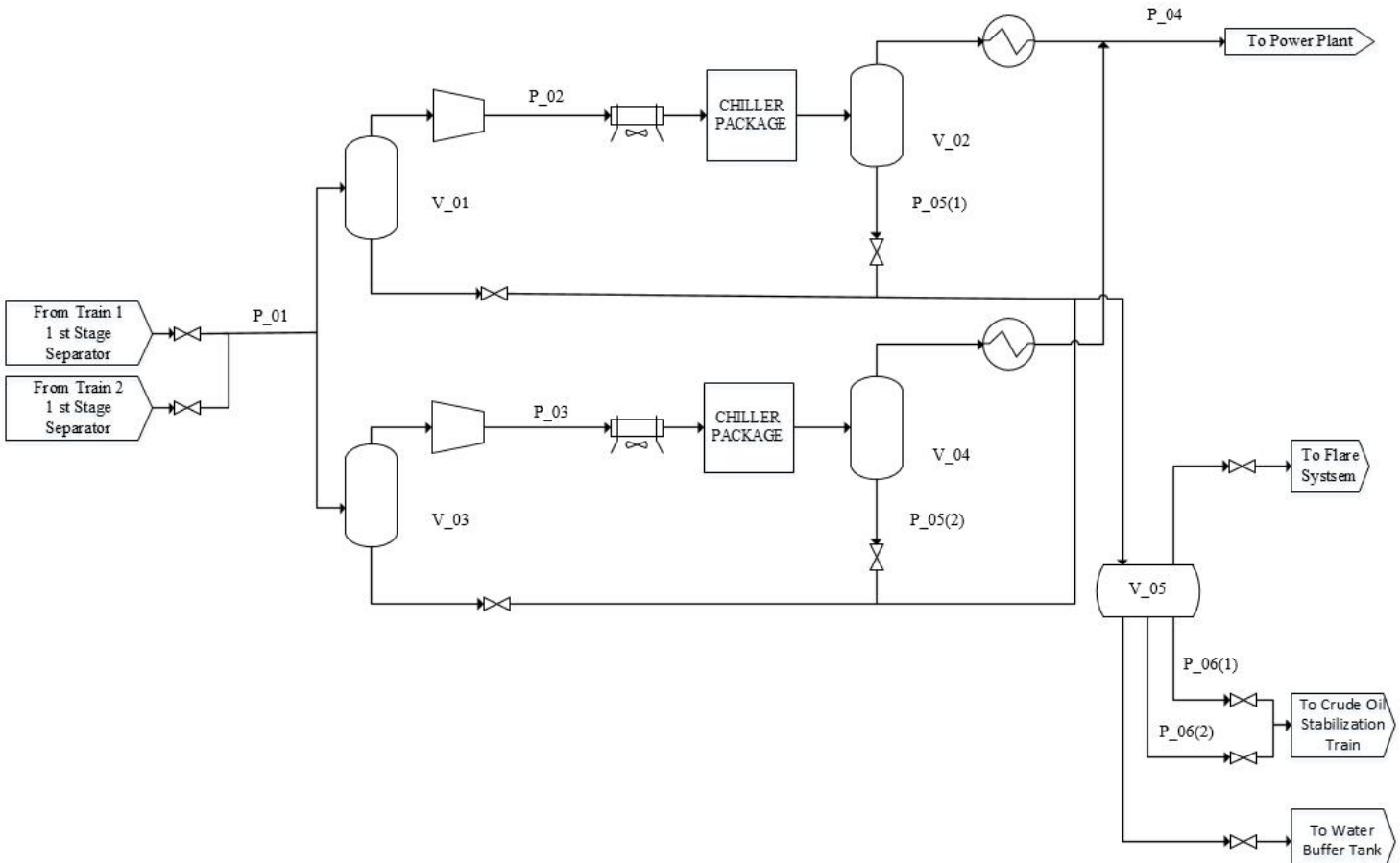

Figure 3-3. Process flow diagram of GTU

Plant layout of the overall GOSP and GTU is softly depicted in Figure 3-4 for the reason of confidential material, and part counts of the associated equipment belonging to each pipeline or vessel (P_01~06, V_01~05) are based on the equipment list and Piping and Instrument Diagram (P&ID) not provided in this paper.

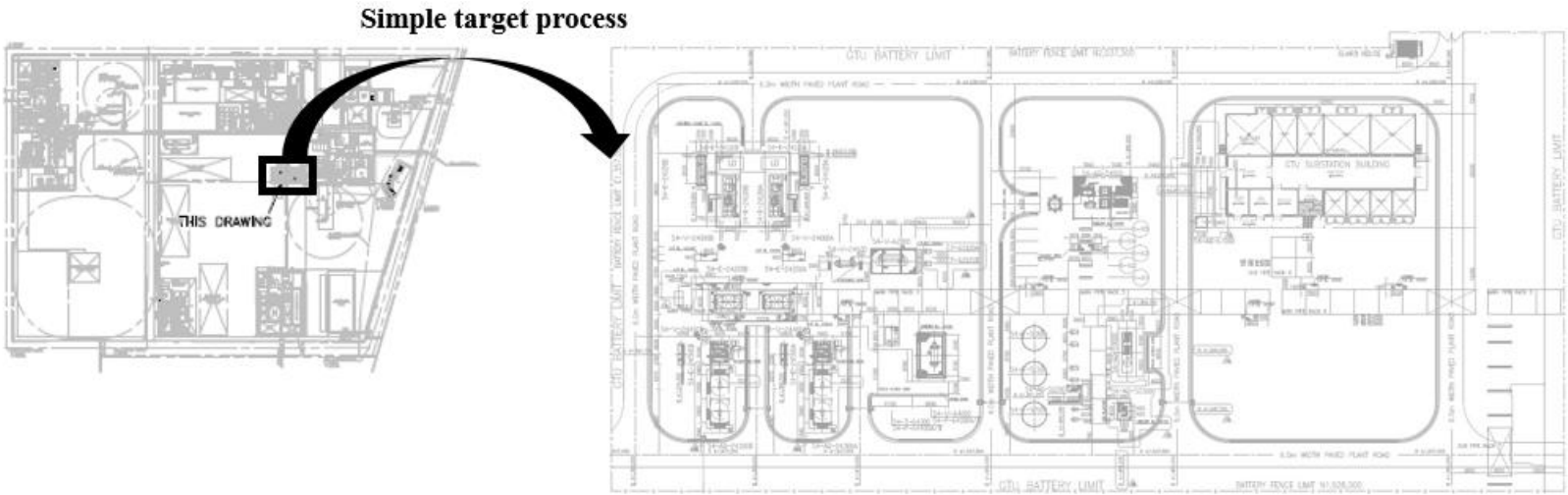

(a) GOSP layout (b) GTU layout

Figure 3-4. Plant layout of GOSP and GTU

Static Inventory Estimation

The risk calculation is basically based on the static storage conditions (pressure, temperature, mixture property, and volume/mass inventory) of each equipment like vessels or pipelines. All of these conditions except static volume/mass inventory could be directly transferred from the process simulation. In this study a non-static parameter of the flow rate (kg/h) of a fluid flowing in a certain equipment is converted to the static inventory (kg) of the same equipment in order to perform QRA based on process simulation. Three additional data of equipment size, fluid mass density, and release duration in case of an accidental release are necessary to estimate the static inventory from the flow rate calculated from process simulation. In particular, the release duration of a flowing fluid is determined by the activation time of isolation process like an emergency shutdown (ESD) system as the fluid would leak continuously until this process is completed. In this study the isolation process is assumed to succeed if it is completed within 5 min after the release occurs (the release duration is 5 min), otherwise the process is judged to fail so that the fluid would be released for 30 min. Hereinafter the former is called the isolation success (IS) case, and the latter is the isolation failure (IF) case which possesses a severe hazard due to its long release duration. Static inventory estimation is expressed in the Eq. 3-1.

$$I = \rho_f V + kM \tag{3-1}$$

- IS case: k = 1/12 (=5min/h)
- IF case: k = 1/2 (=30min/h)

where, I=static inventory of an equipment [kg]; ρ_f=fluid density [kg/m3]; V=internal volume of the equipment [m3]; k=coefficient for release duration; M=mass flow rate [kg/h].

The types of the equipment in our system consist of a cylindrical pipeline, vertical two-phase flash drum, and horizontal three-phase separator as listed in Table 3-1.

Table 3-1. Equipment for static inventory

Equipment	Inventory Figure for Normal Operation
Pipeline	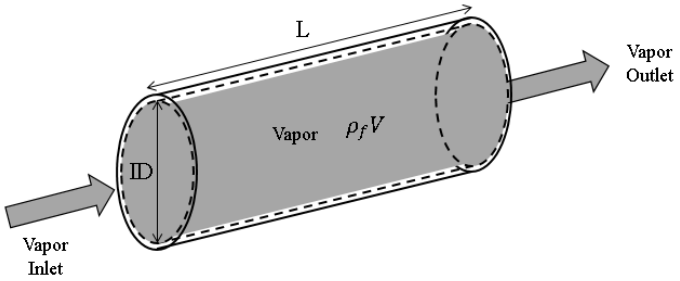 L : the length of pipe between two EIVs* ID : Inner Diameter of the pipe
2-Phase Flash Drum	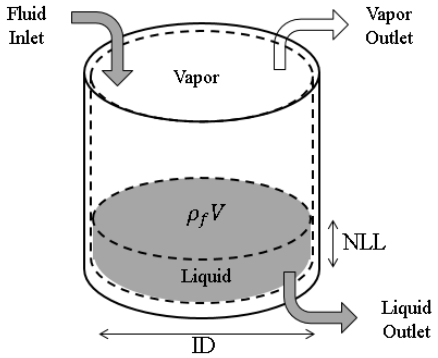 NLL : Normal Liquid Level ID : Inner Diameter of the vertical vessel
3-Phase Separator	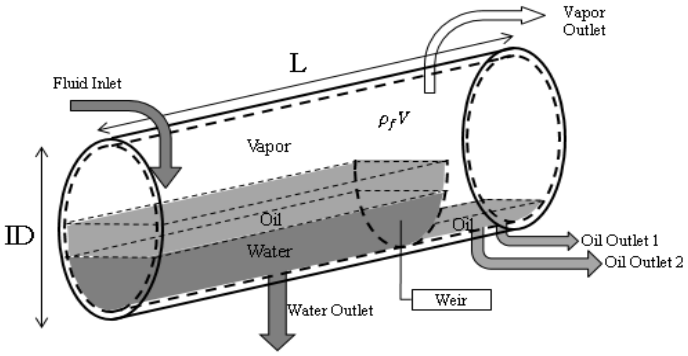 L : Length of the horizontal vessel ID : Inner Diameter of the horizontal vessel

*EIV(Emergency Isolation Valve) : All subsections(P01~06 & V01~05) are

assumed to be independent on each other by the emergency isolation valves at the end of each subsection if the isolation process is done properly in case of an accident.

Hazard Identification (HAZID)

As the chemical (mixture) properties and operating conditions of each stream or equipment would determine its degree of risk, the major hazard targeted for the QRA can be identified considering these factors. Generally, in case of a release scenario, the mass density, pressure, and temperature of a mixture are associated with the orifice discharge velocity (m/s) and total release rate (kg/s), which are highly correlated to the ignition probability. From this perspective, pipelines and vessels operated at a high pressure, high temperature, or large mass flowrate are reasonably chosen as major hazards. As a result, 11 total hazards are identified, as described (P_01~06, V_01~05) in Figure 3-3, and unit descriptions and operating conditions are listed in Table 3-2.

Table 3-2. Unit descriptions and operating conditions of identified hazards

Unit	Description	Pressure (bar-g)	Temperature (℃)	Mass flowrate (kg/h)
P_01	Piping to HP fuel gas suction scrubber (1&2)	13.3	65.0	46,677
P_02	Piping from HP fuel gas compressor (1) to HP fuel gas discharge cooler	35.7	147.6	23,338
P_03	Piping from HP fuel gas compressor (2) to HP fuel gas discharge cooler	35.7	147.6	23,338
P_04	Piping from HP fuel gas discharge super-heater to power plant	34.2	79.8	42,251
P_05	Piping from HP fuel gas discharge scrubber (1&2) to three-phase separator	34.7	34.8	2,734
P_06	Piping from three-phase separator hydrocarbon liquid outlet to crude oil stabilization train	12.0	27.3	2,286
V_01	Fuel gas suction scrubber (1)	13.3	64.7	
V_02	HP fuel gas discharge scrubber (1)	34.7	34.8	
V_03	Fuel gas suction scrubber (2)	13.3	64.7	
V_04	HP fuel gas discharge scrubber (2)	34.7	34.8	
V_05	Three-phase separator	12.0	27.3	

Frequency Analysis

Having assessed the major hazards in the hazard identification (HAZID) step, it is necessary to estimate the frequencies with which possible accidental events could occur. The data are derived from the records of how often an incident has occurred or how often equipment items (such as pumps, pipes, and vessels) have failed in the past. In this paper, the failure frequency data for pipelines including process piping, flanges, and valves are extracted from OGP 2010 [21] and those of vessels are taken from HSE HCR 2013 [22].

At the equipment level, type and size of each equipment item determine its frequencies of possible release scenarios. Typically, a frequency analysis is initiated by conducting a survey of the equipment containing dangerous substances, estimating the number of equipment items (how many pumps, how much pipe, how many vessels, etc.). These numbers are then combined with their respective release frequencies in order to obtain the total frequency of all the releases of hazardous substances at that site.

The event tree analysis (ETA) technique is performed to identify and evaluate all of the possible outcomes resulting from an initiating event. The ETA structure illustrated in Figure 3-5 is constructed based on the several conditions like immediate ignition or delayed ignition, resulting in different accidental outcomes including jet fire, pool fire, flash fire, and explosion etc. At each node, associated conditional probabilities are multiplied consecutively to estimate the final frequencies of each scenario.

In this study, an “isolation success” node at the head of the entire structure is additionally included in order to emphasize the effects of the isolation process in case of an accident. In addition, the criterion for a “short” release duration given immediate ignition is defined by the cut-off time, which in this paper is set at 20s. Thus, for a case where the release duration exceeds this time, the fire ball occurrence frequency is assumed to be zero, and only the jet fire effect is calculated.

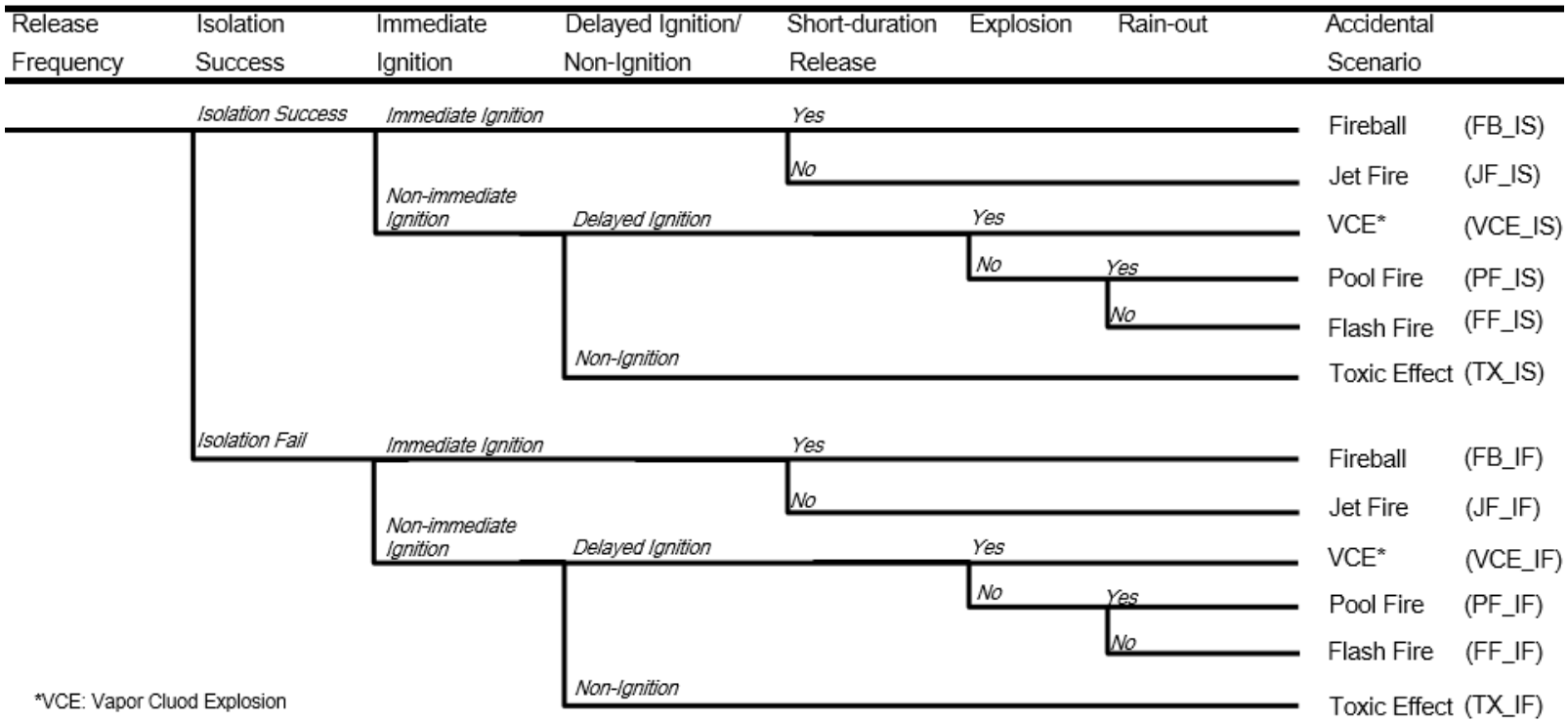

Figure 3-5. ETA structure of each initiating event

The conditional probabilities (Table 3-3) of each node in the ETA structure, are evaluated based on the release rate (kg/s) calculated through a discharge model using DNV PHAST 6.7 and following reasonable assumptions.

▪The ignition probabilities are determined from look-up correlations using a simple cell function formula based on the release rate (kg/s) and scenario types [23].

▪The probability of an immediate ignition is 0.5 for vapor releases or 0.3 for liquid releases.

(Probability of delayed ignition) = 1 – (Probability of immediate ignition)

▪The probability of an explosion is 0.04 for a minor release rate (<1 kg/s) or 0.12 for a major release rate (1–50 kg/s).

▪The probability of success for isolation is 0.5, 0.75, or 0.9 for a small, medium, or large hole- size, respectively.

Table 3-3. Conditional probabilities of each release scenario

Release Scenario	Release rate (kg/s)	Conditional Probability				
		Ignition	Isolation Success	Immediate Ignition	Delayed Ignition	Explosion
P_01_10mm	1.92E-1	8.79E-4	0.5	0.5	0.5	0.04
P_01_50mm	4.79E+0	1.24E-2	0.75	0.5	0.5	0.12
P_01_150mm	1.26E+1	3.19E-2	0.9	0.5	0.5	0.12
P_02_10mm	4.96E-1	1.64E-3	0.5	0.5	0.5	0.04
P_02_50mm	7.16E+0	1.83E-2	0.75	0.5	0.5	0.12
P_03_10mm	4.96E-1	1.64E-3	0.5	0.5	0.5	0.04
P_03_50mm	7.16E+0	1.83E-2	0.75	0.5	0.5	0.12
P_04_10mm	4.58E-1	1.55E-3	0.5	0.5	0.5	0.04
P_04_50mm	1.15E+1	2.90E-2	0.75	0.5	0.5	0.12
P_04_150mm	1.84E+1	4.65E-2	0.9	0.5	0.5	0.12
P_05_10mm	2.89E+0	7.63E-3	0.5	0.3	0.7	0.12
P_05_50mm	1.87E+1	4.70E-2	0.75	0.3	0.7	0.12
P_06_10mm	1.89E+0	5.12E-3	0.5	0.3	0.7	0.12
P_06_50mm	1.21E+1	3.07E-2	0.75	0.3	0.7	0.12
V_01_10mm	1.92E-1	8.79E-4	0.75	0.5	0.5	0.04
V_01_CAT*	4.00E+1	1.00E-1	0	0.5	0.5	0.12
V_02_10mm	5.33E-1	1.73E-3	0.5	0.5	0.5	0.04
V_02_CAT	2.20E+2	5.40E-1	0	0.5	0.5	0.3
V_03_10mm	1.92E-1	8.79E-4	0.5	0.5	0.5	0.04
V_03_CAT	4.00E+1	1.00E-1	0	0.5	0.5	0.12
V_04_10mm	5.33E-1	1.73E-3	0.5	0.5	0.5	0.04
V_04_CAT	2.20E+2	5.40E-1	0	0.5	0.5	0.3
V_05_10mm	1.89E+0	5.13E-3	0.5	0.3	0.7	0.12
V_05_CAT	1.60E+3	6.50E-1	0	0.3	0.7	0.3

*CAT : Catastrophic Rupture

QRA Simulation using Commercial Software

Consequence analysis estimates the scale of a damage caused by an accident through calculating fluid concentrations along with the downwind distance, radiation intensities, and toxic doses. There are two groups of materials considered here causing these damages. One is flammable material group. Outcomes such as fireball, jet fire, and early pool fire from immediate ignition, and flash fire and late pool fire for delayed ignition are caused by flammable fluids. Explosion outcome such as vapor cloud explosion (VCE) also depends on the flammable effect, as well as the extent of congestion and confinement. The risks from these flammable effects are dominant in that the mixtures of concern in the GTU process are mostly composed of hydrocarbons of C_1~C_9. The other one is toxic material group. In case of toxic releases, a longer duration of exposure to the substance or higher concentration at a certain point will increase the probability of fatality. Toxic chemicals in the GTU process include hydrogen sulfide (H_2S) and carbon dioxide (CO_2). Even though the toxic effect will be serious in case of an isolation failure, the amounts of these components are too small to significantly have an effect on the total risk.

After analyzing the hazards, frequencies and consequences of each release scenario, the risk can be quantitatively assessed by built-in models in PHAST_RISK v.6.7. The input data include operating conditions of each equipment with additional weather data of the object area and assumed manning data.

In Figure 3-6, the individual risk (IR) contours are mapped upon the layout of GTU process (Figure 3-4). IR means the annual risk of death to which specific

individuals are exposed at certain position (x, y) in case of an accidental scenario and it could be calculated from Eq. 3-2 and Eq. 3-3 [24].

$$IR_{x,y} = \sum_{i=1}^{N} IR_{x,y,i} \quad (3\text{-}2)$$

$$IR_{x,y,i} = F_i \times P_{fi} \quad (3\text{-}3)$$

where $IR_{x,y}$=individual risk at position (x,y); $IR_{x,y,i}$=individual risk at position (x,y) by an accidental scenario i; N=number of accidental scenarios; F_i=annual frequency of the scenario i; P_{fi}=probability of death by scenario i.

From the figure it could be noted that most of the GTU area is located in the ALARP region between the yellow (1E-03: upper ALARP limit) and red (1E-05: lower ALARP limit) curves. Thus, the risk of GTU could be considered to be tolerable in terms of IR.

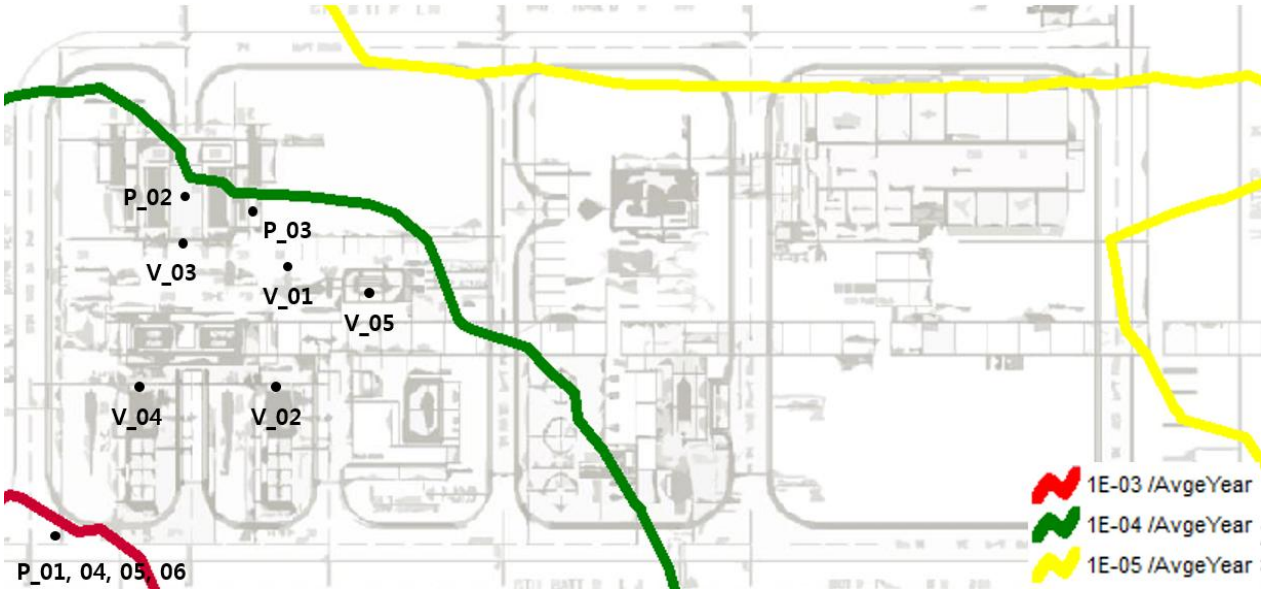

Figure 3-6. IR contours mapping on the GTU layout

In terms of the societal risk (SR) which is a measure of a group risk consisting of the community exposed to the effects of the accident, however, the acceptability of the risk would change compared to that of IR. In the total SR expressed by the F-N curve (Figure 3-7), which is the sum of the societal risks of the IS and IF cases, the curve exceeds the line of the upper ALARP limit for 2 to 10 fatalities. Therefore, the risk should be judged to be unacceptable, and appropriate actions should be taken to drag the frequency of fatalities down into the ALARP region. This F-N curve also shows that the IF case is dominant over the IS case due to more severe consequence outcome of each accidental scenario for the former case, in spite of its low frequencies of failure. These results imply that the risk reduction process should aim to mitigate the scenarios for IF case preferentially.

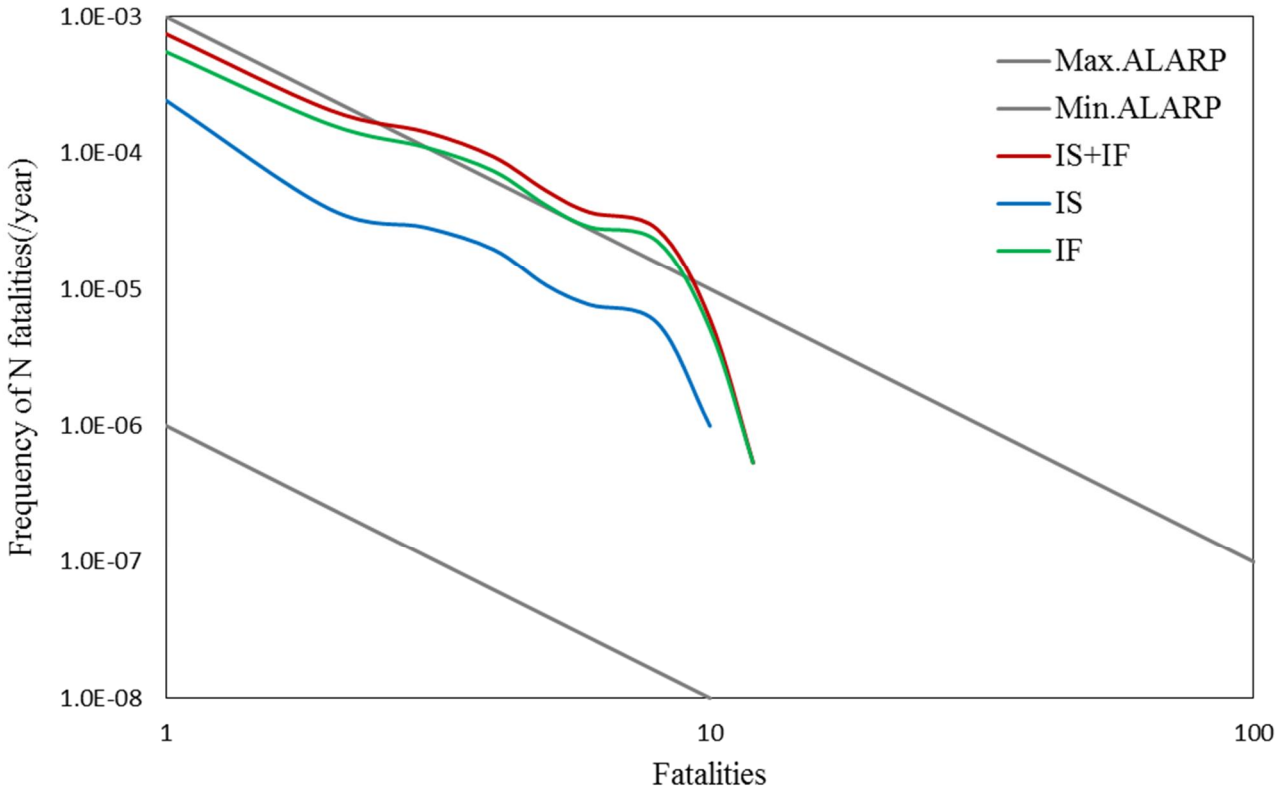

Figure 3-7. F-N curve for SR (=IS+IF) of the base case

Additionally, in order to select the risk reduction target among all of the events, risk integrals (per year) obtained by multiplying the number of fatalities by the frequency of that fatalities are ranked in Figure 3-8 and the values are listed in Table 3-4. Based on the results, a small leak (10mm hole-diameter) scenario at the P_06 equipment in case of isolation failure has the highest risk integral value of 3.04E-04/year which accounts for 21.6% of the total societal risk. The major outcomes for this leak scenario are also listed in Table 3-5, which shows that the continuous release with rainout delayed flash fire and pool fire effects (CRDFFP) scenario is the most dominant scenario, accounting for 18.89% of the total societal risk. These imply that the risk reduction process should target the P_06 equipment alleviating the flash fire and pool fire effects, and enhance the probability of success for isolation process.

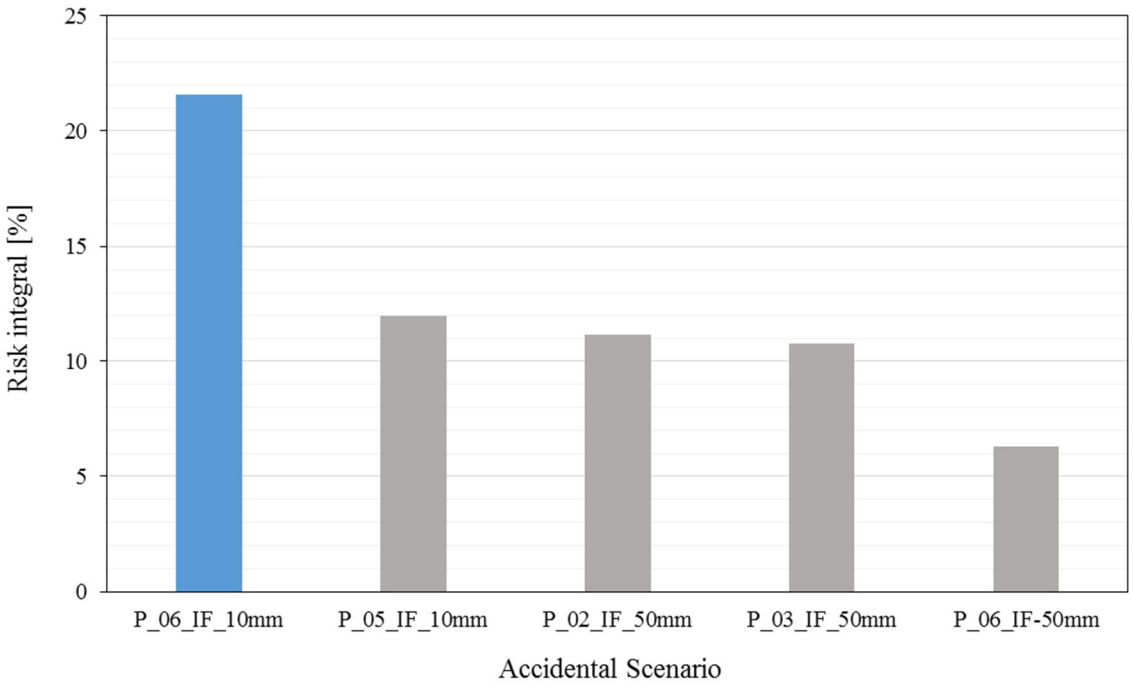

Figure 3-8. Top five risk integrals ranking

Table 3-4. Major leak scenario targeting

	Risk Integral (per year)	Percent (%)	Accumulated Percent (%)
P_06_IF_10mm	3.04E-04	21.6	21.6
P_05_IF_10mm	1.68E-04	12.0	33.6
P_02_IF_50mm	1.57E-04	11.2	44.8
P_03_IF_50mm	1.52E-04	10.8	55.6
P_06_IF-50mm	8.81E-05	6.3	61.9
Total risk integral	1.41E-03	100.0	100.0

Table 3-5. Major outcomes at P_06_10mm

P_06_IF_10mm Outcome	Risk Integral (per year)	Pipe #	Sum	Percent
CRIHJP*	5.51E-07	2	1.10E-06	0.08
CRDFFP**	1.33E-04	2	2.66E-04	18.89
CRDFXP***	1.82E-05	2	3.63E-05	2.59
Total	1.52E-04	2	3.04E-04	21.56

*CRIHJP : Continuous release with rainout immediate horizontal jet fire and additional pool fire effects
**CRDFFP : Continuous release with rainout delayed flash fire and pool fire effects
***CRDFXP : Continuous release with rainout delayed flash fire and explosion effects

3.2.2. Risk Reduction to ALARP

In this chapter, two risk reduction methods, one for the modification of process design based on QRA results and the other for the improvement of the safety systems like isolation process or safety instrumented system (SIS), are proceeded to manage the unacceptable risk. As the standard method for risk reduction is not yet established, those results are expected to give reasonable guidelines to process designers and safety engineers who wants to design a safer process. In this study the former method would be discussed in more detain as it could fundamentally manage the risk through removing or mitigate the major scenarios inherently.

Risk Reduction through Design Modification

Design Consideration

In the scenario ranking results in Figure 3-8, the P_06 equipment is piping from the three-phase separator (V_05) hydrocarbon liquid outlet to the crude oil stabilization train, in which the liquid is maintained at 12.0barg. This pressure affects the vapor-liquid-liquid equilibrium (VLLE) of the vapor, hydrocarbon liquid, and aqueous liquid, which determines the temperature, component composition, and flowrate of the hydrocarbon liquid, more hazardous than the others. A lower pressure will decrease the flowrate of the hydrocarbon liquid outlet and static inventory of P_06, which lessens the potential hazard of the equipment.

In case of leak scenarios, the pressure difference between the vessel and atmosphere determines the discharge rate at the hole-orifice, which is directly connected to the ignition and explosion probability based on the assumption at the ETA. It also determines the extent of liquid flashing into the air which would influence the consequences of accidental outcomes like a pool fire, jet fire, and flash fire. Thermodynamically, higher pressure difference increases the amount of liquid flashing and the effects of a jet fire and flash fire but decreases that of a pool fire.

Based on the QRA results in section 3, the target scenarios for the risk reduction process are those resulting in flash fire and pool fire. Flash fire results from the combustion of a flammable vapor and air mixture, while pool fire occurs as the ignition of a flammable liquid pool formed during rainout of liquid from a leakage hole. Therefore, the modification of the operating pressure of V_05, which will change both the VLLE and the impact of each accidental outcome, can reduce the

risk of the targeted equipment (P_06).

Before the pressure adjustment some factors should be considered. First, the feasible range of operating pressure should be determined to prevent the downstream process from severe inconvenience. Second, at that pressure range, discharge stream condition from the 3-phase separator should not be highly disturbed from the original stream specification.

Four liquid streams, two of which are from fuel gas suction scrubbers (V_01 & 03) at 13.3barg, with the other two from HP fuel gas discharge scrubbers (V_02 & 04) at 34.7barg, are merged into one feed stream routed to the three-phase separator (V_05) after a pressure reduction to 12.0barg through a valve. Because the operating pressure of V_01 & 03 is 13.3barg, considering the pressure drop in the pipe due to frictional losses, the maximum available pressure at the three-phase separator is assumed to be 12.0barg, which is the original condition. In addition, the minimum available pressure is set to be 0.5barg in order to prevent too much loss of hydrocarbon to the vapor stream and excessively low operating temperature.

Furthermore, the pressure specification of the hydrocarbon liquid stream heading to the crude oil stabilization train should be maintained at 5.5barg, while that of the aqueous liquid stream routed to the water buffer tank should be maintained at 1.5barg. For example, if we modify the pressure of the vessel to a value lower than 1.5barg, both the hydrocarbon liquid stream and aqueous liquid stream should be pressurized to their individual specifications using pumps.

Modification Results

For the case considered here, the vessel pressure is reduced until the whole F-N curve of associated societal risk belongs to the tolerable ALARP region. The VLLE and physical properties like the mass density of the P_06 stream are calculated with the Peng–Robinson equation of state (EOS) using the Aspen HYSYS V.8.4. Through the modification, the PFD change near P_06 are illustrated in Figure 3-9 and the results of process simulation are summarized in Table 3-6.

For the modified operating conditions, the hydrocarbon liquid stream in P_06 and aqueous liquid stream from V_05 should be pressurized to 5.5 and 1.5barg, respectively, using pumps to meet the pressure specifications in order to be routed to the downstream process as shown in the figure.

(a) 12.0 barg

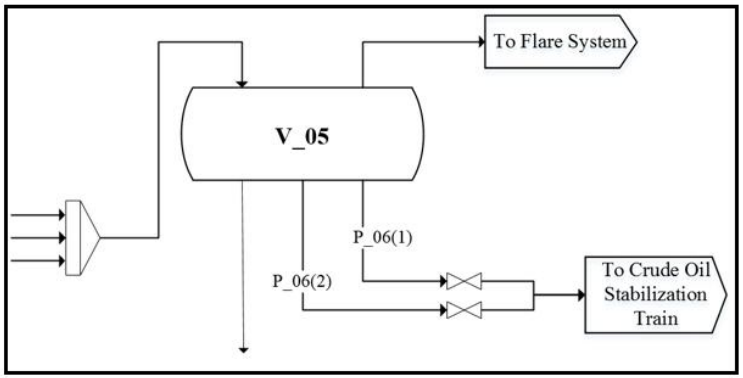

(b) 0.52 barg

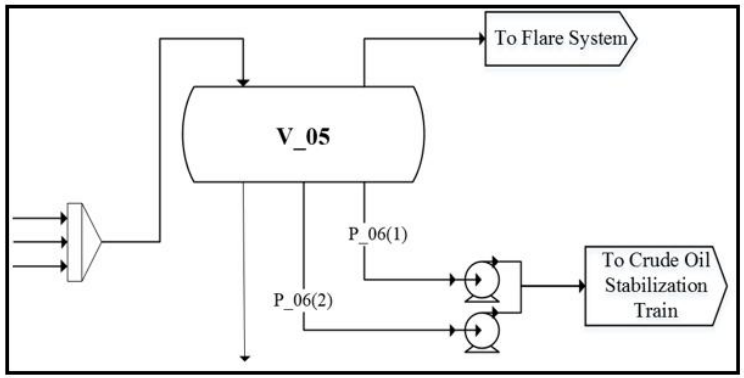

Figure 3-9. PFD for near P_06 of the (a) base case (b) modified case

Table 3-6. Stream data and static inventory of P_06

	Existing condition	Modified condition
Pressure (barg)	12.00	0.52
Temperature (℃)	27.56	3.31
Mass flow rate (kg/h)	2,287	1,879
Gas density (kg/m^3)	14.8	2.5
Liquid density (kg/m^3)	617.8	671.3
IS inventory (kg)	268	236
IF inventory (kg)	1,221	1,019

To evaluate the consequences for the P_06_IF_10mm scenario, the contours of flash fire and pool fire outcomes which accounts for the majority of that scenario are plotted in Figure 3-10 and listed in Table 3-7. The flash fire effect is remarkably reduced at the new operating pressure of 0.52barg due to lower liquid flow rate and static inventory. Meanwhile, the pool fire effect is almost the same as two main factors that increase the associated risk offset each other. One is the extent of the rainout, which increases at a lower pressure because of the weak behavior of liquid flashing into the air, and the other is the liquid flow rate in P_06, which determines the total release quantity and it decreases at a lower pressure because of the VLLE.

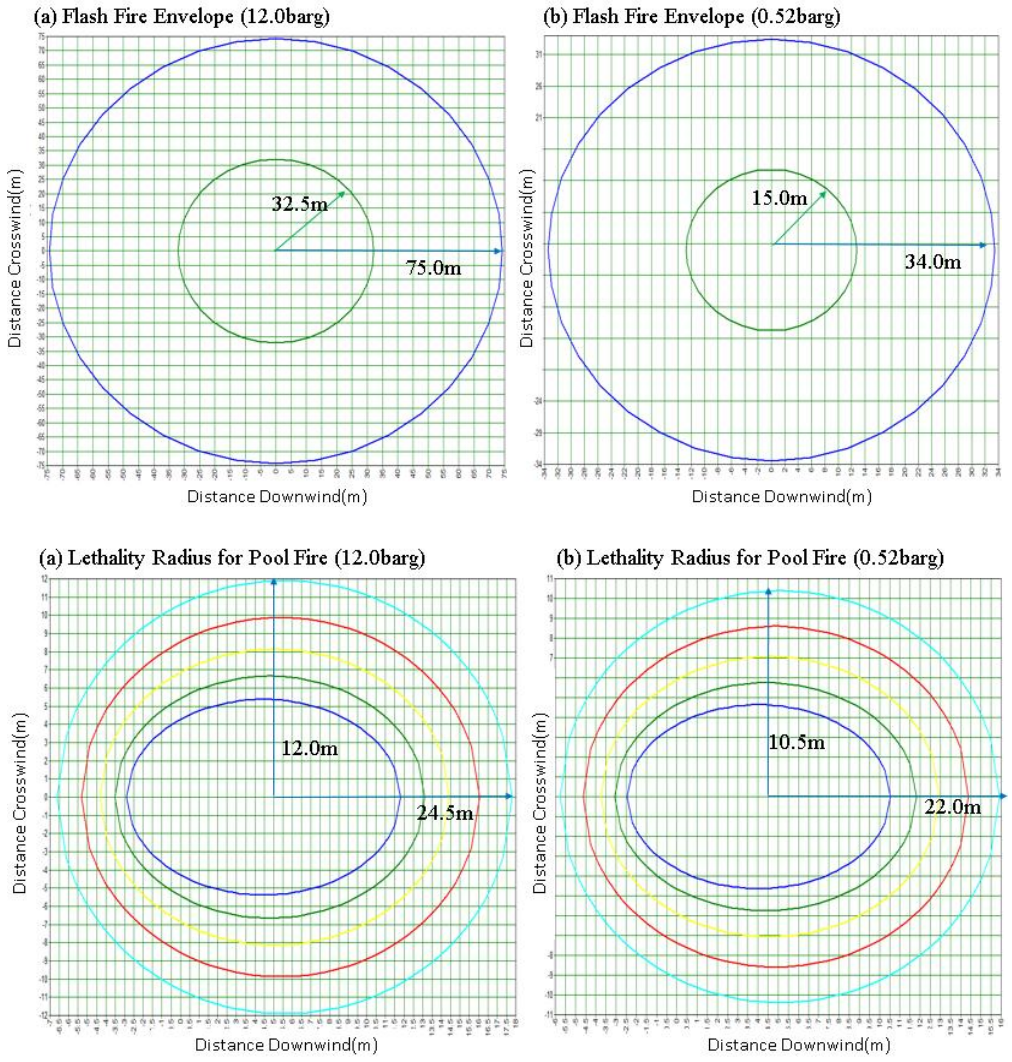

Figure 3-10. Consequence analysis of P_06_IF_10mm for each case

Table 3-7. Consequence analysis of P_06_IF_10mm for each operating pressure

Outcome	Lethality (%)	Color	Operating pressure 12.0barg		0.52barg	
			Radius(m)			
Flash Fire	100 (LFL)	Green	32.5		15.0	
	50 (LFL Frac)	Blue	75.0		34.0	
			Down wind(m)	Cross wind(m)	Down wind(m)	Cross wind(m)
Pool Fire	100%	Blue	15.0	5.5	13.0	5.0
	80%	Green	16.5	7.0	15.0	6.0
	40%	Yellow	19.0	8.0	16.5	7.0
	10%	Red	21.5	10.0	19.0	9.0
	1%	Sky Blue	24.5	12.0	22.0	10.5

The flow rate of the vapor stream from the 3-phase separator also increases due to this modification, but its quantity is small enough not to affect the product specification. This vapor would be disposed of safely at flare system.

In addition, the lower release rate of the 0.52barg case due to the smaller pressure difference between the process stream and atmosphere decreases the ignition probability and explosion conditional probability at the ETA. Based on the new frequency data calculated using the same method as in the original case listed in Table 3-3, the F-N curves for the societal risks of two pressure conditions are shown in Figure 3-11, which clearly shows that the risk is reduced to the level of the ALARP region. Moreover, the total risk integrals decrease from 1.41E-03/year to 1.02E-03 /year, which is more than 27% decrease. Even though the flow rate of the vapor heading to the flare system increases, its quantity is relatively small and is considered to be negligible.

In terms of economic feasibility, a trade-off occurs for different operating pressures. As the pressure decreases, the thickness of V_05 and the capital cost decrease. However, three additional pumps should be installed: two for hydrocarbon liquid streams and one for the aqueous liquid stream. The capital cost of each case is estimated by the equations from Turton et al. [25] with the price in 2012. The cost of the third pump for the aqueous liquid stream is omitted due to its relatively low value. Compared with the total capital cost of the original case, around $50,000 should be additionally invested for the modification case. It is feasible to invest that amount in order to design a much safer process because this amount is negligible enough compared to the total capital cost of the whole plant.

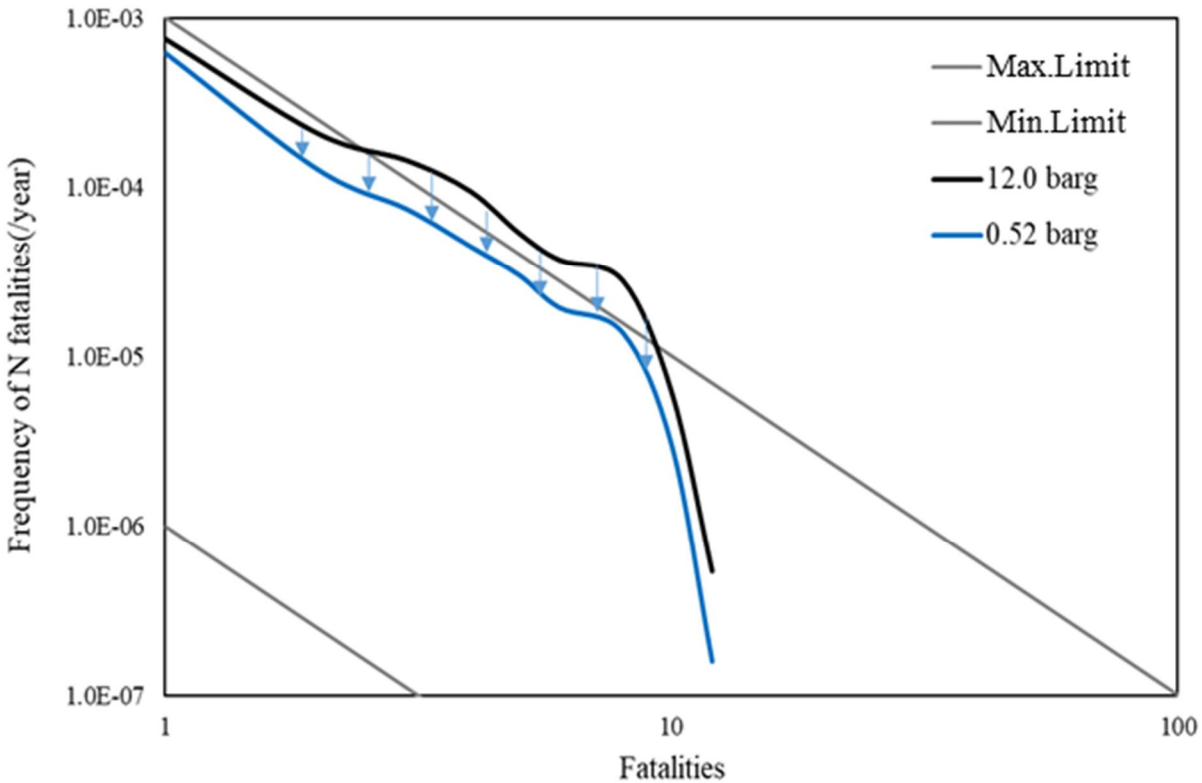

Figure 3-11. F-N curves for SR of two operating pressures at V_05

Risk Reduction through Improving Safety Barriers

The isolation process considered in the ETA in this study has a critical impact on total risk as shown in Figure 3-7. In order to analyze the sensitivity of the total risk to the improvement degree of the safety barriers like the isolation process, a QRA simulation is recursively performed, increasing conditional probabilities of success for isolation up to 50% of that for original case, with a step size of 10%. The F-N curves for the societal risk are shown in Figure 3-12. The associated risk is drastically reduced when the probability of isolation success increases from 30% to 40%, which shows that it is desirable to develop the isolation process until the probability of success is improved to 40%. Economic evaluation with respect to these developments will need to be performed in a future study in order to assess the feasibility more concretely.

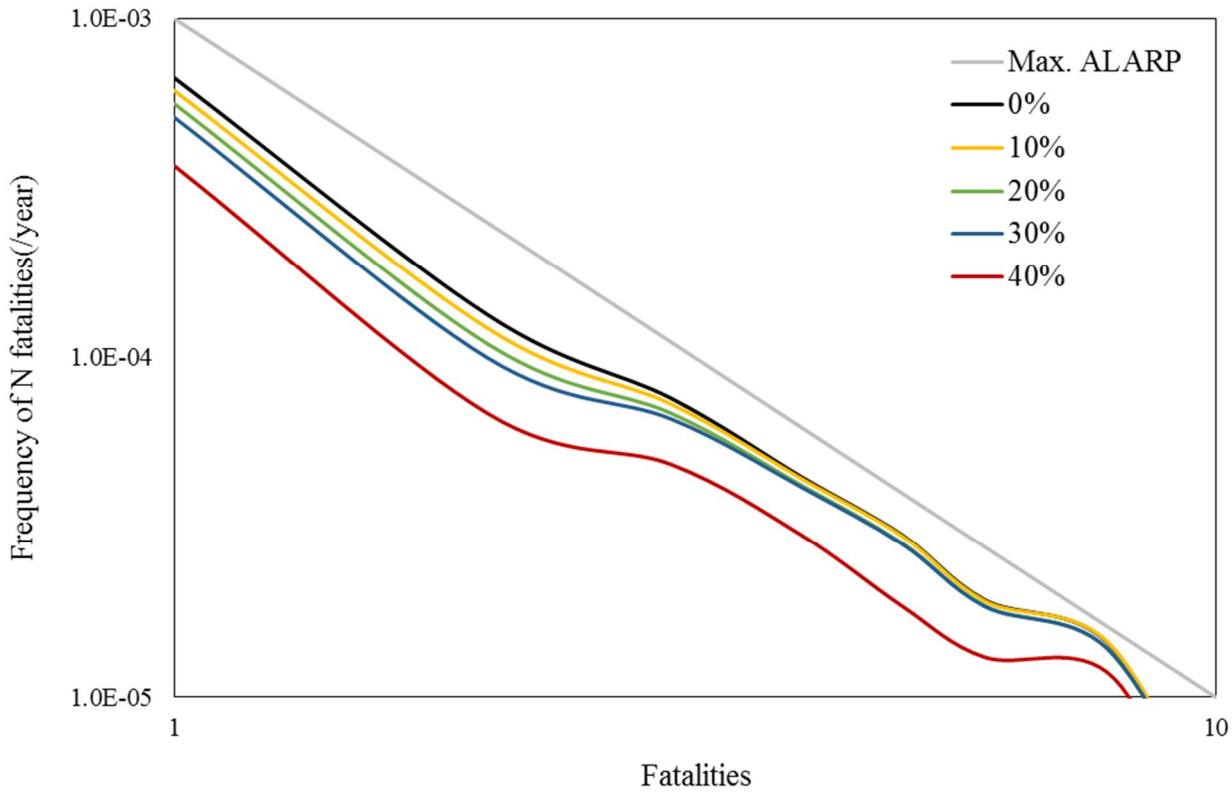

Figure 3-12. Sensitivity analysis with respect to the degree of IS case

3.3. Multi-objective Optimization Including Inherent Safety

Quantitative risk assessment (QRA) of which the main purpose is to evaluate the degree of safety for the designed process or facilities, has played an important part throughout the history of process safety. However, it often requires an expensive cost consuming a long time due to its repetitive nature of the procedure until deciding an acceptable output which satisfies both the risk criteria regulated by each legislative law and the economic feasibility requested by vendors. If the risk could be considered at the preliminary design stage, however, one could avoid this recursive loop caused by intolerable degree of safety. Inherent safety approach is appropriate for such tasks among four fundamental strategies of achieving safety: inherent, passive, active and procedural [26].

Inherent safety approach is one of the systematic strategies to achieve safety in the chemical plant. Unlike external methods, it avoids or reduce hazards inherently through designing a safer process rather than control them through reducing the probability of an accidental event [27]. Hence this approach is often used and applied in the design stage in the way of making alterations to the process design or materials used. It yields the best results when applied during the preliminary design stage [28]. There are six fundamental principles for designing an inherently safe process [29]: (1)Intensification: use smaller quantities of hazardous substances; (2)Substitution: replace chemicals with less hazardous substances; (3)Attenuation: reduce the volumes of hazardous materials, operate at less hazardous conditions; (4)Limitation of effects: design facilities that could minimize the impact of a release of hazardous materials or energy; (5)Simplification: avoid complexities such as

multi-product or multi-unit operations; (6)Error tolerance: make operating errors less likely with robust equipment. Through following these principles, inherently safer design could reduce either the magnitude or the likelihood of an accident so that it would require less layers of protection [26].

For more than a decade, various researches aiming at evaluating the inherent safety level are studied and several systematic approaches to apply it to the chemical process design are developed. They could be classified into largely two categories in evaluating the inherent safety level: one using an inherent safety index they developed according to its usage, and the other using a consequence modeling for directly assessing the outcome effects in case of an accident. The former is relatively easy and fast as the index could be calculated simply with some process parameters but it is susceptible to being meaningless if the index cannot represent the overall process safety. Due to its simplicity, the index-based approach occupies the majority of the associated research field for which extensive literature reviews are provided by Jafari et al. [30] where total 35 indicators are classified into six categories and six estimation approaches are sorted out among 62 literatures.

Leong and Shariff [31] developed an inherent safety index module (ISIM) where the process simulator is integrated to evaluate the inherent safety level based on the operating conditions and stream explosiveness. They then proposed a new index for explosion outcomes called process routed index (PRI) [32] which assesses the severity of hazard in a certain process route based on the mass, energy and combustibility of flammable materials in all process streams. It then can prioritize the inherently safer option among several process routes which produce the same products. PRI was benchmarked against three pioneering indexes for inherent safety

(PIIS [33], ISI [34] and i-Safe [35]) resulting in a close agreement with them. Shariff et al. [36] further developed a process stream index (PSI) which shares the common principle with PRI, but it assesses the safety level for an individual stream not the overall process route. Ortiz-Espinoza et al. [37] combined these two indexes where PRI is used to rank the process alternatives of producing ethylene or methanol with economic and environmental measures and PSI to identify the target streams to be managed for reducing overall process hazards.

Meanwhile relatively few studies are performed for the latter one using consequence modeling as it requires complex theories and equations consuming high computation cost and a long time. Shariff et al. [38] developed an explosion consequence evaluation module called integrated risk estimation tool (iRET) based on TNT equivalence method with TNO correlation one. Similarly, Shariff and Zaini [39] developed a toxic release consequence analysis tool (TORCAT), and later Shariff et al. [40] developed an inherent fire consequence estimation tool (IFCET) to assess the boiling liquid expanding vapor explosion (BLEVE) scenario.

Recently, researchers tried to consider the plant economics in inherent safety design through optimization. Ruiz-Femenia et al. [41] performed a multi-objective optimization for the simple super-structure of monochlorobenzene production process minimizing both the annual plant cost and Dow's fire and explosion index. Later, Vazquez et al. [42] expands the super-structure to complete separation of 4 components, and performed a large-scale multi-objective MILP problem through objective reduction strategies. Eini et al. [43] proposed an optimization procedure that integrates both processing and accident costs from consequence modeling techniques through defining an objective function as the sum of accident costs and

plant lifecycle processing costs. Later Eini et al. [44] developed a multi-objective optimization framework for simultaneously minimizing each cost for a simple refrigeration cycle.

Above studies contributed a lot to the inherent safety design in that they formulated a superstructure for the target process and perform a multi-objective optimization considering inherent safety using consequence modeling or inherent safety indexes. For the first two references [41,42] evaluated the risk through simplified consequence modeling, however, they decided only whether the parallel n trains with 1/n capacity or a single train with full capacity would be better without considering the thermodynamic efficiencies in the heat exchanger which are the critical issue in liquefaction process. Also for the last two references [43,44], as they assessed the inherent safety level of the separation structure using some indexes which cannot consider the accidental situation, the optimization results showed that more distributed structures are prioritized over thermally coupled one in the safety manner even though the more distributed the system is, the more prone it is to be exposed to the accidental releases. Due to those limitations, it is hard for those conclusions to provide reasonable guidelines to the process designers.

In this chapter, two systematic approaches aiming at simultaneously considering the economic feasibility and safety of the process would be proposed: one using inherent safety indexes considering the accidental situations with commercial QRA software and the other directly calculating the risk through rigorous custom modeling. Only the former approach would be performed in this paper while the latter would remain in the future work. As the QRA basically requires a lot of process information including process flow diagram (PFD), piping and

instrumentation diagram (P&ID), equipment counts list, plant layout and manning data etc., if the practicality of each approach is to be verified, it should effectively represent the original QRA method only with limited information available at the preliminary step such as operating conditions of process streams and equipment.

The developed approach is applied to designing an optimal natural gas liquefaction processes as they could verify the effectiveness of the method in that the feasible operating range for the pressure, flowrate and composition of the refrigerant cycles they use are broad enough to see the trade-off relation between economic feasibility and safety. Generally, with higher pressure at which the cycle is discharged from the compressor, less flowrate of the cycle and smaller heat transfer area are required for the same liquefaction but with higher hazards in case of an accident. The structure of a liquefaction process could vary with respect to different refrigeration cycles it uses. In this study, three structures are selected of a single-stage mixed refrigerant process (SMR), pre-cooled process without phase separators (Precooled), or dual-mixed refrigerant process with the precooling refrigerant evaporated at double pressures (DMR). These processes share similar heat transfer structures in producing the same amount and quality of product LNG, only different in the number of multi-stream heat exchangers and that of refrigerant cycles. Due to these similar structures, it could approximate the super-structure of a liquefaction process through expanding its structure from SMR to DMR. Then proposed approach could give reasonable guidelines to the designer who want to decide not only the optimal design conditions but the structure of heat transfer also.

3.3.1. New Decision Making Schemes for Inherent Safety

Inherent Risk Assessment for Design Modification

Inherent risk assessment (IRA) firstly proposed by A. Shariff et al [14,31], is to roughly evaluate the risk inherent to a process owing to the chemical it uses and the process conditions it is operated at in early design stages. The main aim of this method is to reduce or eliminate the root causes of potential hazards in the plant through modifying the process design itself instead of relying on additional safety systems and procedural controls which could often fail. As the risk assessment tool is integrated with process flowsheeting simulator like ASPEN HYSYS providing necessary process data, design modifications based on inherent safety principles could be incorporated in early design stages to enhance the process safety of the plant. The procedure of IRA is quite similar to that of QRA, and the whole decision making scheme which was called 2TISI (Two-tier inherent safety index) by A. Shariff et al. [32] for deciding the final process design is described in Figure 3-13.

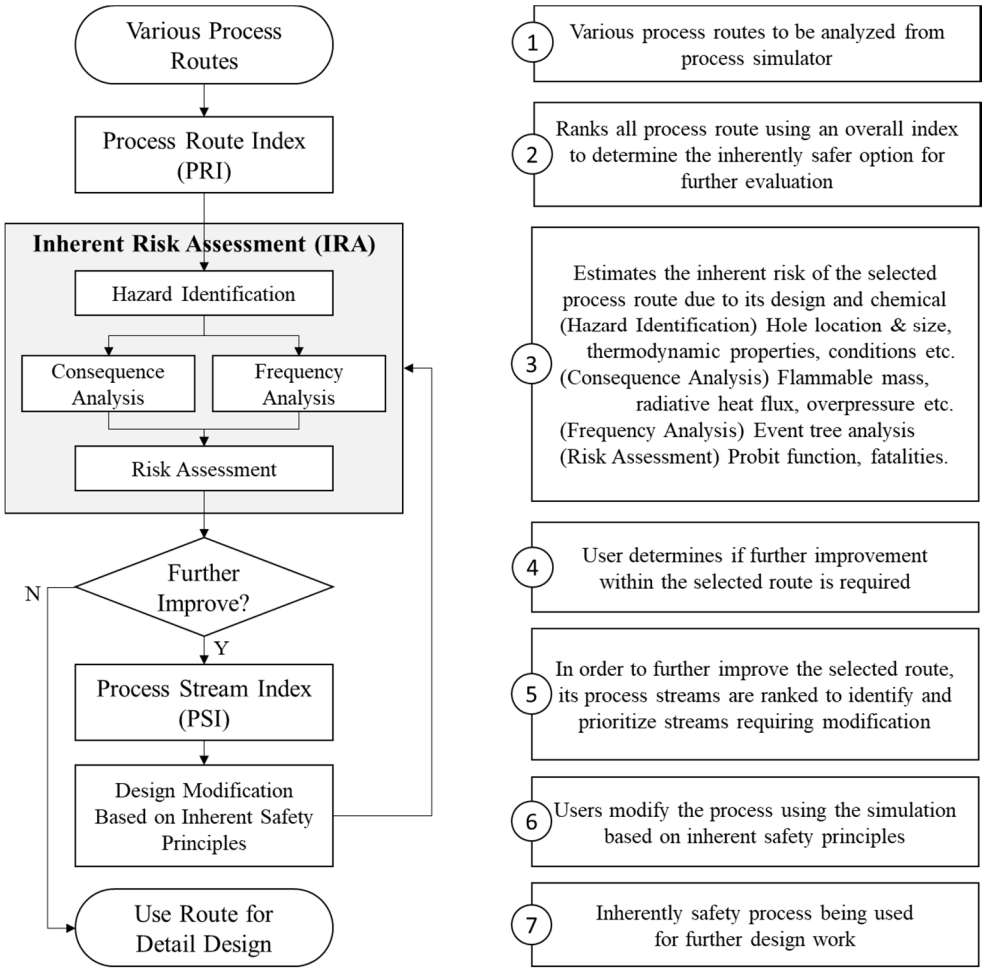

Figure 3-13. The framework of two-tier inherent safety index (2TISI)

In this procedure, two inherent safety indexes are used: one for Process Route Index (PRI) to select an inherently safer option among all possible process routes for further evaluation ahead of IRA, and the other for Process Stream Index (PSI) to target certain process streams with high severity to be modified for further improvement of selected route after the IRA step. These two indexes and IRA could be calculated in a single composite model in Microsoft Excel including a risk assessment model linked with a process simulator where the overall heat & material balances and thermodynamic equations are solved and the results of process conditions are automatically transferred to the composite model. As these two indexes (PRI, PSI) will also be utilized with importance in the new method developed in this study, the definition and derivation of each one is explained in the following.

The PRI is derived based on fundamental process parameters that influence the outcome effect of an explosion [32]. The maximum distance wherein certain damage could be expected is the function of the product of total mass of flammable material in the cloud [kg] and lower heat of combustion [kJ/kg] according to Crowl & Louvar [45]. As the combustibility of the released mixture should also be considered in assessing the explosion hazard, it is included in defining the PRI as in Eq. (3-4)

$$\text{PRI} = f(mass, energy, combustibility) \tag{3-4}$$

From principles of fluid mechanic, amount of mass flowing through a hole in case of a leak is a function of density and pressure differential between the system and surrounding. Then Eq. (3-4) could be expressed with process parameters of density

and pressure like Eq. (3-5)

$$\text{PRI} = f(density, pressure, energy, combustibility) \tag{3-5}$$

The combustibility of a mixture could be expressed as the gap [%] between UFL (Upper flammable limit) and LFL (Lower flammable limit) of individual components. The derivation of that of a mixture from those of individual components and its temperature dependence could be expressed in Eq. (3-6), (3-7), (3-8), and (3-9) by Crowl & Louvar [45].

$$LFL_T = LFL_{25}[1 - \frac{0.75(T-25)}{\Delta H_c}] \tag{3-6}$$

$$UFL_T = UFL_{25}[1 + \frac{0.75(T-25)}{\Delta H_c}] \tag{3-7}$$

where LFL_T, UFL_T = lower and upper flammable limit [%] at temperature, T [C] of a single component; ΔH_C = heat of combustion for the component [kcal/mol]

$$LFL_{mix} = \frac{1}{\sum_{i=1}^{n}(y_i/LFL_i)} \tag{3-8}$$

$$UFL_{mix} = \frac{1}{\sum_{i=1}^{n}(y_i/UFL_i)} \tag{3-9}$$

where LFL_{mix}, UFL_{mix} = lower and upper flammable limit [%] of a mixture; LFL_i, UFL_i = lower and upper flammable limit [%] of a i-th single component among n components; y_i = volume or mole fraction of i-th component in mixture.

As the PRI represents the overall process route, actual value of each property would rather have a form of average value for all process streams and the final

expression could be like Eq. (3-10).

$$\text{PRI} = \bar{\rho} \cdot \bar{P} \cdot \overline{LHV} \cdot \Delta\overline{FL}_{mix}/1\text{E}8 \tag{3-10}$$

where $\bar{\rho}$ = average fluid density [kg/m3] for all process streams; $\bar{P}$ = average pressure [bar]; $\overline{LHV}$ = average mass heating value [kJ/kg]; $\Delta\overline{FL}_{mix}$ = average combustibility of a mixture.

The PSI is the same concept to the PRI except that it represents the explosion hazard of each stream rather than that of overall process route, so that it could compare and prioritize the level of inherent safety of an individual stream against all streams [36]. The definition of PSI is expressed in the following Eq. (3-11).

$$\text{PSI} = \frac{\rho}{\bar{\rho}} \cdot \frac{P}{\bar{P}} \cdot \frac{LHV}{\overline{LHV}} \cdot \frac{\Delta FL_{mix}}{\Delta\overline{FL}_{mix}} \tag{3-11}$$

where $\rho, P, LHV, \Delta FL_{mix}$ in the nominator are the associated properties of each stream.

All the parameters in Eq. (3-10) and (3-11) could be obtained directly from process simulator so that these indexes could be automatically calculated with process simulation.

New Decision Making Schemes for Inherently Safer Process Design using Multi-objective Optimization

Previous researches dealing with inherent risk assessment mainly focused on the design modifications fast and easily through assessing risk while maintaining the existing QRA methodology and using some indexes or custom modeling with certain parameters related to process operation or facilities etc. automatically transferred from process simulation However those suggestions for the design modification could be unreasonable as these approaches unwillingly excluded the dimension of the equipment which is the key factor for the risk assessment. For example, a pipeline with lower hazard in terms of inherent safety could be most risky equipment among overall process if its length is longer enough with lots of flanges and valves which cannot be identified in the PFD, even in the P&ID.

Due to this limitation, the reasonable way of considering inherent safety in the preliminary design stage is to focus on providing some practical guidelines through multi-objective optimization with economic feasibility, not suggesting modifications to the existing designs as IRA tries to do. Even the recent multi-objective optimization works concerning about similar considerations to this study are lack of practicability as mentioned earlier in that they missed key factors of either the process design or the risk assessment.

The new decision making schemes for designing an inherent safer process this study proposes are the improved versions from the original IRA, and they differ each other in defining an objective function for inherent safety whether it is the

PRI value for representing the risk for hazardous equipment identified from PSI analysis (Figure 3-14) or the fatality value [1/yr] directly calculated from risk assessment modeling including consequence analysis and frequency estimation (Figure 3-15). The former could be easy and fast in giving a pareto optimal points but it could be hard to validate the suitability of the defined index for representing the risk. For the latter, optimization results could be led to the final decisions but there could be some problems of the accuracy of consequence modeling and high cost of computation load and time. In this study only the former approach will be applied to the natural gas liquefaction processes and the other will remain in the future work.

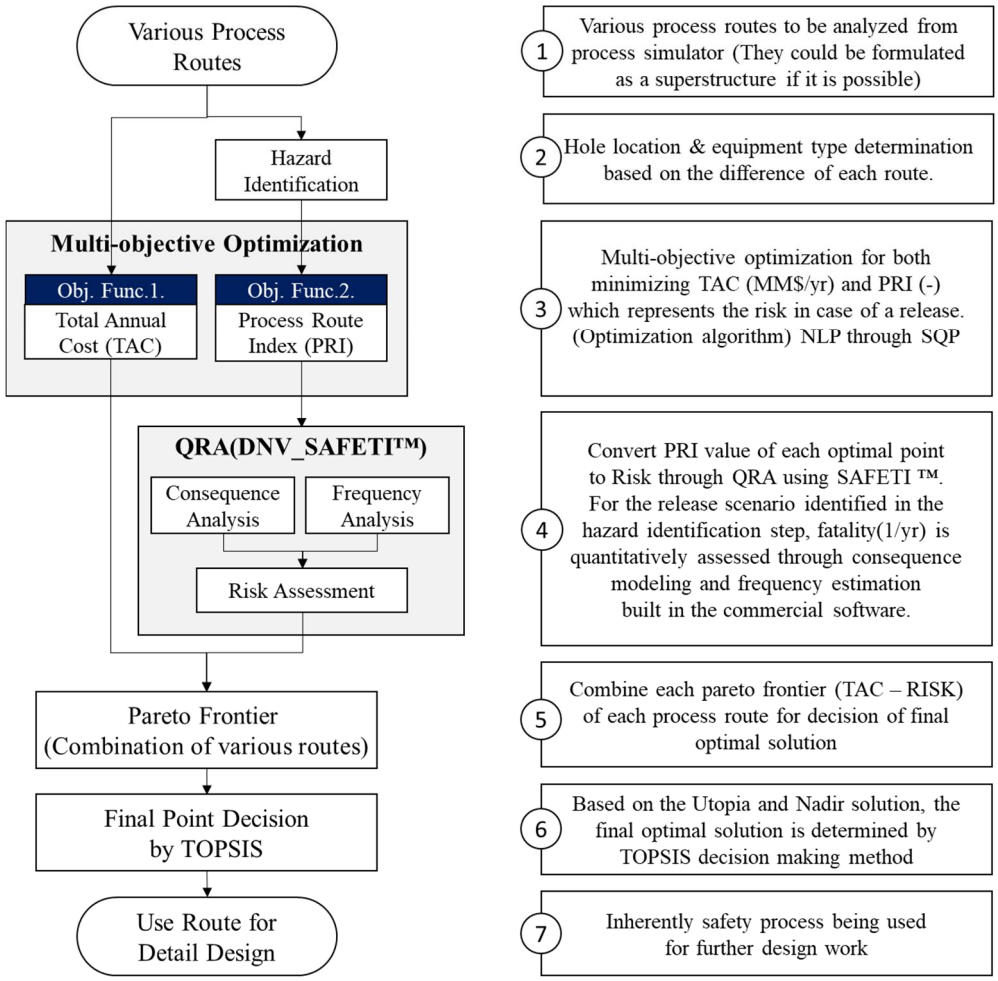

Figure 3-14. The framework of proposed decision making scheme – 1 (PRI)

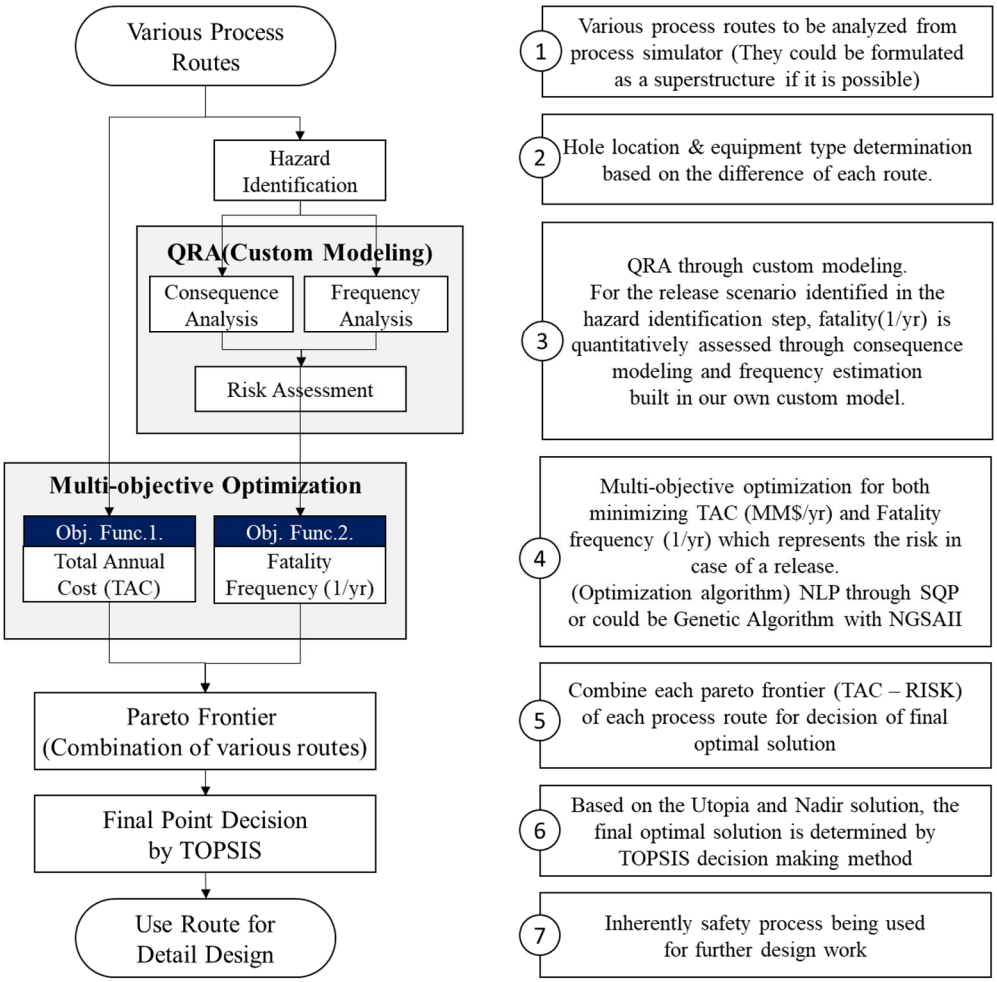

Figure 3-15. The framework of proposed decision making scheme – 2 (FATALITY)

3.3.2. Superstructure for Natural Gas Liquefaction Process

Simple Liquefaction Process

A simple natural gas liquefaction process of 3mtpa using single-stage mixed refrigerant (SMR) shown in Figure 3-16 [46] produces LNG and some flash gas from natural gas feed gas of which the physical conditions are listed in Table 3-8. Especially the mixed refrigerant (MR) conditions are optimized values maximizing thermodynamic efficiency of the process. As the pressurized MR stream is expanded at the throttling valve, V-1, it provides the cryogenic heat source to the cold-box for liquefying natural gas. As the pressure outlets of the compressor and V-1 are 17.6bar and 1.6bar respectively from the optimal solutions, for lowering irreversibility in the compressor the compressor is operated by two-stage with one after-cooler which is not depicted in Figure 3-16. Thermodynamic efficiency could be maximized by minimizing specific power [kWH/kg_LNG] or maximizing exergy efficiency [%] which were defined in chapter 2. As a result, 1kg LNG could be produced consuming 0.28kWH with overall exergy efficiency of 48.39% in the SMR process.

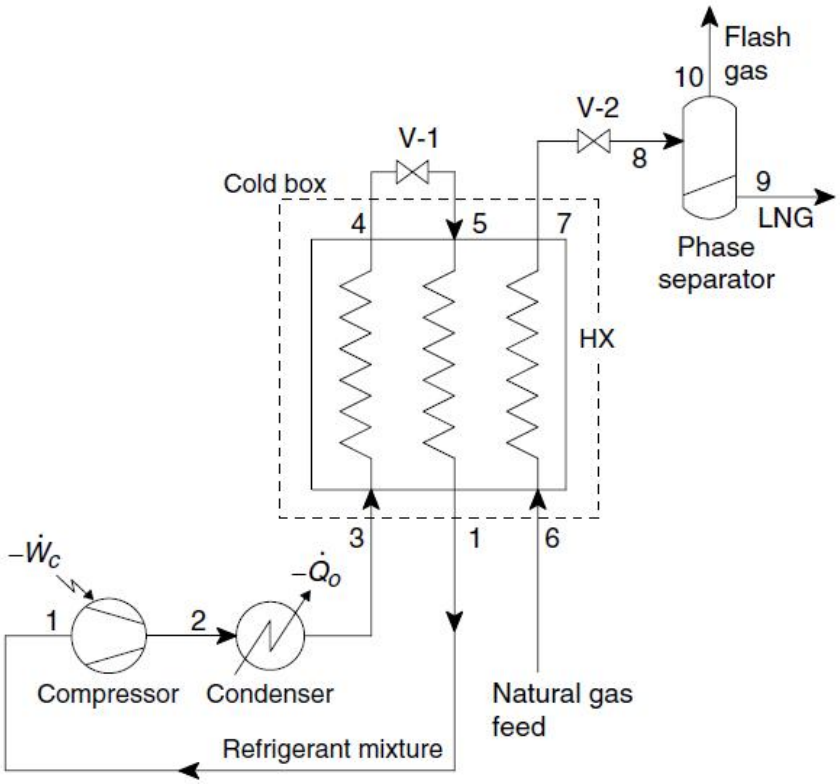

Figure 3-16. Single-stage mixed refrigeration process without a phase separator [46]

Table 3-8. Main stream data for 3mtpa SMR process

		NG FEED	Mixed Refrigerant		LNG (3mtpa)
			Condenser outlet	V-1 outlet	
Pressure	bar	65	17.6	1.6	1
Temperature	K	300.00	310.00	110.00	107.18
Flowrate	kg/s	114	541	541	106
	kmol/h	22549	49687	49687	21001
Composition					
N2	mol/mol	0.0400	0.0680	0.0680	0.0162
C1	mol/mol	0.8750	0.2291	0.2291	0.8926
C2	mol/mol	0.0550	0.3294	0.3294	0.0591
C3	mol/mol	0.0210	0.0904	0.0904	0.0223
nC4	mol/mol	0.0050	0.0494	0.0494	0.0054
iC4	mol/mol	0.0030	0.0000	0.0000	0.0032
iC5	mol/mol	0.0010	0.2333	0.2333	0.0011

Structure Expansion to Complex Process for Approximating a Superstructure

In order for deciding an optimal structure of heat transfer in producing LNG, the sole powerful way would be to formulate a single superstructure encompassing possible liquefaction processes. The superstructure formulation could be somewhat easily applied to the parallel systems like reactors or separators which would not affect the internal thermodynamic behaviors largely. For the liquefaction process, however, as the structure of heat transfer differs by the number of heat exchangers or that of cycles, thermodynamic aspects in the overall cycle behavior changes a lot. Also these liquefaction structures could not be simply combined as a superstructure as they operate in a sequential manner not the parallel.

In this study, the liquefaction structure is expanded as in Figure 3-17 from SMR with a single multi-stream heat exchanger (MSHE) and a single MR cycle, to the Precooled process with two MSHEs and two MR cycles, finally to the DMR process with 4 MSHEs and two MR cycles.

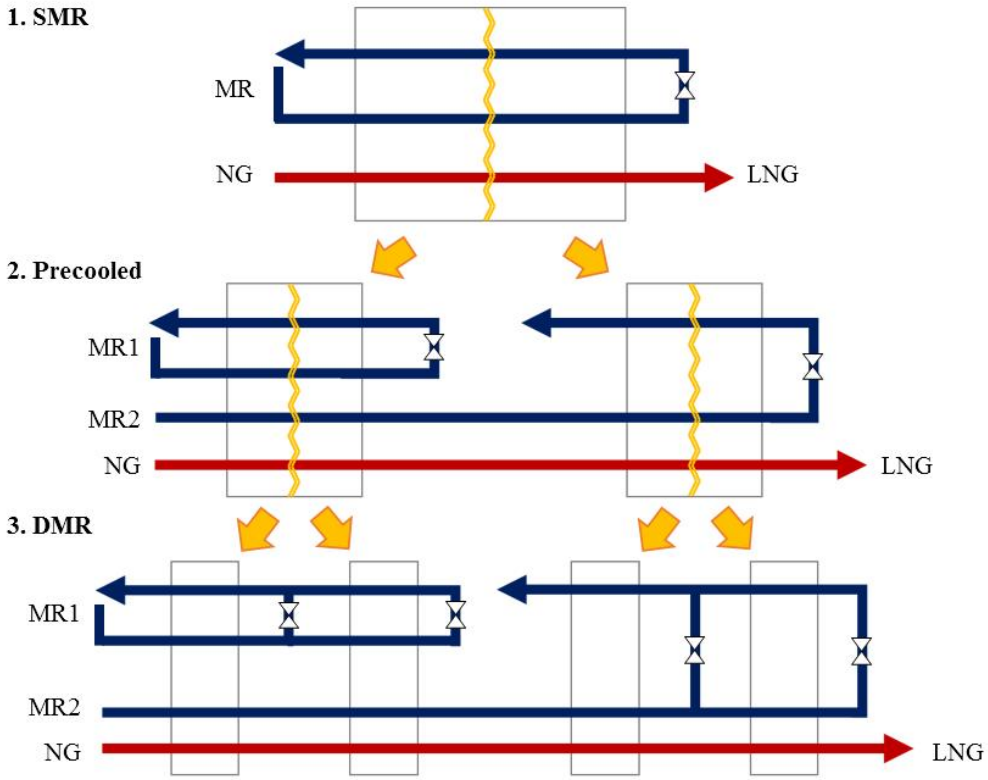

Figure 3-17. Structure Expansion from SMR to Precooled to DMR

As the simple SMR structure is divided to others, thermodynamic efficiency in the overall liquefaction would be expected to increase as more sophisticated heat transfer would be possible at each divided section of MSHE with a different refrigerant. The actual results would be dealt in the following section of the single optimization for maximizing the thermodynamic efficiency of each process.

In the inherent safety aspect, however, the fact that one single MSHE is divided to two or four means they become more prone to be exposed to the accidental release with larger surface area for each equipment. For example, two MSHEs need two throttling valves and two MR cycles need two independent compressor sections with additional pipelines, which all affect the release scenarios and event frequencies. Detailed consideration for these expectations would also be discussed in later section of hazard identification.

The additional PFDs of Precooled and DMR process are shown in Figure 3-18 and Figure 3-19 [46] and main stream data after optimization are listed in Table 3-9 and Table 3-10.

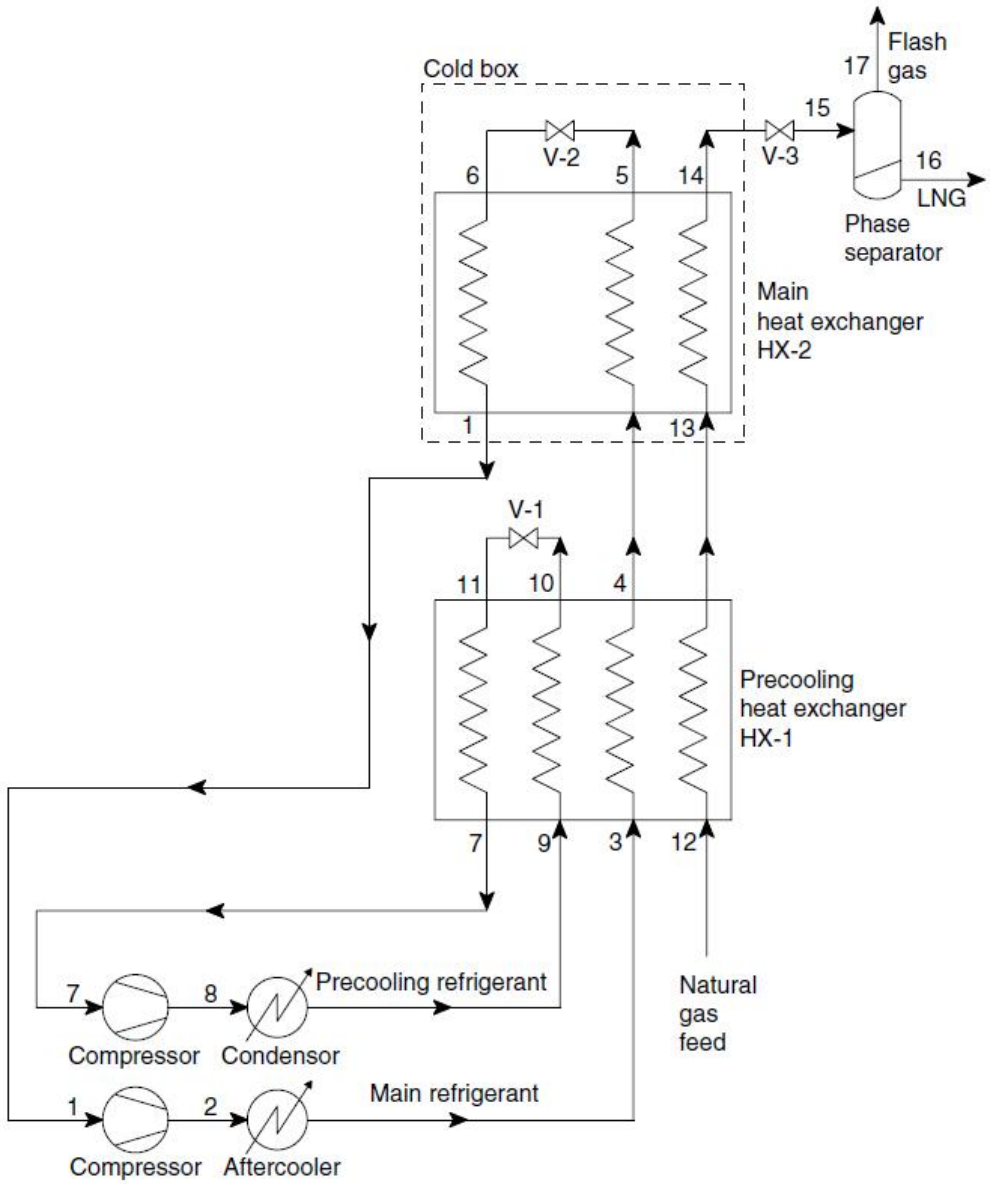

Figure 3-18. Pre-cooled process without phase separators [46]

Table 3-9. Main stream data for 3mtpa Precooled process

		NG FEED	Mixed Refrigerant 1		Mixed Refrigerant 2		LNG
			Cond outlet	V-2 outlet	Cond outlet	V-1 outlet	
Pressure	bar	65.0	23.7	1.8	17.3	1.6	1.0
Temperature	K	300.00	310.00	108.95	310.00	219.56	107.18
Flowrate	kg/s	114	197	197	326	326	106
	kmol/h	22549	26030	26030	25113	25113	21001
Composition							
N2	mol/mol	0.04	0.0768	0.0768	0.0000	0.0000	0.0162
C1	mol/mol	0.875	0.3447	0.3447	0.0000	0.0000	0.8926
C2	mol/mol	0.055	0.4228	0.4228	0.2947	0.2947	0.0591
C3	mol/mol	0.021	0.1557	0.1557	0.2264	0.2264	0.0226
nC4	mol/mol	0.005	0.0000	0.0000	0.4789	0.4789	0.0054
iC4	mol/mol	0.003	0.0000	0.0000	0.0000	0.0000	0.0032
iC5	mol/mol	0.001	0.0000	0.0000	0.0000	0.0000	0.0011

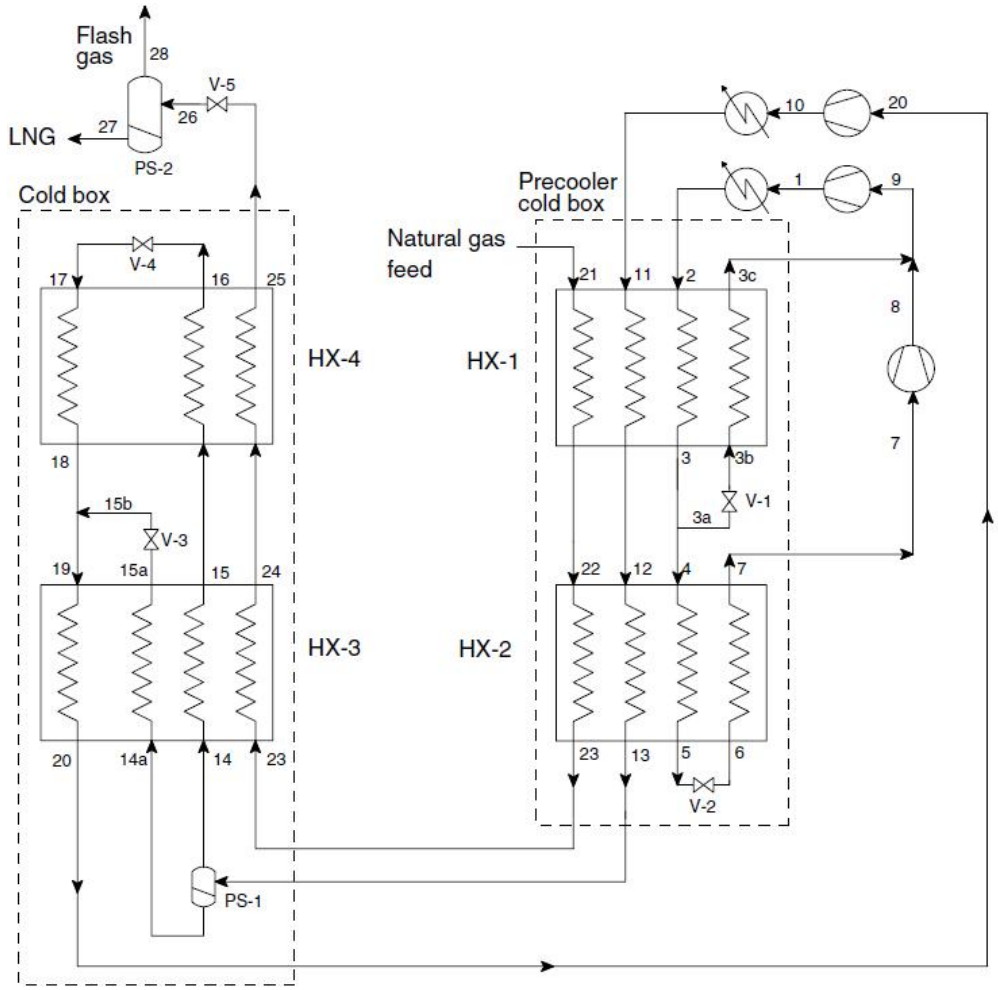

Figure 3-19. Dual mixed refrigerant process with the precooling refrigerant evaporated at different pressures [46]

Table 3-10. Main stream data for 3mtpa DMR process

		NG FEED	Mixed Refrigerant 1			Mixed Refrigerant 2			LNG (3mtpa)
			Cond outlet	V-1 outlet	V-2 outlet	Cond outlet	V-3 outlet	V-4 outlet	
Pressure	bar	65.0	19.4	5.0	1.6	31.4	3.0	3.0	1.0
Temp	K	300	310	254	220	310	152	113	107
Flow-rate	kg/s	114	374	224	150	215	146	68	106
	kmol/h	22549	31389	18802	12587	30327	18197	12130	21001
Composition									
N2	mol/mol	0.040	0.00	0.00	0.00	0.064	0.02	0.14	0.02
C1	mol/mol	0.875	0.00	0.00	0.00	0.43	0.27	0.69	0.89
C2	mol/mol	0.055	0.27	0.27	0.27	0.39	0.53	0.16	0.06
C3	mol/mol	0.021	0.54	0.54	0.54	0.12	0.19	0.01	0.02
nC4	mol/mol	0.005	0.19	0.19	0.19	0.00	0.00	0.00	0.005
iC4	mol/mol	0.003	0.00	0.00	0.00	0.00	0.00	0.00	0.003
iC5	mol/mol	0.001	0.00	0.00	0.00	0.00	0.00	0.00	0.001

Single Optimization for Thermodynamic Efficiency

Three liquefaction processes mentioned above are optimized for a single objective function of specific power [kWH/kg_LNG] and compared with each other in this section. Optimization is performed through the sequential quadratic programming for the complex non-linear problems using gProms Processbuilder v.1.1 as the same way that in chapter 2 did. Thermodynamic efficiency of each process could be compared intuitively through overall composite curves of MSHEs which show the heat transfer between hot and cold streams in them as in Figure 3-20. Generally, as the temperature gap between hot and cold stream curves is getting narrower, the exergy efficiency of MSHEs becomes higher. Also with smaller amount of heat flow for the required heat transfer, cycle compressors consume less power.

In Figure 3-20, as the MSHEs is divided into more sections, temperature gap and total amount of heat flow decrease which would result in lower specific power later. SMR transfer the heat around 395MW between hot and cold streams, 305MW for Precooled and 297MW for DMR process. This trend is because each section could be optimized independently with different properties of refrigerants for maximizing thermodynamic efficiency.

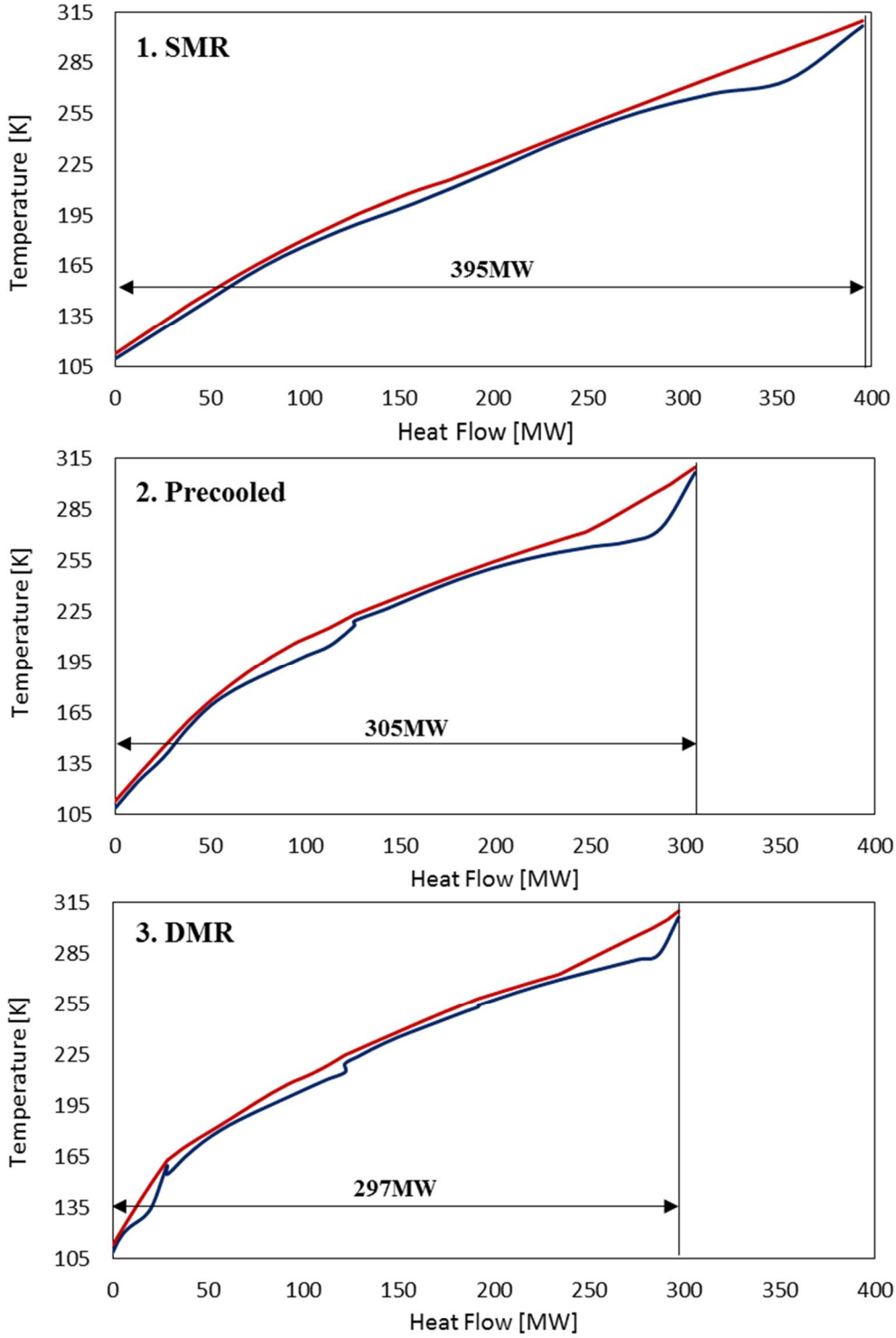

Figure 3-20. Overall composite curves in MSHEs of each process

In overall exergy analysis for each process, as expected earlier, DMR has lowest specific power of 0.26kWH/kg_LNG (SMR of 0.28; Precooled of 0.27) and highest exergy efficiency of 52.17% (SMR of 48.39; Precooled of 50.63) as shown in Figure 3-21.

For the process components of MSHEs, air-coolers, compressors, and valves, tables from Table 3-11 to Table 3-14 summarized the performances of unit operations and associated exergy destructions (or irreversibility) and efficiencies for each process. Exergy destructions of process components for each process are compared in Figure 3-22 which shows that the difference in irreversibility of air-coolers followed by MSHEs between each other accounts the most for that in total irreversibility.

In the following section, potential hazard in each process would be identified for evaluating the inherent safety level of each process before performing a multi-objective optimization.

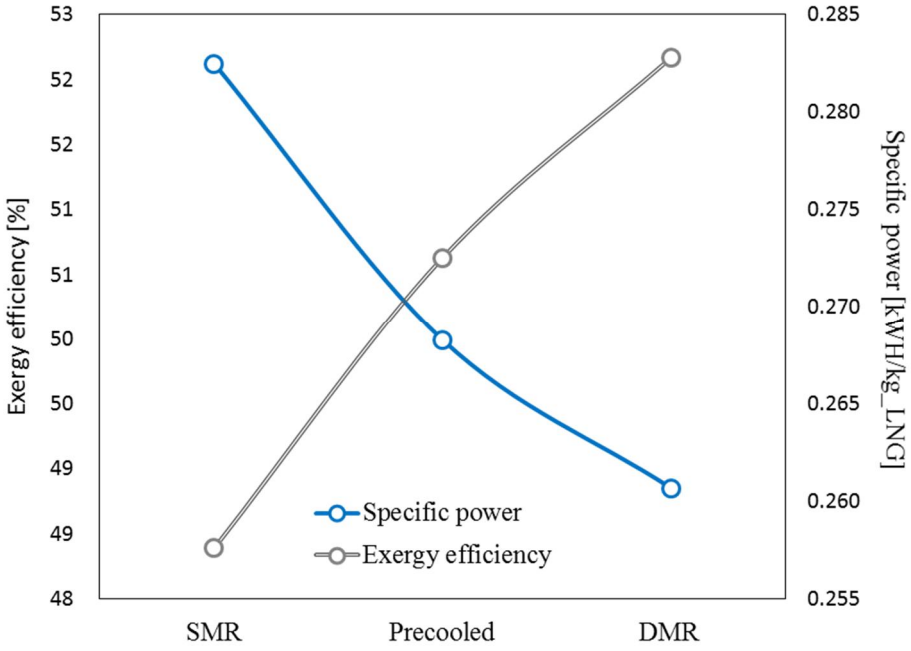

Figure 3-21. Thermodynamic efficiencies of each process

Table 3-11. Exergy Analysis of MSHEs for each Process

Exergy analysis MSHE		LMTD [K]	MTA [K]	Heat flow [MW]	E.D.* [MW]	E.E.* [%]	Number of sides
SMR	HX1	3.0	3.0	395.17	15.90	95.98	3
	Total			395.17	15.90	95.98	3
Precooled	HX1	3.4	3.0	179.35	6.23	96.53	4
	HX2	5.2	3.0	125.83	7.98	93.66	3
	Total			305.18	14.20	95.09	7
DMR	HX1	3.8	3.0	105.03	3.02	97.19	4
	HX2	5.0	3.0	69.97	1.44	97.94	4
	Hx3	9.2	3.0	93.24	4.53	95.14	4
	HX4	3.7	3.0	28.61	3.80	86.73	3
	Total			296.85	12.78	94.25	19

* E.D. = Exergy destruction, E.E. = Exergy efficiency

Table 3-12. Exergy Analysis of Air Coolers for each Process

Exergy Analysis		Fan power	Air flow	T_air	ΔP	Eff	E.D.*	E.E*
Air cooler		[kW]	[kg/s]	[K]	[Pa]	[%]	[MW]	[%]
SMR	AC1	125	1753	328.15	50	0.7	3.52	94.09
	AC2	340	4756	328.15	50	0.7	9.80	90.27
	Total	465	6508	-	-	-	13.32	92.18
Precooled	MR1_AC1	41	581	328.15	50	0.7	0.99	98.06
	MR1_AC2	27	376	323.14	50	0.7	0.35	99.37
	MR2_AC1	77	1075	328.15	50	0.7	2.17	93.47
	MR2_AC2	311	4359	328.15	50	0.7	7.79	83.61
	Total	456	6391	-	-	-	11.29	93.63
DMR	MR1_AC1	383	5364	328.15	50	0.7	7.91	87.68
	MR2_AC1	30	426	319.71	50	0.7	0.35	99.50
	MR2_AC3	40	561	328.15	50	0.7	0.81	98.77
	Total	454	6352	-	-	-	9.07	95.32

* E.D. = Exergy destruction, E.E. = Exergy efficiency

Table 3-13. Exergy Analysis of Compressors for each Process

Exergy Analysis		P_in	P_out	Ratio	Eff*	Work	E.D.**	E.E.**
Compressor		[bar]	[bar]		[%]	[MW]	[MW]	[%]
	C1	1.6	5.0	3.09	81.24	51.83	8.67	83.27
SMR	C2	5.0	17.6	3.51	81.53	55.66	9.00	83.84
	Total					107.49	17.67	83.55
	MR1_C1	1.8	17.0	9.38	83.39	43.57	7.58	82.61
	MR1_C2	17.0	23.7	1.39	80.59	7.19	1.29	82.01
Precooled	MR2_C1	1.6	6.0	3.74	81.29	30.04	5.02	83.28
	MR2_C2	6.0	17.3	2.88	81.37	21.29	3.57	83.24
	Total					102.09	17.46	82.78
	MR1_C1	1.6	5.0	3.18	81.42	10.83	2.16	80.07
	MR1_C2	5.0	19.5	3.88	81.7	36.14	5.83	83.87
DMR	MR2_C1	3.0	24.0	8.01	83.41	45.62	8.07	82.31
	MR2_C2	24.0	31.4	1.31	80.52	6.60	1.20	81.84
	Total					99.19	17.26	82.02

* Eff = Polytrophic efficiency
** E.D. = Exergy destruction, E.E. = Exergy efficiency

Table 3-14. Exergy Analysis of Valves for each Process

Exergy Analysis		Pressure drop	E.D.*	E.E.*
Valve		[bar]	[MW]	[%]
SMR	V1	15.9	4.66	93.10
	V2	64.0	4.17	93.31
	Total		8.83	93.21
Precooled	V1	15.7	1.12	95.62
	V2	21.9	2.39	94.52
	V3	64.0	4.17	93.31
	Total		7.68	94.49
DMR	V1	3.4	0.68	92.56
	V2	14.4	0.61	96.10
	V3	21.0	2.06	92.27
	V4	7.4	1.03	94.57
	V5	64.0	4.17	93.31
	Total		8.55	93.76

* E.D. = Exergy destruction, E.E. = Exergy efficiency

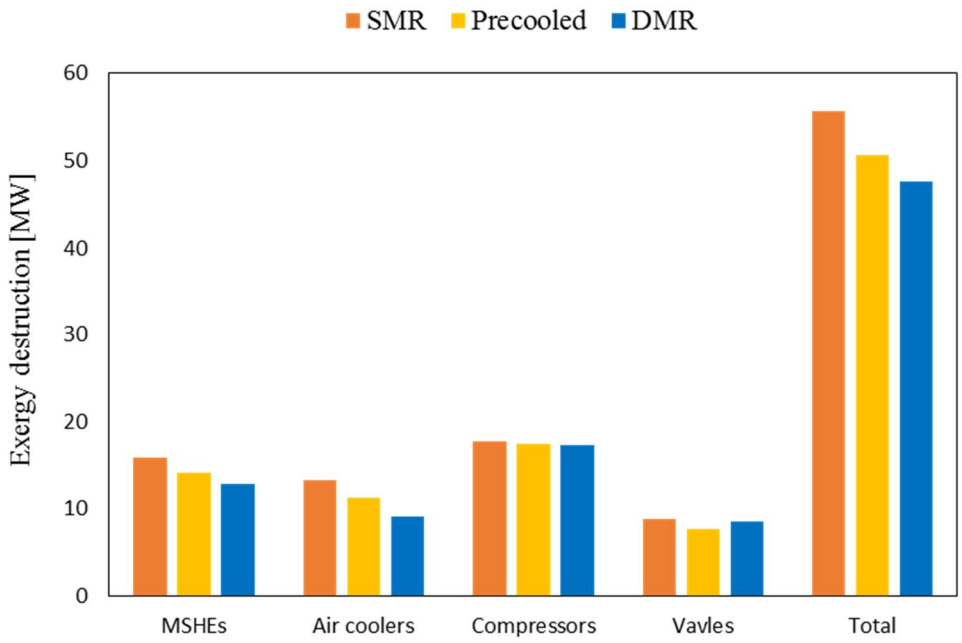

Figure 3-22. Exergy destructions of process components for each process

3.3.3. Multi-objective Optimization

Total Annual Cost (TAC) Estimation for Objective Function1.

Even though the specific power we analyzed before could effectively evaluate the thermodynamic efficiency of a process and could be reasonable criteria for comparing the operating expenditure of each process in producing the same products. However, if we consider it as one of multi-objective functions and the other function is the PRI as we defined before, there could be infinite points having different PRI values with the same value of specific power as shown in Figure 3-23 for SMR process. This is caused by the relation between refrigerant pressure and heat transfer area as listed in Table 3-15. As the MR pressure decreases from 18bar to 9bar, mass flowrate and total heat flow in MSHE varies with different specific heat capacity, resulting in the trend shown in the figure. In terms of PRI, pressure term dominates its value when each case shares almost similar properties of MR. Meanwhile in terms of TAC, with same feed gas and product values, total heat transfer dominates its value due to the expensive cost of MSHE.

Hence hereinafter the TAC is designated as the first objective function in the multi-objective optimization. The estimation method of TAC is referenced by Wang et al. [47].

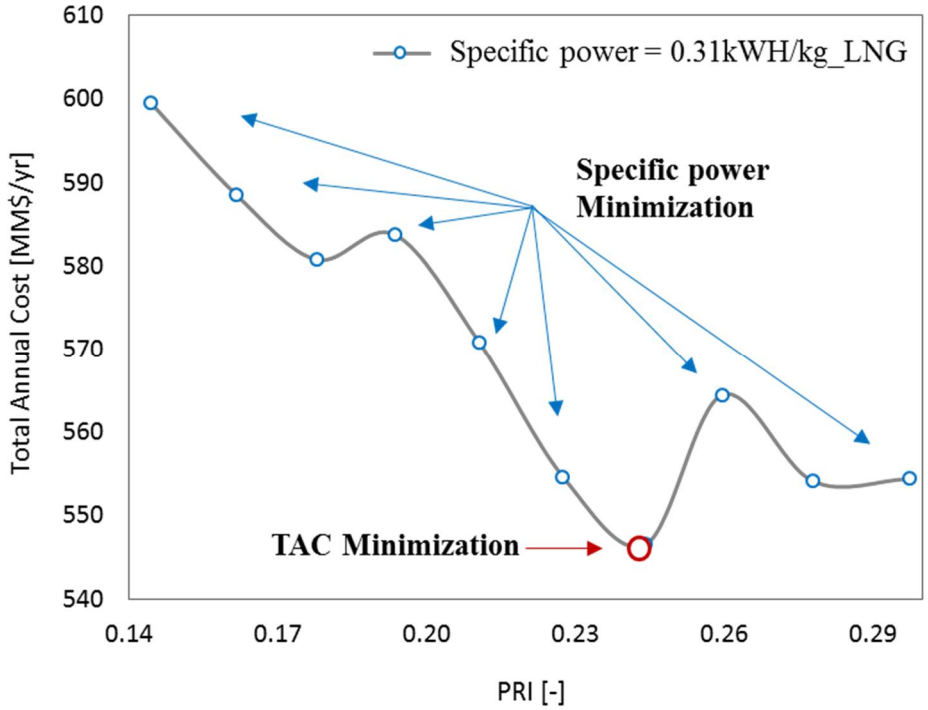

Figure 3-23. Optimization points with different PRI values and same specific power

Table 3-15. Optimization points with different PRI values and same specific power

Specific power	PRI	MR(V_in)		HX			COST		
		P	Mass flow	Heat Flow	LMTD	UA	OPEX	CAPEX	TAC
kWH/ kg_LNG	-	bar	kg/s	MW	K	kJ/s-K	MM$/yr	MM$/yr	MM$/yr
0.31	0.30	18	571	419	3.0	16.5	326	228	554
0.31	0.28	17	592	433	3.1	16.5	326	228	554
0.31	0.26	16	618	454	3.0	18.1	326	238	564
0.31	0.24	15	633	462	3.6	15.3	326	220	547
0.31	0.23	14	603	441	3.2	16.6	326	229	555
0.31	0.21	13	671	491	3.1	19.2	326	245	571
0.31	0.19	12	729	534	3.0	21.2	326	258	584
0.31	0.18	11	765	559	3.2	20.8	326	255	581
0.31	0.16	10	778	567	3.1	21.9	326	262	589
0.31	0.14	9	820	596	3.0	23.7	326	273	599

Defining PRI for Objective 2 through Hazard Identification (HAZID) using PSI.

In this section, target streams of high severity are selected for defining PRI index and release locations of accidental release in quantitatively assessing the risk later. Generally, in QRA, the hazard identification (HAZID) starts with dividing the whole process into subsections based on the major process components like separators which normally contain large amount of gas or liquid. In each subsection, the worst case scenario is defined based on stream properties and operating conditions. For example, the discharge stream of a compressor is regarded as a worse scenario than the suction stream due to the pressure and temperature conditions. Then the HAZID counts several equipment in each subsection like 150m of 7″-12″ pipework with 70 numbers of 7″-12″flanges, 30 numbers of 7″-12″ manual valves and 1 centrifugal compressor (conns > 150mm). This parts count has an important role in assessing risk as it is directly related to the event frequency.

For evaluating the inherent safety level at the preliminary design stage, however, this parts count is not possible. To overcome this limitation, we defined the possible process routes as the Precooled and DMR processes which have similar structures with SMR as they are all expanded from it. Hence the HAZID can only consider the difference between each other in identifying the release location, assuming that other parts have almost the same number and dimension resulting in the same event frequency. For example, from SMR to Precooled, as the single MSHE is divided into two MSHEs, one additional throttling valve between MSHEs is counted as a new possible release location. Also, as one additional MR cycle is operated in the Precooled, it generates one additional release location near the compressors.

In this chapter, firstly PSIs for all streams in each process are calculated for identifying the worst case scenario, and the streams with high value of PSI (red, range and/or blue in Figure 3-24) which are regarded as having high severity are firstly targeted in defining PRI. This could make the optimization algorithm focus on these streams in lowering the potential risk. Besides these identified severe streams, in order to consider the additional release locations generated when Precooled and DMR are expanded, throttling valve inlet streams and compressor outlet streams of high pressures are additionally included in calculating PRI even though they have relatively low values of PSI.

In Figure 3-24, for SMR the "V_in" stream is most severe in terms of PSI so that this stream is included in defining PRI with additional "Comp_out" stream. For Precooled process, "V2_in" is most severe followed by "V1_in" and "MR2_AC_out". PRI for this process is defined by theses streams with additional "MR1_Comp_out" and "MR2_Comp_out". For DMR process, "V4_in", "V3_in", "PS_v_HX3_out", "PS_liquid", "V2_in", and "V1_in" are selected with additional "MR1_C1_out", "MR1_C2_out", and "MR2_C2_out".

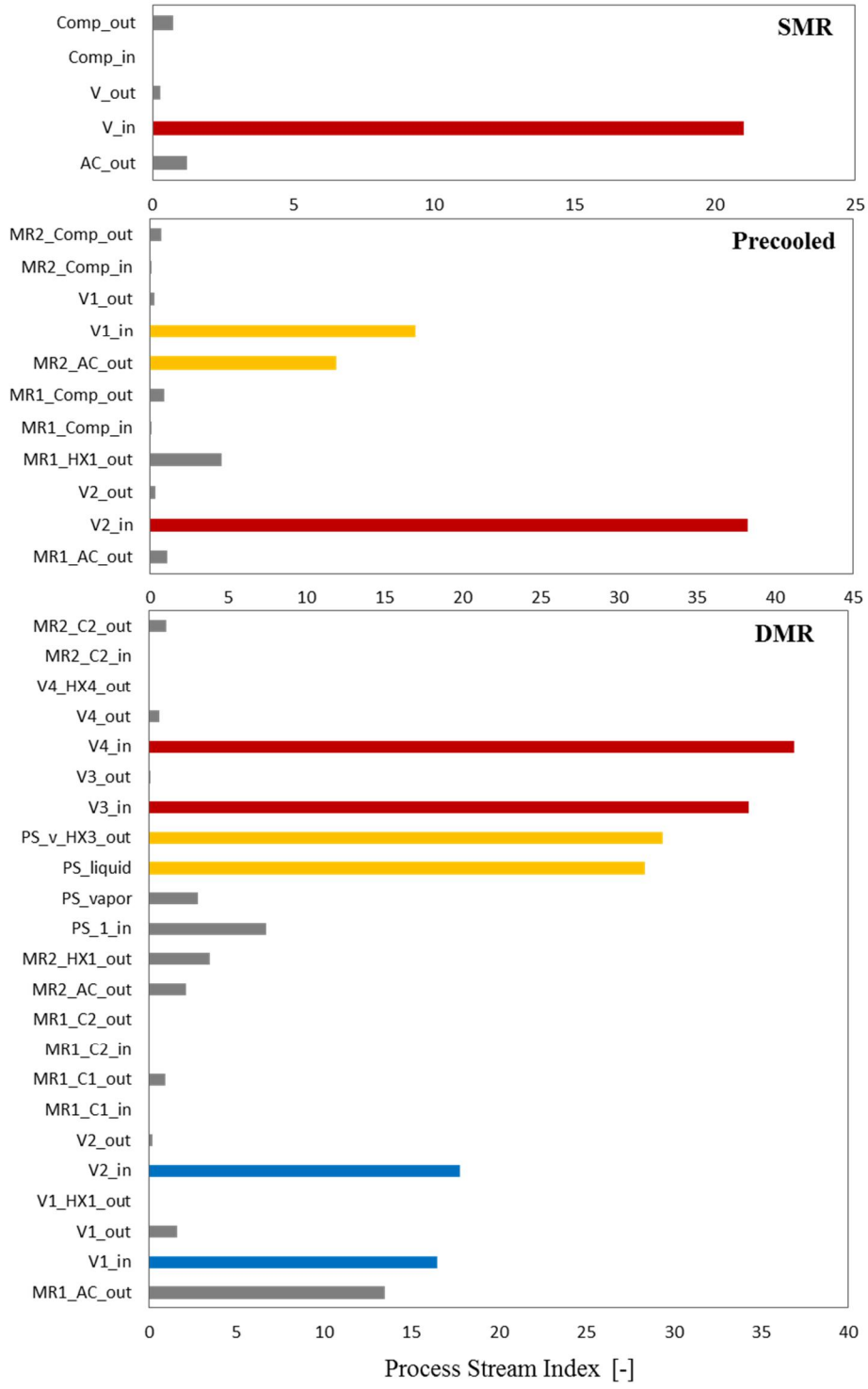

Figure 3-24. PRI of the streams in each process

Fitness function with Weighted Sum Approach

Fitness function of our multi-objective optimization is formulated through weighted sum approaches with assigned scalar weights, ω_i. This method allows the multi-objective optimization problem to be cast as a single objective mathematical optimization problem like Eq. 3-12 [48].

$$\min \sum_{i=1}^{k} \omega_i f_i'(x) \quad \text{s.t.} x \in \Omega \tag{3-12}$$

where $\omega_i \geq 0, \forall i = 1, \ldots, k$ and $\sum_{i=1}^{k} \omega_i = 1$. $f_i'(R^n \rightarrow R)$ is the i-th normalized objective function $f_i(R^n \rightarrow R)$ and $\Omega(\in R^n)$ is the feasible region. k = 2 for this problem.

Each objective function is normalized by the differences of optimal values in the Nadir (negative-ideal) and Utopia (positive-ideal) points that give the length of the intervals where the optimal objective functions vary within the Pareto optimal set.

$$z_i^U = f_i\left(x^{[i]}\right) \quad where\ x^{[i]} = argmin_x\{f_i(x): x \in \Omega\} \tag{3-13}$$

$$z_i^N = max_{(1 \leq j \leq k)}\left(f_i\left(x^{[j]}\right)\right), \qquad \forall i = 1, \ldots, k \tag{3-14}$$

$$f_i'(x) = \frac{f_i(x) - z_i^U}{z_i^N - z_i^U} \tag{3-15}$$

where z^U, z^N are Utopia and Nadir points respectively.

Since the two objective functions (TAC, PRI) we defined compete with each other, there is no unique solution that optimizes both objectives simultaneously. An optimal solution in multi-objective optimization is a solution where there is no other feasible solution which improves at least one objective function value without deteriorating any other objective. This is the notion of Pareto optimality [48]. A

decision vector $x^* \in \Omega$ is Pareto optimal if there exists no another $x \in \Omega$ such that $f_i(x) \leq f_i(x^*)\ \forall i = 1, \ldots, k\ and\ f_j(x) < f_j(x^*)$ for at least one index j.

Firstly, each objective function is solely minimized for determining the Utopia and Nadir solutions. Then with the equally spaced weight factors from 0 to 1, the fitness function is optimized finding the Pareto optimal solutions. As in this study the optimization problem is solved through the NLP-SQP method using commercial software, the weight factors are manually designated and updated based on the distribution of optimal points from previous optimization step. The final results of Pareto optimal set for each process are listed in Table 3-16 and plotted in Figure 3-25.

Table 3-16. Pareto frontier with PRI for each process

Number of points	SMR				Precooled				DMR			
	A*		N**		A*		N**		A*		N**	
	TAC	PRI	F1	F2	TAC	PRI	F1	F2	TAC	PRI	F1	F2
1	613	0.71	0.00	1.00	583	0.41	0.00	1.00	580	0.43	0.00	1.00
2	615	0.54	0.02	0.75	585	0.37	0.02	0.89	587	0.38	0.09	0.79
3	617	0.50	0.04	0.69	586	0.31	0.03	0.76	588	0.37	0.10	0.77
4	620	0.43	0.06	0.57	588	0.30	0.05	0.72	594	0.34	0.18	0.65
5	627	0.34	0.11	0.44	595	0.24	0.11	0.57	595	0.34	0.19	0.64
6	630	0.31	0.14	0.40	599	0.22	0.14	0.54	600	0.29	0.25	0.48
7	633	0.28	0.17	0.35	605	0.19	0.19	0.47	604	0.26	0.31	0.35
8	639	0.24	0.21	0.29	612	0.16	0.25	0.38	612	0.22	0.41	0.22
9	655	0.16	0.34	0.16	618	0.13	0.30	0.32	614	0.22	0.43	0.20
10	664	0.13	0.42	0.13	624	0.11	0.35	0.27	624	0.19	0.57	0.10
11	687	0.10	0.60	0.08	633	0.08	0.43	0.20	635	0.18	0.70	0.06
12	706	0.09	0.76	0.05	642	0.07	0.50	0.16	643	0.17	0.81	0.03
13	723	0.06	0.90	0.01	655	0.03	0.61	0.08	658	0.17	1.00	0.00
14	735	0.05	1.00	0.00	673	0.01	0.77	0.03				
15					697	0.00	0.97	0.00				
16					700	0.00	1.00	0.00				

*A: Actual objective function values
**N: Normalized objective function values [48]

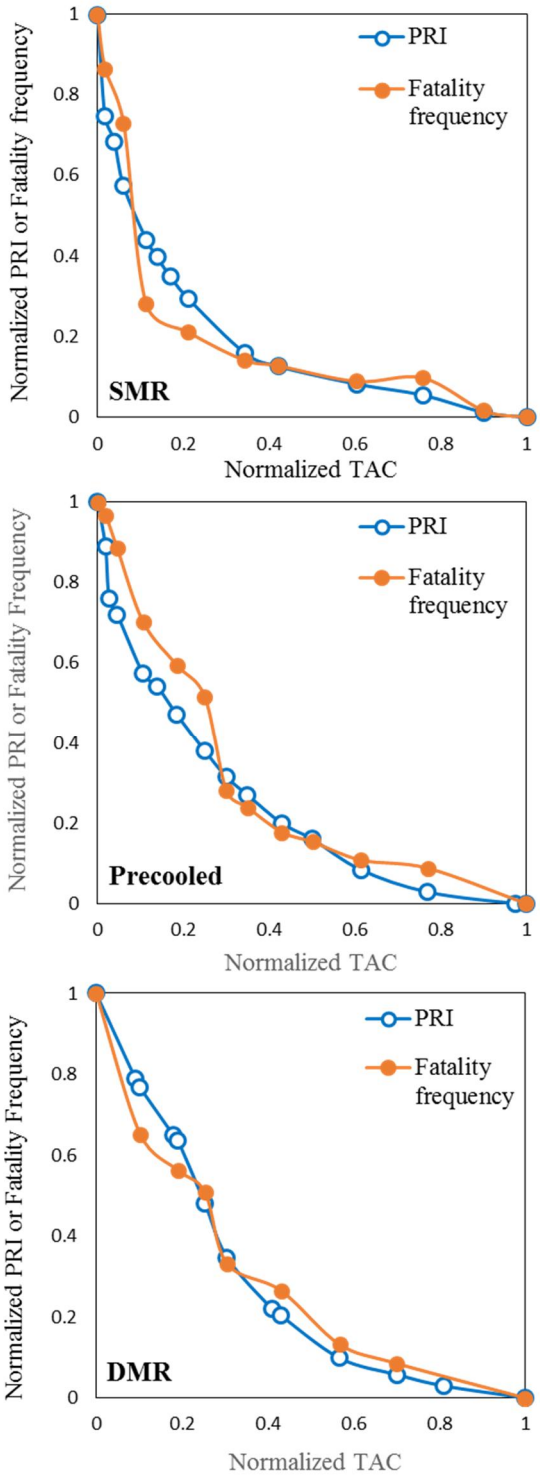

Figure 25. Pareto frontiers of PRI or fatality frequency for each process

Risk Assessment for Pareto Optimal Solutions

PRI as one of objective functions in multi-objective optimization is reasonably defined before to closely approximate the actual risk like fatality frequency [1/yr] through firstly targeting the severe streams by PSI analysis and considering their physical properties of pressure, density, energy, and combustibility which are all related to the accidental release behavior via a hole with associated outcomes of fire and explosion.

However properly defined this simple index is, it should be converted to the actual risk value through QRA for verifying its accuracy and finalizing the optimal solution having the risk value, not the PRI. In this study, QRA is simulated using SAFETI™ software developed by DNV_GL, which can accurately assess the risk of input plant. Necessary inputs like equipment counts and dimension, which are important in estimating event frequency but not able at the preliminary design stage, are assumed to be equal for each process except the additional components of cycle compressors and throttling valves between MSHEs which were generated as the heat transfer structure was expanded. Then we should only assess the risk related to the release scenario at this additional parts and just compare the risk value with each other. Simulation model setting including equipment and scenario generation and frequency estimation is summarized in Figure 3-26 in the SAFETI user interface.

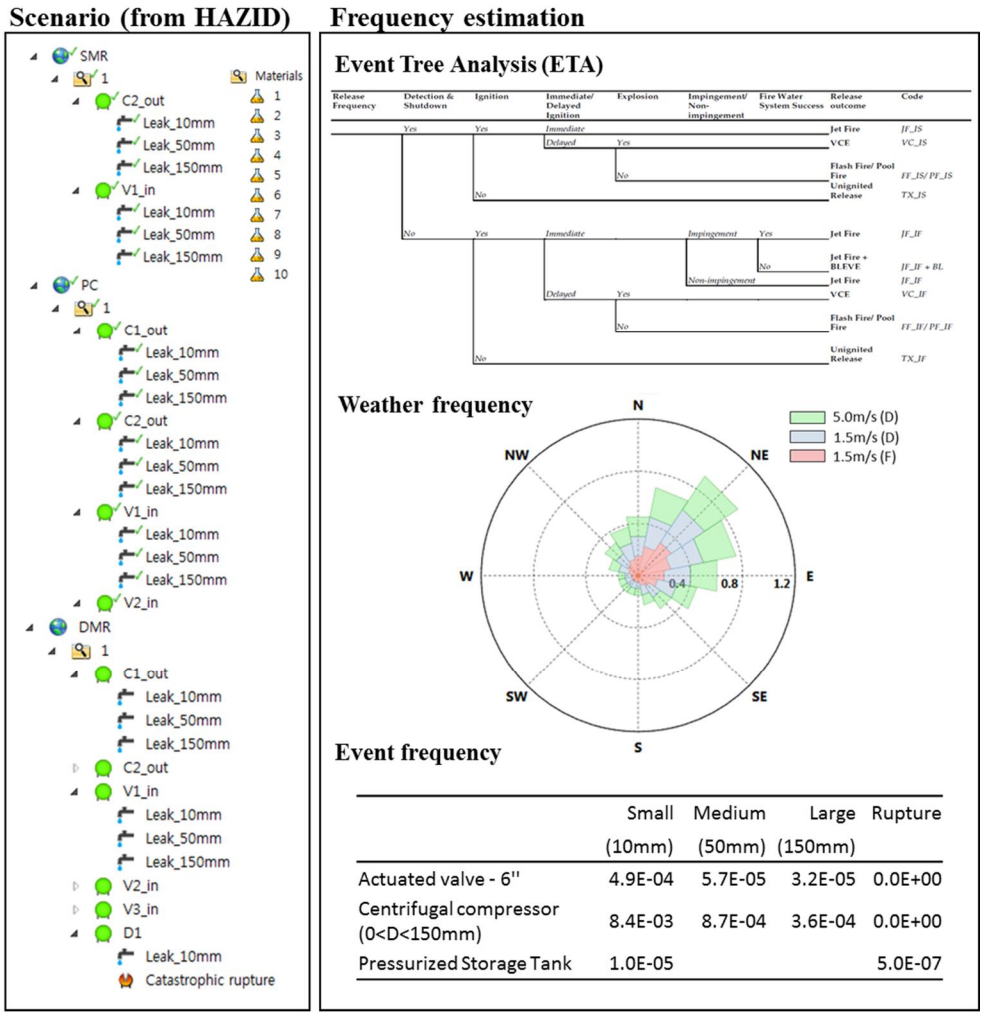

	Small (10mm)	Medium (50mm)	Large (150mm)	Rupture
Actuated valve - 6''	4.9E-04	5.7E-05	3.2E-05	0.0E+00
Centrifugal compressor (0<D<150mm)	8.4E-03	8.7E-04	3.6E-04	0.0E+00
Pressurized Storage Tank	1.0E-05			5.0E-07

Figure 3-26. Simulation settings for QRA simulation using SAFETI™

Event frequency data shown in the figure are retrieved from the data directory by Oil & Gas Producers [21]. Additionally for assessing societal risk which assesses the multiple fatality in case of an accident, the population geometry is set as a rectangle with 180m×80m where there are total 16 operators (0.001/m2).

After QRA simulation for each process, the FN curves which show the frequency of N fatalities with respect to N fatalities are plotted in Figure 3-27. Each line in the figure means the societal risk of an accidental release at the conditions of each point in Pareto optimal set. Generally, with the same simulation settings except the scenarios of each process, DMR has the highest frequency of N fatalities than others. It should be noted that despite some lines exceed the maximum limit of ALARP region, it does not mean that their associated risks are intolerable as we focused only on the difference of the risk value between each other, not the actual risk in the plant with actual population and layout data

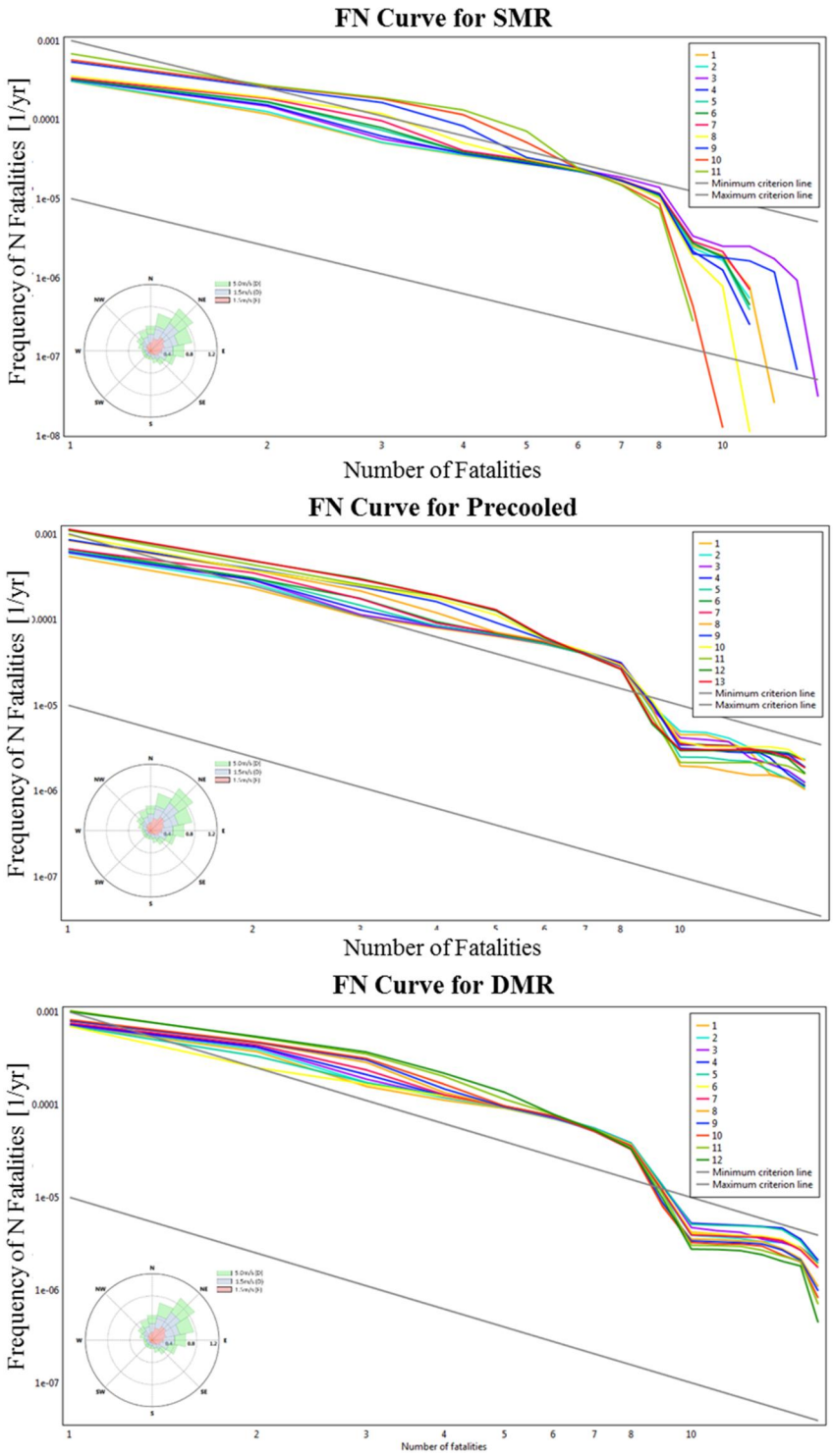

Figure 3-27. Societal risk results of each process in FN curve

From this QRA, the PRI value of each Pareto optimal point can be converted to the risk value of fatality frequency per year. Then the Pareto optimal set of PRI with respect to TAC could also be converted to the solutions of Fatality frequency with respect to TAC as shown in Figure 3-25 and summarized in Table 3-17.

It should be noted that these set of solutions for fatality frequency are actually not the Pareto optimal set as the Pareto optimality conditions are satisfied only in the multi-objective optimization. However, as can be seen in the Figure 3-25, two Pareto frontiers of each process, one for PRI and the other for fatality frequency, are close to each other and the mean squared errors (= $E(\|\hat{\theta} - \theta_0\|)$ of normalized PRI compared to the normalized fatality frequency assessed by QRA are 0.007, 0.009, 0.003 respectively for each process which is low enough to verify the Pareto optimality of converted solution sets very closely.

Table 3-17. Pareto frontier with Fatality frequency for each process

Number of points	SMR				Precooled				DMR			
	A*		N**		A*		N**		A*		N**	
	TAC	F.F.***	F1	F2	TAC	F.F.	F1	F2	TAC	F.F.	F1	F2
1	613	1.33	0.00	1.00	583	2.37	0.00	1.00	580	2.30	0.00	1.00
2	615	1.23	0.02	0.87	585	2.34	0.02	0.97	588	2.09	0.10	0.65
3	620	1.13	0.06	0.73	588	2.24	0.05	0.88	595	2.04	0.19	0.56
4	627	0.80	0.11	0.28	595	2.03	0.11	0.70	600	2.00	0.25	0.51
5	639	0.75	0.21	0.21	605	1.90	0.19	0.59	604	1.89	0.31	0.33
6	655	0.70	0.34	0.14	612	1.81	0.25	0.52	614	1.85	0.43	0.27
7	664	0.68	0.42	0.13	618	1.53	0.30	0.28	624	1.77	0.57	0.13
8	687	0.66	0.60	0.09	624	1.48	0.35	0.24	635	1.74	0.70	0.09
9	706	0.66	0.76	0.10	633	1.41	0.43	0.18	658	1.69	1.00	0.00
10	723	0.60	0.90	0.02	642	1.38	0.50	0.15				
11	735	0.59	1.00	0.00	655	1.33	0.61	0.11				
12					673	1.31	0.77	0.09				
13					700	1.20	1.00	0.00				

*A: Actual objective function values
**N: Normalized objective function values [48]
***F.F.: Fatality frequency [1/yr] * 1E-03

3.3.4. Decision Making for Final Optimal Solution

Combination of Each Pareto Frontier

In order to finally determine the optimal solution, each Pareto set of each process in Figure 3-28 should be combined to a single Pareto frontier with real TAC and fatality frequency values, not the normalized one, to see the structural preferences with respect to each objective function. In Figure 3-28, the gray frontier of SMR is located at the far down – right position with highest TAC and lowest fatality frequency, as expected earlier. The Pareto frontier of Precooled (blue) and DMR (red) are moved up – left from that of SMR with decreased TAC and increased fatality frequency as the heat transfer structure is divided to improve the thermodynamic efficiency and economic feasibility at the cost of safety. Then the combined Pareto frontier could be determined as the orange line in the figure of which the points have the closest distances from the Utopia points. The data points are listed in Table 3-18. In the following chapter the decision making method and results for the final solution will be discussed.

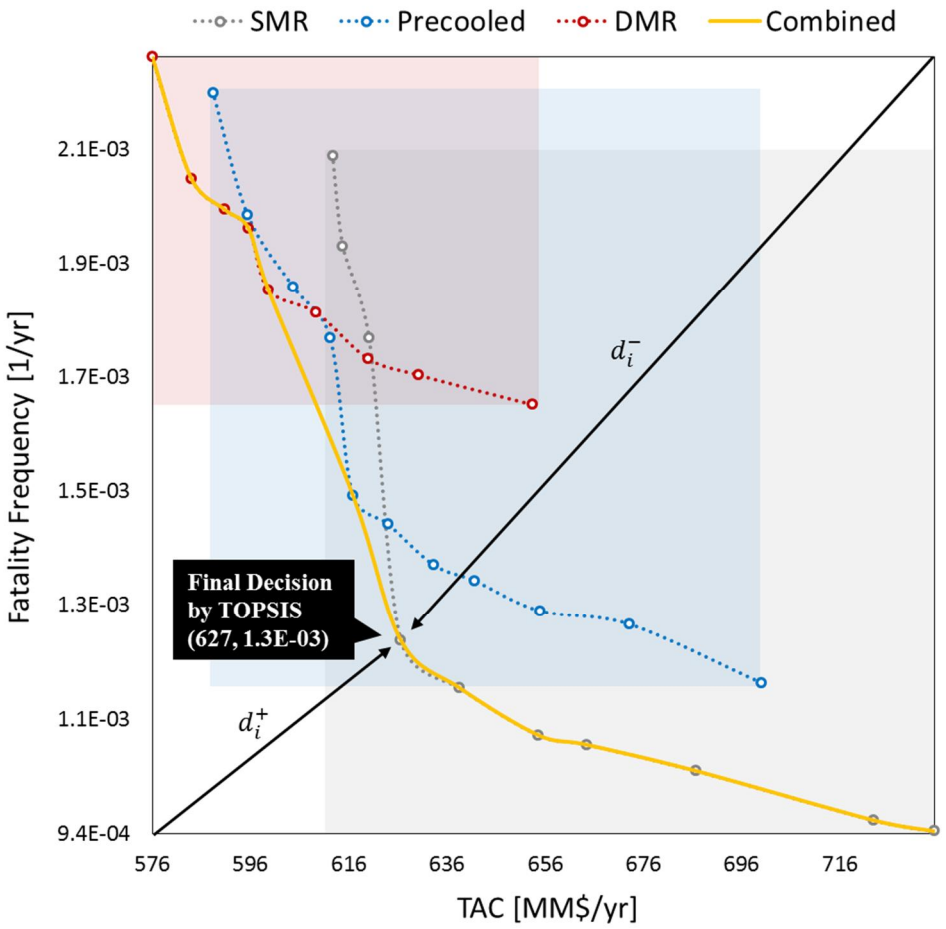

Figure 3-28. Final optimal solution in the combined Pareto frontier

Table 3-18. Combined Pareto frontier and the final optimal solution

Combined Pareto frontier							
Number		A*		N**		TOPSIS	
of points	TAC	F.F***.	F1	F2	d+	d-	Y
1	576	2.30	0.00	1.00	1.00	1.00	0.50
2	584	2.09	0.05	0.84	0.85	0.96	0.53
3	591	2.04	0.09	0.80	0.81	0.93	0.53
4	596	2.00	0.12	0.78	0.79	0.90	0.53
5	600	1.89	0.15	0.70	0.72	0.90	0.56
6	617	1.53	0.26	0.43	0.50	0.93	0.65
7	627	1.28	0.32	0.25	0.40	1.02	0.72
8	639	1.19	0.39	0.18	0.43	1.02	0.70
9	655	1.11	0.49	0.12	0.51	1.01	0.67
10	664	1.10	0.56	0.11	0.57	0.99	0.64
11	687	1.05	0.70	0.08	0.70	0.97	0.58
12	723	0.96	0.92	0.01	0.92	0.99	0.52
13	735	0.94	1.00	0.00	1.00	1.00	0.50

*A: Actual objective function values
**N: Normalized objective function values [48]
***F.F.: Fatality frequency [1/yr] * 1E-03

TOPSIS Decision Making and Deviation Index

TOPSIS decision making technique [49] aims at determining the order of preference by the similarity to (positive and negative) ideal solutions. For the Utopia point, z^U and Nadir point, z^N in Eq. (3-13) and Eq. (3-14), each could be expressed as $z^U = (v_1^+, v_2^+)$, $z^N = (v_1^-, v_2^-)$, where 1 and 2 denotes the value of TAC and Fatality frequency respectively. Then the separation of each alternative (v_{i1}, v_{i2}) from the Utopia and Nadir solutions is given as Eq. 3-16 and Eq. 3-17.

$$d_i^+ = \sqrt{\sum_{j=1}^{n}(v_{ij} - v_j^+)^2}\ ,\ i = 1, \dots, m \tag{3-16}$$

$$d_i^+ = \sqrt{\sum_{j=1}^{n}(v_{ij} - v_j^-)^2}\ ,\ i = 1, \dots, m \tag{3-17}$$

where m is the number of optimal points in the Pareto frontier set.

The relative closeness of the *i*-th alternative with respect to the Utopia solution is defined in Eq. 3-18.

$$Y_i = \frac{d_i^-}{d_i^- + d_i^+}\ ,\ i = 1, \dots, m \tag{3-18}$$

A set of alternatives now can be prioritized by the descending order of the value of Y_i, which is ideal when having the value of 1. Y_i value for each point is listed in the last column of Table 3-18 which leads to the decision of final optimal point of (SMR, 626.6MM$/yr, 1.28E-03/yr) as shown in Figure 3-28.

The final optimal point could be moved to the upper - left points when we expand the heat transfer structure more from the DMR process to such a mixed fluid cascade (MFC) process which have 4 MSHEs with 3 different mixed refrigerant cycles. Even though this process could have a higher thermodynamic efficiency (lower specific power and higher overall exergy efficiency) and lower TAC than any other processes, it is not covered in this study as selected three process routes of SMR, Precooled, and DMR are enough to verify the effectiveness of the proposed method and to give reasonable guidelines to the process designers.

3.3.5. Future Works

Three limitations in this study could be pointed out as below:

1. Pareto optimality of the solutions of fatality frequency with respect to TAC
2. Cost estimation of a certain fatality frequency value
3. Global optimality of the solutions

Firstly, as mentioned in above chapter, the solutions of fatality frequency could not verify its Pareto optimality as they were determined by converting those of PRI values through QRA simulation. This limitation could be overcome through the other decision making scheme proposed in Figure 3-14, where the risk is directly assessed through the rigorous custom modeling and it is designated as the second objective function in multi-objective optimization. The custom modeling of consequence analysis like calculating radiative flux (x,y,z) [kW/m2] for fire outcomes and overpressure (x,y,z) [gauge bar] for explosion outcomes would be a time-consuming work and high computation load would be burdened to the multi-objective optimization solver for finding Pareto optimal set. This modeling work is now in progress and the effectiveness of this decision making scheme will be tested in the future.

Secondly, when we finalize the decision of determining an optimal point through TOPSIS method, as the risk value was represented by the fatality frequency per year [1/yr], not the economic value [MM$/yr] like TAC, the meaning of the final decision could be vague. Extremely if the risk cost of a certain fatality frequency is much cheaper than TAC, the final solution should be the point at the far left which has the structure of DMR with lowest TAC and highest fatality frequency. When the

cost of the risk is properly estimated, the final decision could give more practical guidelines to the process designers.

Finally, the optimization solver used in this study was the sequential quadratic programming which is powerful at solving the complex non-linear optimization problems. The algorithm is built-in the gProms software, so the users can use this tool with additional custom modeling when they want to modify it or additionally define new models for accelerating the optimization. However powerful it is, the main issue is the global optimality of resulted solutions as it is often confined at the local optimum region and finalized with it which satisfies the optimization criteria for stationary, feasibility, complementarily and Taylor conditions. Among several methods for verifying this global optimality, the elitist non-dominated sorting genetic algorithm (NGSA-II) would be selected as the optimization solver for future work, which is recently used in multi-objective optimization problems.

3.4. Concluding Remarks

This chapter covered largely two themes for safer process design: one for risk reduction methodology through process design modifications following the general design procedures, and the other for deciding an optimal solution using multi-objective optimization for economic feasibility and safety by introducing the inherent safety concept in the preliminary design stage.

First, it dealt with the risk-based process safety management for a GTU of a GOSP through the implementation of a process simulation into a general QRA procedure using the concept of static inventory. The proposed integration methodology could connect two different natures of simulation in a reliable manner: the static nature of a QRA simulation based on the storage conditions of a fluid, and the dynamic nature of a process simulation dealing with the fluids flowing through a pipe or separated by the phase equilibrium.

The QRA results were utilized to concretely determine the risk reduction targets through the total risk integral ranking of all the accidental scenarios and major outcomes that had a dominant impact on the risk. Consequently, a small leak (10mm hole-diameter) scenario at the hydrocarbon liquid stream from the three-phase separator in case of an isolation failure and the associated flash fire and pool fire effects from that scenario were targeted to be managed.

The risk reduction approach was applied in two different ways according to the risk target. First, in order to reduce the risk by mitigating the flash fire and pool fire probabilities under the selected leak scenario, modification of the process design by altering the operating pressure of the three-phase separator from 12.0barg to

0.52barg was proposed. Modification resulted in a 27% decrease in the total societal risk from 1.41E-03/year to 1.02E-03/year with an additional capital cost of around $50,000, which dragged down the risk to the tolerable ALARP region. Second, a sensitivity analysis of the total societal risk to the isolation success probabilities was performed. As a result, the improvement of the success probability up to 40% drastically reduced the risk from 1.02E-03 to 5.82E-04/year.

Second, a new decision making scheme for optimal process design minimizing both the economic feasibility and potential risk was proposed using multi-objective optimization and inherent safety indexes. The proposed method firstly found the Pareto optimal set for the total annual cost (TAC) and process route index (PRI) with identified hazardous streams. Then for those points, the fatality frequencies representing the actual risk were calculated through quantitative risk assessment (QRA) simulation resulting in an optimal solution set having the fatality frequencies, not PRI. The final optimal solution was determined based on the closeness to the ideal solutions through TOPSIS decision making method. This overall procedure was applied to the natural gas liquefaction processes of SMR, Precooled and DMR which share the similar heat transfer structure so that the Pareto optimal solutions of each process could be combined approximating a superstructure optimization. Finally, the SMR process with TAC of 627MM$/yr and fatality frequency of 1.28E-03/yr is determined as the final optimal solution.

CHAPTER 4. Safer Operation

With the aim of safely operating a chemical plant, this study focuses on developing a new operator training module which mainly targets the field operators through using advanced simulation and data processing technologies.

This chapter proposes a method of interactive simulation modeling which delivers the online simulation results to the field operators and induces them to take proper actions in case of a random accidental situation among pre-identified scenarios in a chemical plant. Developed model integrates the real-time process dynamic simulation with the off-line database of 3D-CFD accident simulation results in a designed interface using OLE technology so that it could convey the online information of the accident to trainees which is not available in existing operator training systems. The model encompasses the whole process of data transfer till the end of the training at which trainees complete an emergency shutdown system in a programmed model.

The developed module is applied to a natural gas pressure regulating station where the high pressure gas is depressurized and distributed to the end-users like households or offices. An overall scenario is simulated in the interactive simulation model, which starts from an abnormal increase of the discharge (2^{nd}) pressure of the main valve due to its malfunction, and spreads to an accidental gas release through the crack of a pressure recorder. Then the magnitude of the accident outcomes with respect to the lead time of each trainee's emergency response is analyzed. The module can improve the effectiveness of operator training system through interactively linking the trainee actions with the model interface so that the

associated accident scenarios would vary with respect to each trainee's competence facing an accident.

4.1. Introduction

Reference to 2011, total revenue of the whole chemical industry came to about 100 billion euros [1]. While this development of modern chemical plants has created high economic profits, the issues of less operability and increased risk are inevitably brought about due to complicated processes and large quantity and variety of treating chemicals.

Chemical accidents result in productivity loss, equipment and environment damage, and fatalities which we can observe in several cases from Bhopal toxic gas release accident in 1984 [2] to Texas BP refinery explosion in 2005 [3-4]. According to several studies dealing with main causes of the accidents, mal-operation of plant equipment by human error is one of the most frequent causes [5-7], and accidents recur mainly due to inefficient structure of information sharing between each operator and insufficient education about past accident cases [8]. Particularly, fast and accurate communication between physically separated operators in spacious site of chemical plants requires high competence.

Although established operator training systems based on dynamic process simulation like UniSim® OTS by Honeywell and Aspen® OTS by AspenTech have taken great roles in training of proficiency in operation procedure and control of risk factors in chemical process for CROPs [9-13], they have a difficulty in enhancement of training efficacy due to limited information delivery for FOPs generally not equipped with systematic knowledge of process simulation. As field

operations are manually performed based on communication with control room, FOPs are highly reliant on the control room commands and heuristics based on personal experience in case of an accident. As the existing education for FOPs is limited to studying text manuals of operation and emergency procedures or handling method of each equipment, however, a systematic FOP training system which can induce the series of process from correct estimation of accidental situation to active management is necessary [14].

Cha et al developed a fire suppression training program which generate a fire scenario in virtual reality, calculate the fire effect using 3D-CFD, and deliver the situation information to trainees so that they can actively suppress the fire using an avatar [15-16]. Schneider Electric performed and evaluated operator training with 30 operation scenarios (15 scenarios for CROPs and FOPs, respectively) via EYESIM® immersive training package in plant virtual reality environment [17-20]. Even though above two researches try to develop FOP customized training solutions by integration of accident simulation or process simulation with immersive virtual reality system respectively, they are not able to train the whole process of accident initiated from process upsets and terminated at emergency response as they do not link the process simulation to accident simulation directly.

To solve this limitation, Manca et al [21-26] interlinked the process simulation with self-developing accident simulator, AXIM by OLE technology, and implemented this module into immersive virtual reality. Through this combined model they realized the pool formation and pool fire scenario by liquid release, and let the fire results affect process simulation model so that trainees could experience the fault propagation realistically. Nazir et al [27, 28] evaluated and validate the

training efficacy by applying this model to FOPs directly. As the AXIM simulator is based on parametric calculation with simple heat and material balances only for liquid phase, however, the accuracy of this model could not be sufficient for vapor phase or two-phase jet release, dispersion, and fire & explosion calculation.

Based on the analysis of existing technologies which all try to develop a more realistic operator training module targeting the field, Figure 4-1 compares four most recent technologies including one which is developed in this study, in terms of their capabilities and limitations.

For the proposed model located at the down – left position in the figure, it is now implemented in the virtual reality (dotted line), but this chapter only covers the technology of interactive simulation between dynamic process and accident model (solid line). The detailed information of the proposed model would be described later.

Additionally, it should be noted that even though the Virthualis located at right – left position has lower accuracy of the model and can only deal with limited scenarios, it has higher degree of freedom for field actions as they can update the accident simulation very quickly whenever a field operator takes any actions.

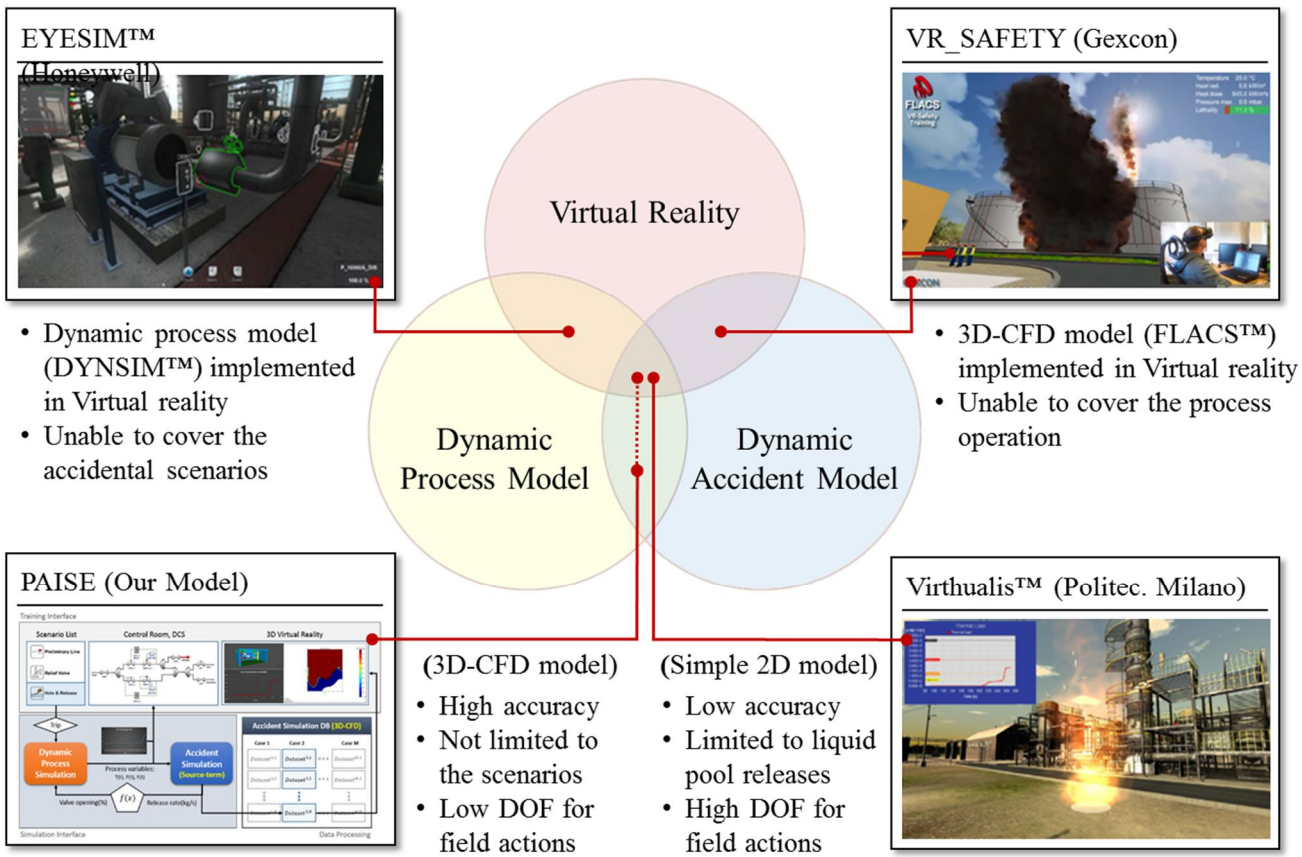

Figure 4-1. Recent advanced technologies of operator training module

This study aims to develop an interactive simulation model in which dynamic process simulator of Aspen Hysys and self-developed source-term model which calculates the discharge conditions for a release are directly linked via Microsoft Excel Visual Basic, and especially for gas dispersion scenario, pre-calculated off-line 3D-CFD data via Gexcon FLACS are processed real-time with respect to trainees' emergency actions. Simulated results are delivered to the trainees so that they can correctly percept the abnormal situation based on the information from the model and actively take proper actions in the programmed interface. Then the actions affect the process and accident simulation simultaneously. As our model utilizes a commercial 3D-CFD simulator to calculate the effect of an accident, the model is assumed to guarantee sufficient accuracy for the accident outcomes like gas dispersion, fire and explosion of a released fluid at any phase of equilibrium. A case study deals with a natural gas pressure regulating station in South Korea, and evaluates the applicability of our model to practical operator training by generating process upsets and accident scenarios, constructing dynamic process and accident simulation models, and developing a demonstration program.

4.2. Interactive Simulation Modeling

4.2.1. Model Structure

Interactive simulation model interlinks process and accident simulation model in an overall training scenario from process upsets to accident occurrence and propagation (Fig. 4-2). In this model, three simulations are linked based on certain sequence of accident scenarios: Dynamic process simulation, Source-term model discharge calculation, and pre-calculated 3D-CFD simulation. As the scenarios are initiated with certain process upset like equipment failure, dynamic process simulation firstly calculates the effect of the failure to the process for each time. The real-time results are automatically conveyed to the integration domain like Microsoft Excel via the export port of the simulator. When the accidental release conditions are met at certain time as an error is accumulated, source-term model built in the domain is activated to calculate the discharge at the leakage point in equipment. Calculated discharge flowrate is transmitted back to the dynamic process simulator via the export port of the domain and affects the simulator to realize the leak through generating an additional stream. As the same time, pre-calculated 3D-CFD simulation results for dispersion and explosion of discharged fluid are selectively sent to the domain for each time via the export port of a CFD database according to the leakage conditions like pressure, temperature and hole-size. This whole sequence partly by OLE technology is visualized in the training system so that trainees can see the results and take actions in it.

Through this simulation linking structure, the model leads trainees to actively analyze process variable trends based on the simulation results and take proper

actions with their own decision to stabilize the variables or minimize operational losses. When stabilization fails and accident occurs, associated results like gas cloud concentration and explosion overpressure at each time and position are additionally provided to the trainees. Their actions like emergency shutdown can be inputted by clicking a mouse or a joystick control.

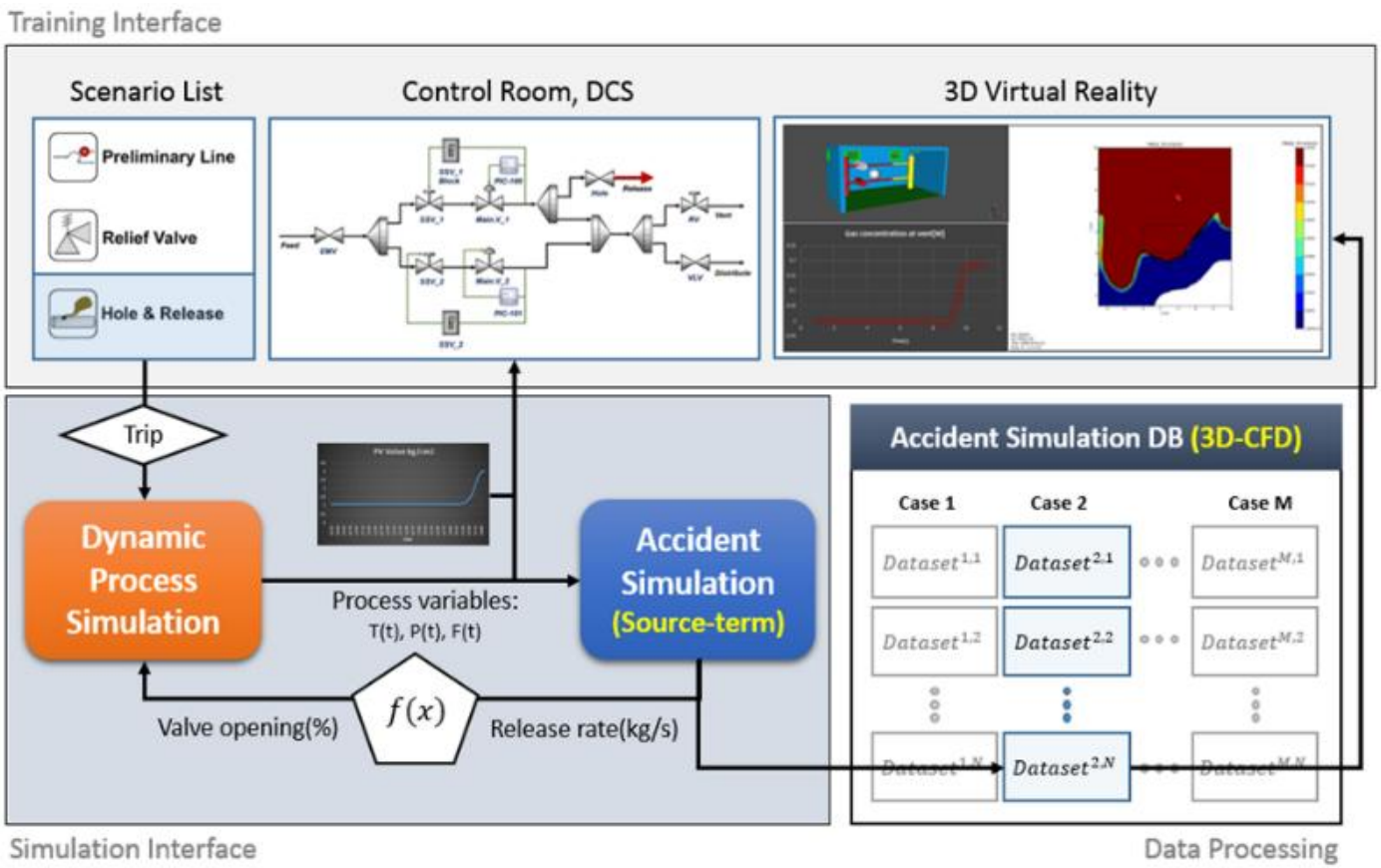

Fig.4-2. Schematic design of interactive simulation model

4.2.2. Dynamic Process and Accident Simulation Engine

Dynamic Process Simulation Model

Dynamic process simulation using Aspen Hysys gives trainees almost the same trend of process variables with that of a real plant. As a scenario is initiated, physical and thermodynamic calculations are conducted online and variable trends deviating from set points or being stabilized to those points can be analyzed. As errors are accumulated and the variables reach the pre-defined conditions of an accidental release scenario, values of the variables at that time are automatically inserted into the accident simulation model. When trainee' actions like emergency shutdown by clicking a manual valve in the training environment are taken, associated signal is transferred to the process simulation model so that the actions are reflected in the model.

Dynamic Accident Simulation Model

In order to separate the linking point with process simulation model, accident simulation model is divided into two sub-models: One is 'Source-term model' calculating discharge from inside of the equipment to outside through an orifice. And the other is '3D-CFD model' calculating indoor or outdoor dispersion and fire & explosion effects after the discharge.

Source-term model calculates the release mass flowrate, Q [kg/h] with given process simulation results at the time when a fluid starts to release (Eq. 4-1) and transfers the results to 3D-CFD model. As this release should be simultaneously reflected in the process simulation model, we generate an additional stream and a valve at the release position right behind the main valve in the process model and automatically adjust the valve openings (Eq. 4-2: *f*(x) in Figure 4-2) so that the fluid is to be released with the quantity calculated from source-term model (Figure 4-3).

$$Q_1 = C_{disc} A \sqrt{\gamma \cdot \rho_i \cdot P_i \cdot (2/\gamma + 1)^{(\gamma+1)/(\gamma-1)}} \quad (4\text{-}1)$$

where Q_1=release mass flowrate [kg/h] in an orifice model; C_{disc}= discharge coefficient; A=hole area [m2]; γ=specific heat ratio (=C_p/C_v); ρ_i=inlet fluid density [kg/m3]; P_i=inlet pressure [kPa].

$$Q_2 = k \sqrt{V_{open} \cdot dP \cdot \rho} \quad (4\text{-}2)$$

where Q_2=mass flowrate [kg/h] from a pressure-flow relation in the valve; k=valve conductance [kg/h]; V_{open}=valve opening [%]; dP=friction delta pressure [kPa]; ρ=gas density[kg/m3].

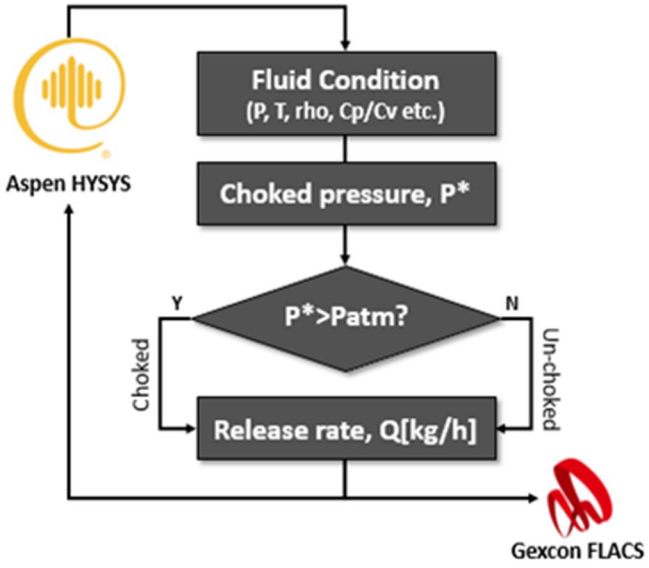

Figure 4-3. Real-time source term modeling

3D-CFD model utilizes commercial software (FLACS® by Gexcon) in order to guarantee the accuracy of dispersion calculation. As CFD calculation requires heavy computational load unlike source-term model, this study develops a method of real-time processing the offline CFD data for applying the CFD model to our training system in which the real-time data transfer between the simulation model and training environment is essential. For this purpose, we construct a big database, save the CFD results in it with respect to each scenario, and provide them to trainees selectively as they take a certain action in the training interface.

4.2.3. Real-time 3D-CFD Data Processing Method

Training with pre-defined operating scenarios and pre-calculated CFD data holds low degree of freedom in that the trainees cannot do anything but certain actions designated by the system in advance. In order to overcome this limitation, this study suggests a real-time CFD data processing method consisting of four steps described below and increases the training effectiveness of our model.

(1) Trainee Action List - Generate trainee action list in a certain scenario and process. For the case of pressure regulating station this study will address later, 'Manually close the emergency shutdown valve inside the station' is a representative action in case of a gas release.

(2) Release Duration - Determine the range of release duration based on a field operator's average site arriving time (15min for pressure regulating station) and the mission fails if the training time exceeds the maximum time (30min for the same process) without a series of proper actions.

(3) 3D-CFD Database - Divide the range of release duration (15-30min) with one minute interval, and save total 16 simulation results, labeling each gas concentration dataset $C^i(x, y, z, t)$ as $Dataset^i(i = 15, 16, \cdots, 30)$.

(4) Data Processing with respect to Trainee Action (Eq. 4-3, Figure 4-4) - As the release start $(\mathrm{t} = t_{rel})$, firstly the dataset of maximum release duration, $Dataset^{30}$ is transferred to a trainee in the training environment in real-time. The reason for the selection of this dataset is that anyone can know at which time the trainee would do the proper action. When the trainee receives the message to move, an avatar in the program heads for the site by trainee's

manipulation. When the avatar closes the shutdown valve at a certain time ($t = t_{act}$), the CFD data after that time are automatically replaced by those in $Dataset^{(t_{act}-t_{rel})}$ not in $Dataset^{30}$ (Figure 4-5).

$$
\begin{aligned}
&C(x, y, z, t) \qquad (4\text{-}3)\\
&= 0 \qquad\qquad 0 \le t < t_{rel}\\
&= C^{30}\left(x, y, z, (t - t_{rel})\right) \qquad t_{rel} \le t < t_{act}\\
&= C^{(t_{act}-t_{rel})}\left(x, y, z, (t - t_{rel})\right) \qquad t_{act} \le t \le t_{max}
\end{aligned}
$$

For instance, if a gas release occurs 10min after the training starts ($t_{rel} = 10$) and a trainee close the valve 20min after the release ($t_{act} = 30$), concentration data of $Dataset^{30}(= C^{30}(x, y, z, t), 0 \le t \le 20)$ during the time between release and action ($10 \le t \le 30$) are real-time transferred, and after that time ($30 < t \le t_{max}$) the data are replaced by those of $Dataset^{20}(= C^{20}(x, y, z, t), 20 \le t \le (t_{max} - 10))$.

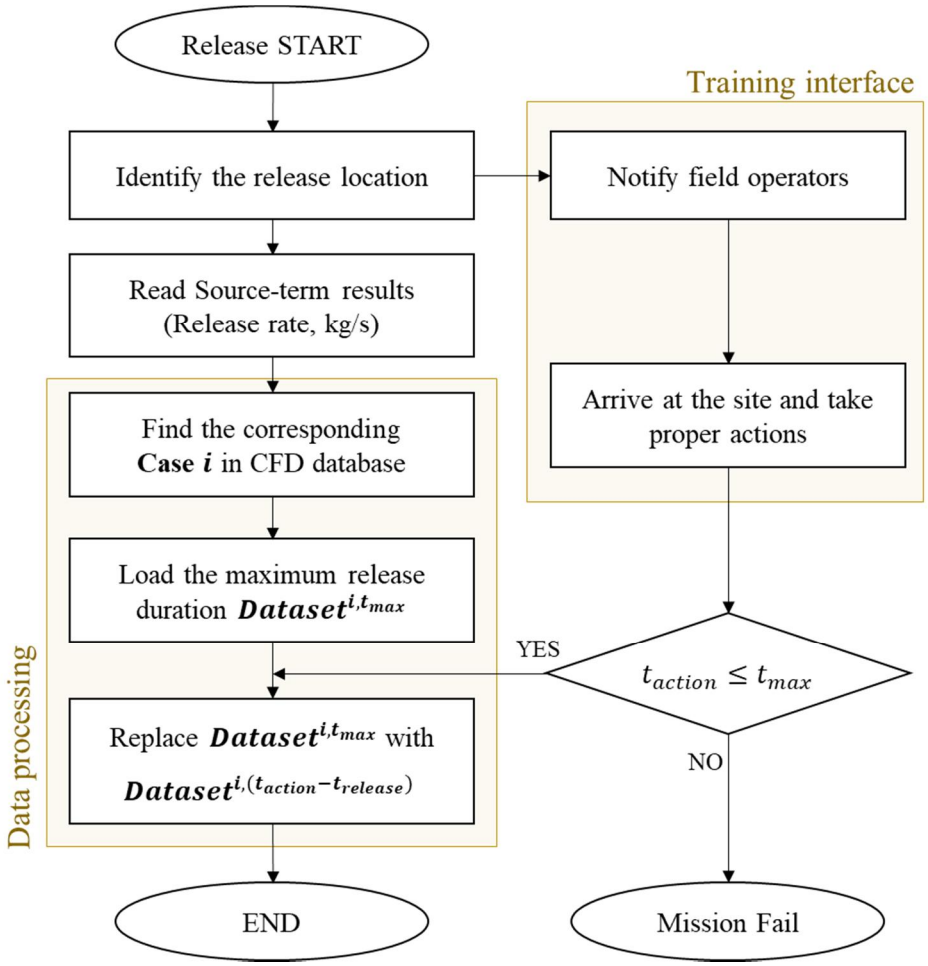

Figure.4-4. Real-time CFD data processing method

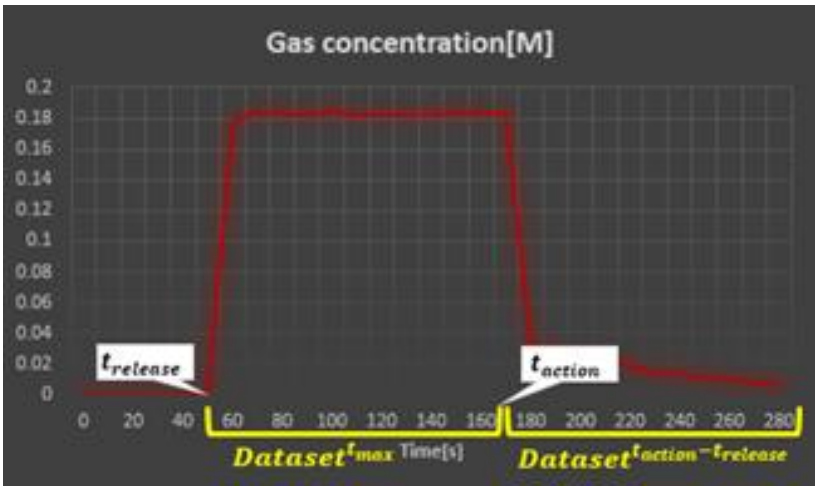

Figure 4-5. Real-time CFD data selection and switch for gas concentration

Figure 4-6 briefly describes the configuration of 3D-CFD simulation database and shows how it works for a single accidental scenario. Each rectangular box means a certain 3 dimensional dataset of all positions (x,y,z) and the saturation of color inside the box shows the intensity of accident outcomes like the total quantity of released gas or overpressure degree by explosion. The boxes (x,y,z) at different times aligning vertically in the figure constitute the dataset *i* (t,x,y,z) with respect to the release duration in case of an accident. For example, dataset 1 in the figure means the release lasts more than t=5 so that all boxes in that column are dark. Meanwhile dataset 3 means it stops between t=3 and t=4 so that the saturation of color is getting blurred after t=4.

These datasets would be selected and switched according to the time at which the operator takes actions for emergency shutdown. The arrow line in the figure shows how they works for the operator 3 who shutdowns the plant between t=3 and t=4. At the time when the release occurs, the dataset 1 of which the release duration is longest is automatically transferred to the module following the real time scale, and the dataset would be switched from 1 to 3 if the operator takes actions at that time.

From this method, each operator whose action time differs each other has different accident outcomes like the boxes below. And it would be reflected to the training evaluation.

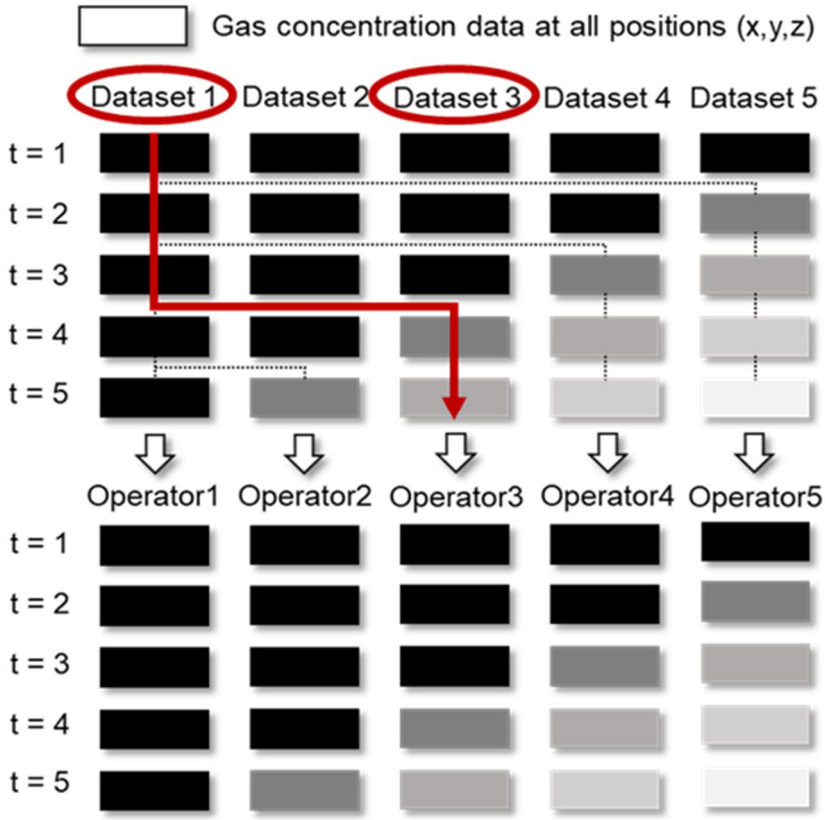

Figure 4-6. Real-time CFD data implementation method for each operator

4.3. Cast Study – Pressure Regulating Station

4.3.1. Developing a Program Prototype

Pressure Regulating Station

Natural gas in South Korea is supplied from LNG receiving terminal to residences or offices through KOGAS (Korea Gas Corporation) supply management station at 6.86MPa and then two pressure regulating stations operating at 0.8MPa or 0.6MPa respectively. Pressure regulating stations reduce pressure of the high-pressure supplied gas toward proper level of 2kPag for safe distribution [29].

In this study pressure regulating station near residential area is chosen as the target process for implementing our model as it has a high risk of fire and explosion accident (Figure 4-7). It consists of main (upper) and preliminary (lower) lines including main valves for reducing and controlling the gas pressure, gas heater for compensating lowered temperature due to abrupt expansion, gas filter for preventing inflow of other substance, SSV (Slam Shutoff Valve) for automatically block the flow and relief valves in case of an emergency.

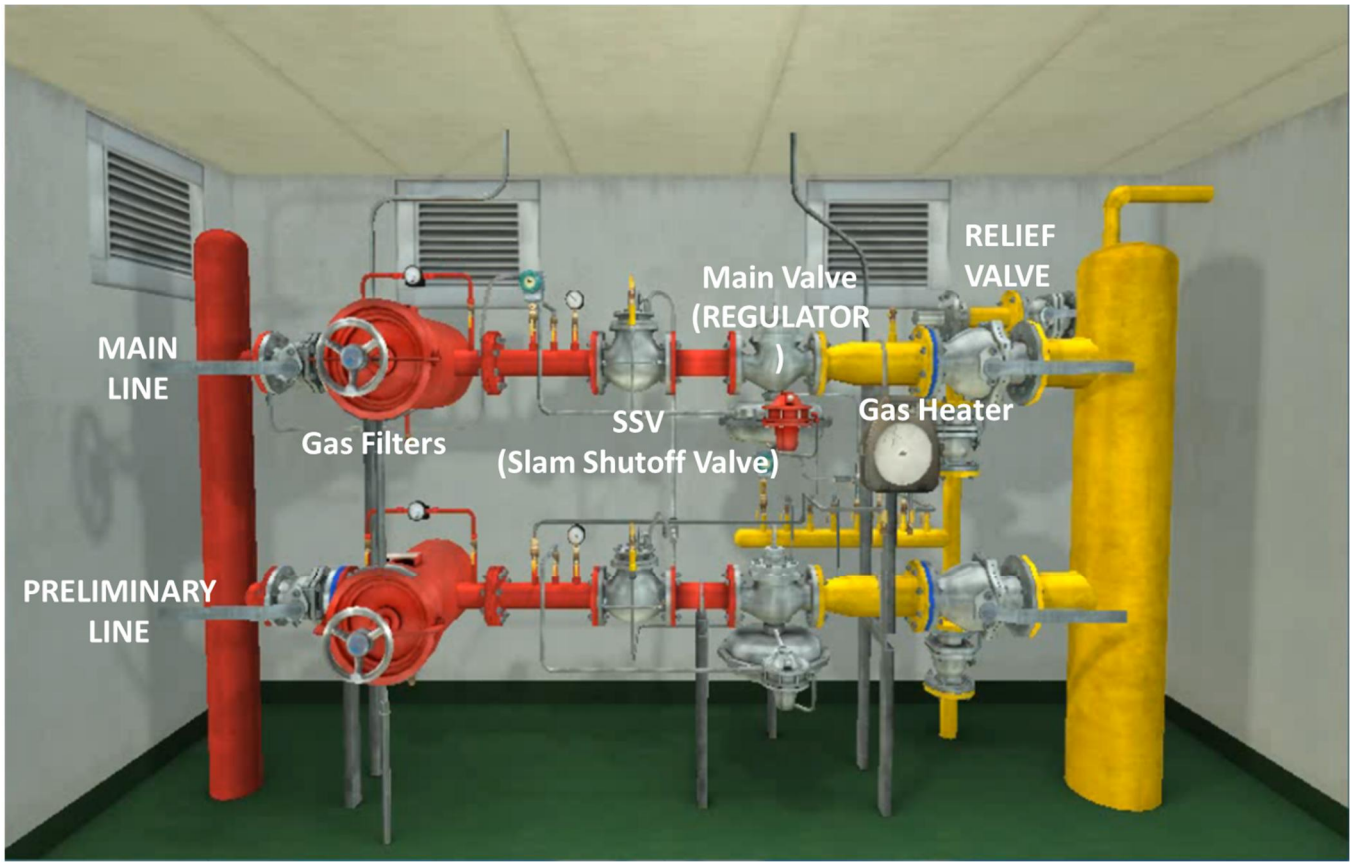

Figure 4-7. 3D image of pressure regulating station

Process Simulation Modeling

Process model can be constructed (Figure 4-8) based on controller set pressures of pressure regulating station (Table 4-1). Yellow region of the figure is one additional stream and valve in order to simulate the gas release right behind the main valve. When a gas releases opening percentage of the valve is set by discharge calculation in source-term model, otherwise it is set to be zero at normal operation.

Dynamic simulations of controller normal operations are tested in Figure 4-9. As in the figure, main valve controller tracks the set point change well and SSV controller block the gas stream at the set pressure.

The model uses Aspen Hysys v.8.4 as a process simulator and PR-LK EOS as a thermodynamic model for simulating the natural gas with the composition of (C1: C2: C3: nC4: iC4=0.90: 0.05: 0.03: 0.01: 0.01). Main valve type is 1098-EGR, and pressure-flow correlation at choked flow is as the following Eq. 4-4 [30].

$$Q_{main} = P_i \cdot C_g \cdot 1.29 \quad (4\text{-}4)$$

where Q_{main} =volumetric gas flowrate through the main valve [SCFH]; C_g=regulator or wide-open gas sizing coefficient

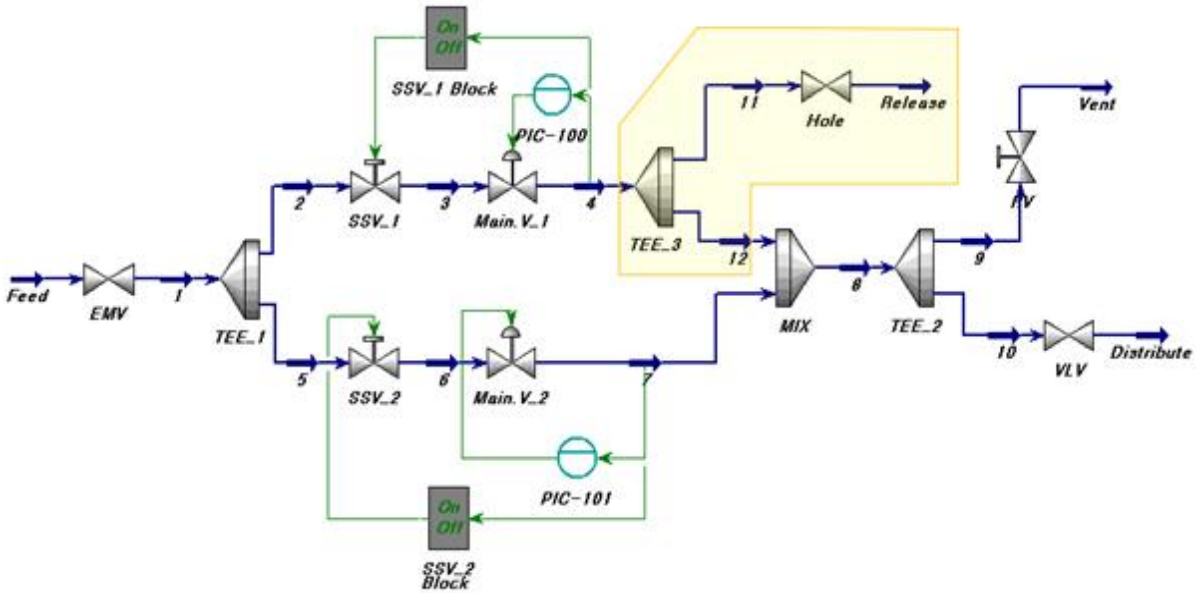

Figure 4-8. Process simulation model of pressure regulating station

Table 4-1. Controller Set Pressure

Controller		Set Pressure (kPag)
Failure Alarm	Lower limit	1.2
	Upper limit	3.2
SSV-1 (Main line)		3.6
Relief Valve		4.0
SSV-2 (Preliminary line)		4.4

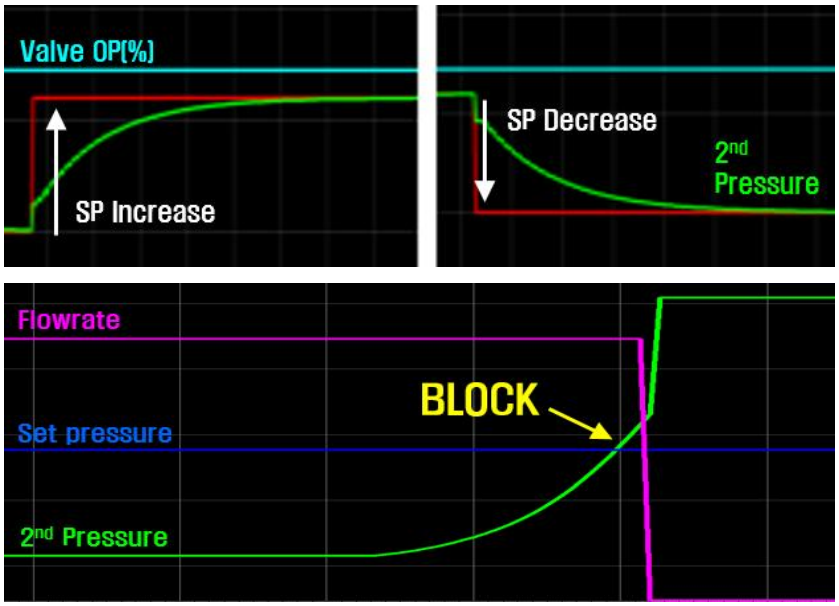

Figure.4-9. Controller operation test (top-Main valve, bottom-SSV)

Scenario Generation

Scenarios are generated based on the historical data of process upsets or accidents. As these cases are documented with real process data and event sequence, scenario generation process is initiated at the cased-based analysis of historical data. The resultant scenario tree is formulated in Figure 4-10 starting from top initiating event of pressure rise to the final state of process stabilization or accidents. Among all these scenarios of pressure regulator, three representative scenarios are selected in this case study and listed in Table 4-2.

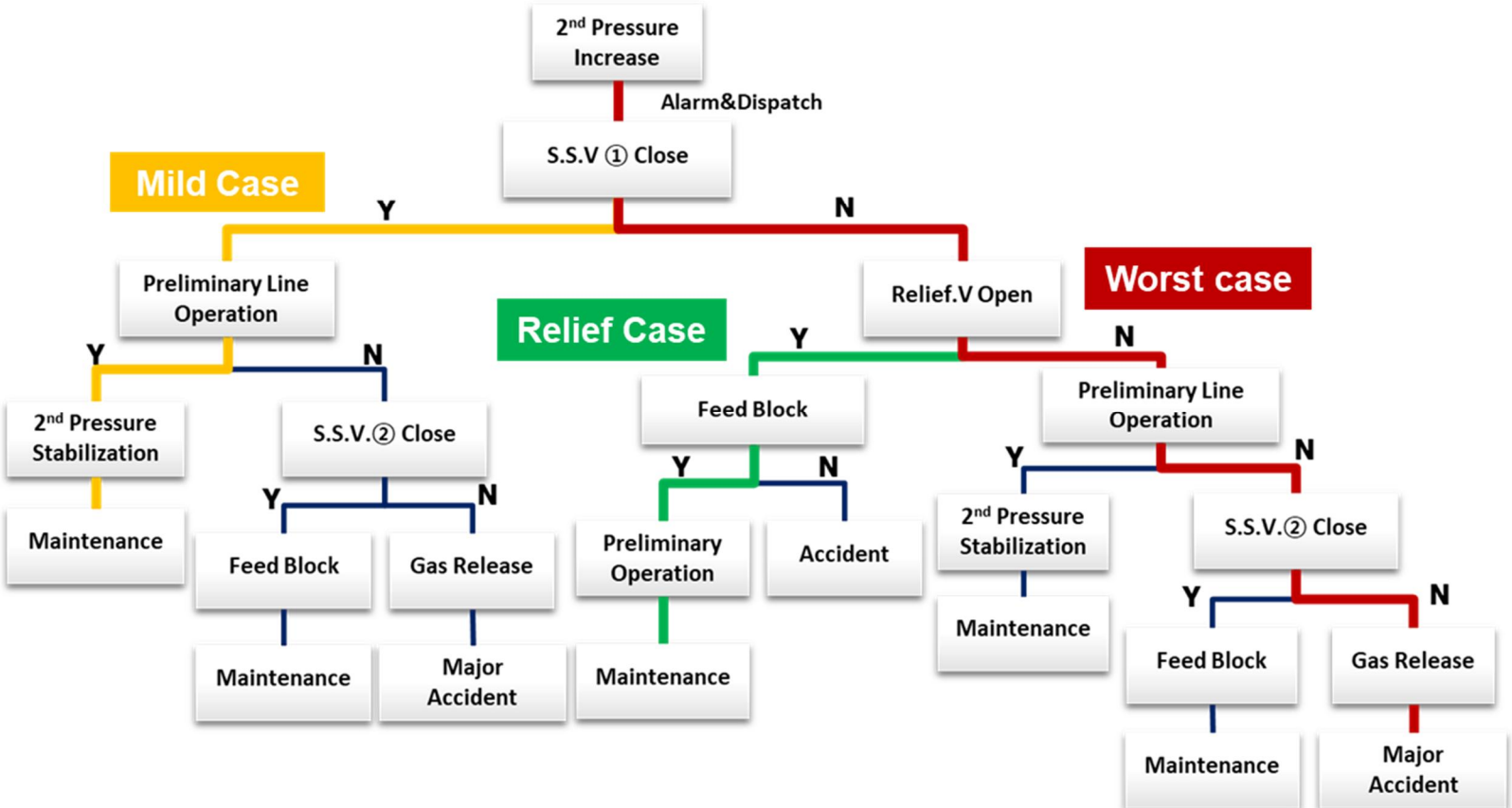

Figure.4-10. Scenario tree of a pressure regulator in case of pressure rise

Table 4-2. Three Representative Scenarios

Case	Scenario
Mild	2nd Pressure Increase → SSV_1 Block → Preliminary line Operation
Relief	2nd Pressure Increase → SSV_1 Block Fail → Relief valve Operation → Supply Block
Worst	2nd Pressure Increase → SSV_1 Block Fail → Relief valve Fail → Gas Release

The process is normally operated as the Figure 4-11(a) where the natural gas of 6bar is regulated to 2kPag via the regulator main valve through only the main line.

The mild case (Figure 4-11(b)), however, occurs when 2nd pressure reaches the SSV set pressure due to certain malfunctions of the equipment or mal-operations by operators, then SSV is automatically closed immediately and the main valve in preliminary line opens by the sensing line to stabilize the gas flowrate and 2nd pressure.

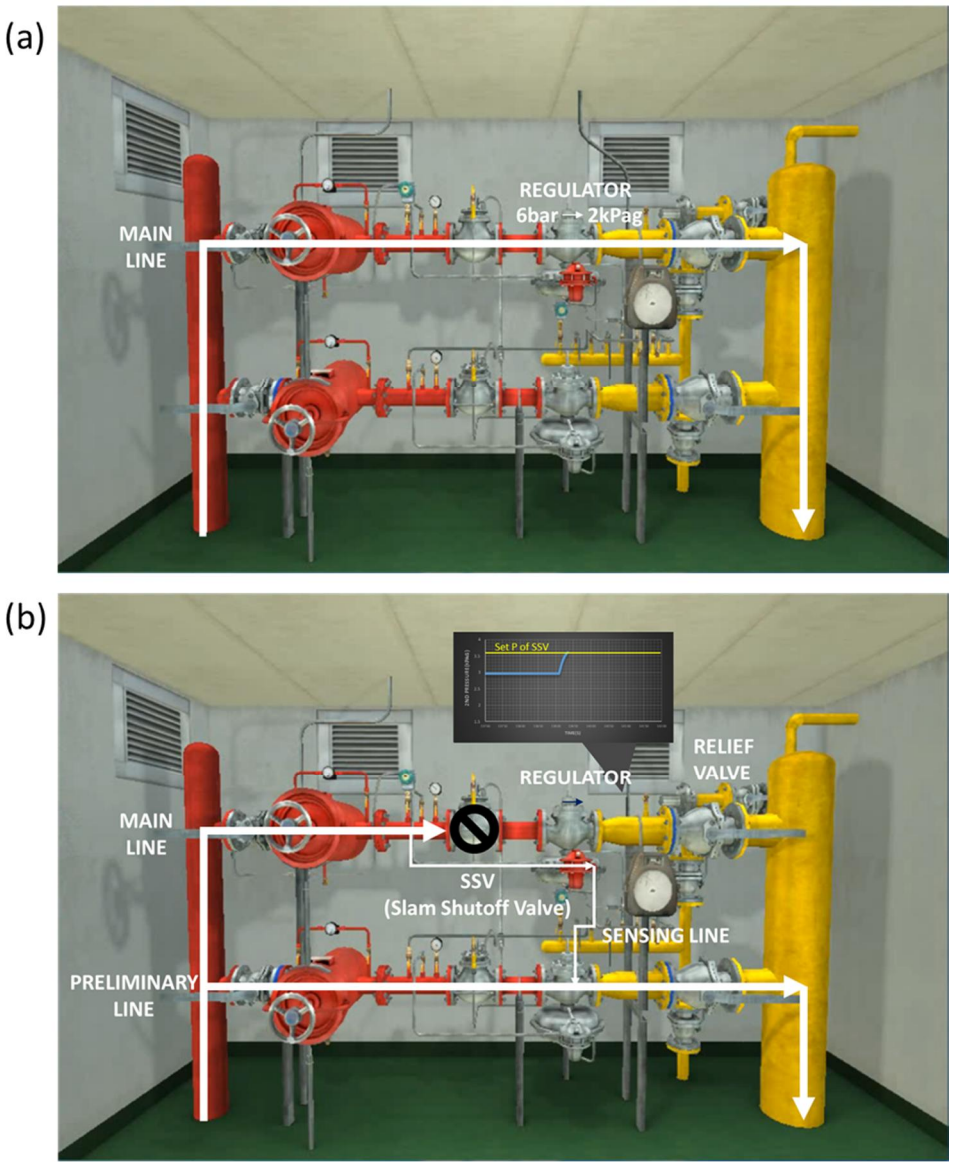

Figure 4-11. Operation Scenarios (a) Normal operation, (b) Mild case

In relief case (Figure 4-12(a)), as SSV fails to block the supply and gas pressure

reaches the relief valve set pressure the valve vents pressurized gas outside the station as much as the quantity its size is capable of.

For worst case (Figure 4-12(b)), gas is released at high pressure due to a series of malfunction of all safety devices. In this study worst case scenario is performed among three main scenarios in order to evaluate our model linking of the process simulation and accident simulation for operator training system in the pressure regulating station.

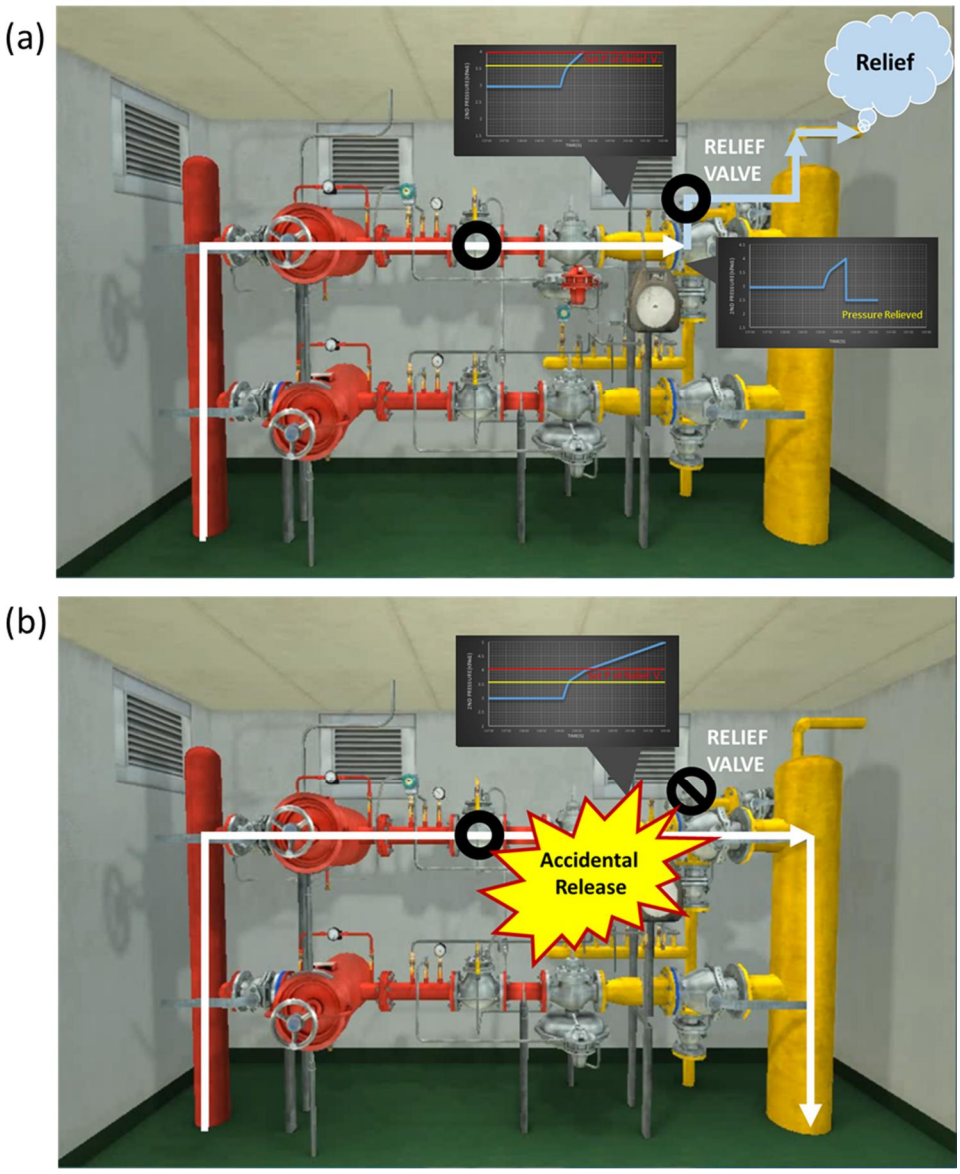

Figure 4-12. Operation Scenarios (a) Relief case, (b) Worst case

Accident Simulation Modeling

After the onset of training, the instructor starts the 2nd pressure rise scenario. The stepwise course of training is as follows. First, the value of 2nd pressure from dynamic process simulation model is transmitted to the trainee in real-time. Next, the 2nd pressure reaches the release pressure which was set by the instructor (1.1kg/cm2 - changeable depending on the scenario), which leads to the automatic source-term simulation based on the values of process variables like temperature and pressure at the leakage spot. At the same time, corresponding 3D-CFD dispersion simulation results in the database whose input is from source-term simulation are provided to the trainee. Finally, based on this process variables and accident data the trainee is induced to take appropriate actions.

Figure 4-13 indicates the gas concentration (Red:1.0, Green:0.5, Blue:0.0 m3/m3) from 10 to 600 seconds after the release stops at the height of ventilation inside the station by 2D (Figure 4-13(a)) and at the outside of the station by 3D (Figure 4-13(b) when a gas releases near the pressure recorder due to 2nd pressure rise(1.1kg/cm2).

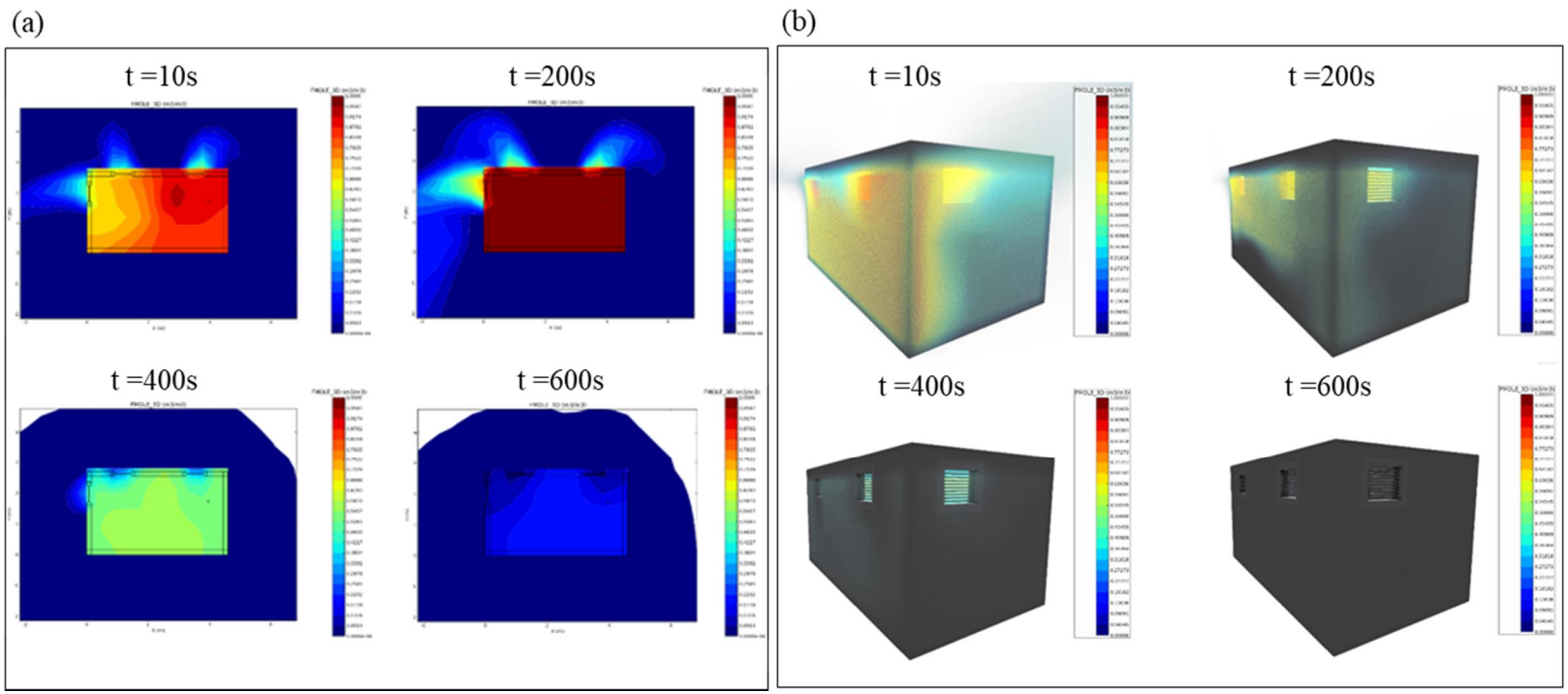

Figure 4-13. Gas dispersion results by 3D-CFD (a) inside the station at the height of ventilation (b) outside the station

For simulating the explosion outcome inside the station after the release, based on the indoor dispersion results which show the time dependent gas concentration at a certain position inside the station (t, x, y, z), the highest flammable positions at different times are extracted and the explosion outcomes are simulated for this position as an ignition point. The gas flammability is assessed by the ratio of the flammable gas concentration in the air and the stoichiometric ratio of that gas over air in the combustion, which would be higher as it approaches to 1.

Figure 4-14(a) shows the gas dispersion results of concentration between lower and upper flammable limit (LFL and UFL) with the front view of the gas station 200s after the release stops, and Figure 4-14(b) shows the associated explosion results of overpressure for the 15 monitoring points inside the gas station. Two highest overpressure of around 2.7barg and 2.3barg are detected at the two outlets of ventilation windows near the release position.

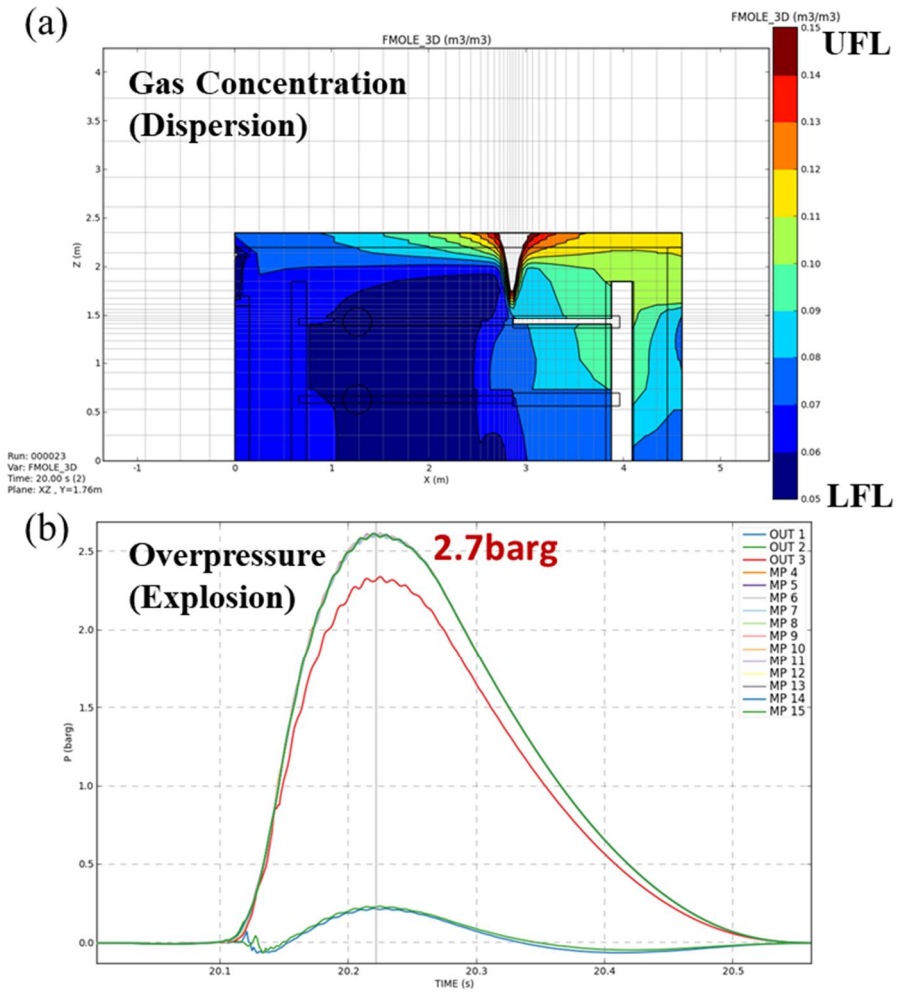

Figure 4-14. Gas dispersion and explosion results inside the station

Interactive Simulation Modeling

The demo version of interactive simulation module is designed as in Figure 4-15.

In the center is PFD (Process Flow Diagram) of pressure regulating station, on the left are process upsets & accident scenarios, at the top are controllers and process variable information, on the right is single variable chart, and at the bottom is gas concentration of dispersed gas.

The trainee can shut off gas supply by clicking the red circle above the emergency shutdown valve. The message above the PFD indicates the status of controller alarms such as High or Low when 2nd pressure goes beyond or below each limit.

The process upsets & accident scenarios on the left list was set up to initiate the desired scenario by clicking the button. Each scenario is identical to Mild case, Relief case, and Worst case in Table 4-2.

On the top are several tables of Dynamic Integrator, Regulator Operation, Source-term Model and Main & Preliminary Controller. In the Dynamic Integrator table, the trainer can specify the simulation speed and display interval, and in the Regulator Operation table the opening% of supply and safety valve is displayed. In the Source-term Model table, discharge calculation is done in real time, and in the Main & Preliminary table, the status of controllers (PV, OP, SP) is displayed. By clicking the right end cell of each table, trainee can monitor the trend of univariate chart on the right corner. Dispersed gas concentration results at the bottom is only activated in worst case among three scenarios, which shows 3D geometry of the pressure regulating station, gas concentration at the height of ventilation in the form of univariate chart and 2D & 3D image.

By clicking the play button on the left top corner, training starts from the initial

state.

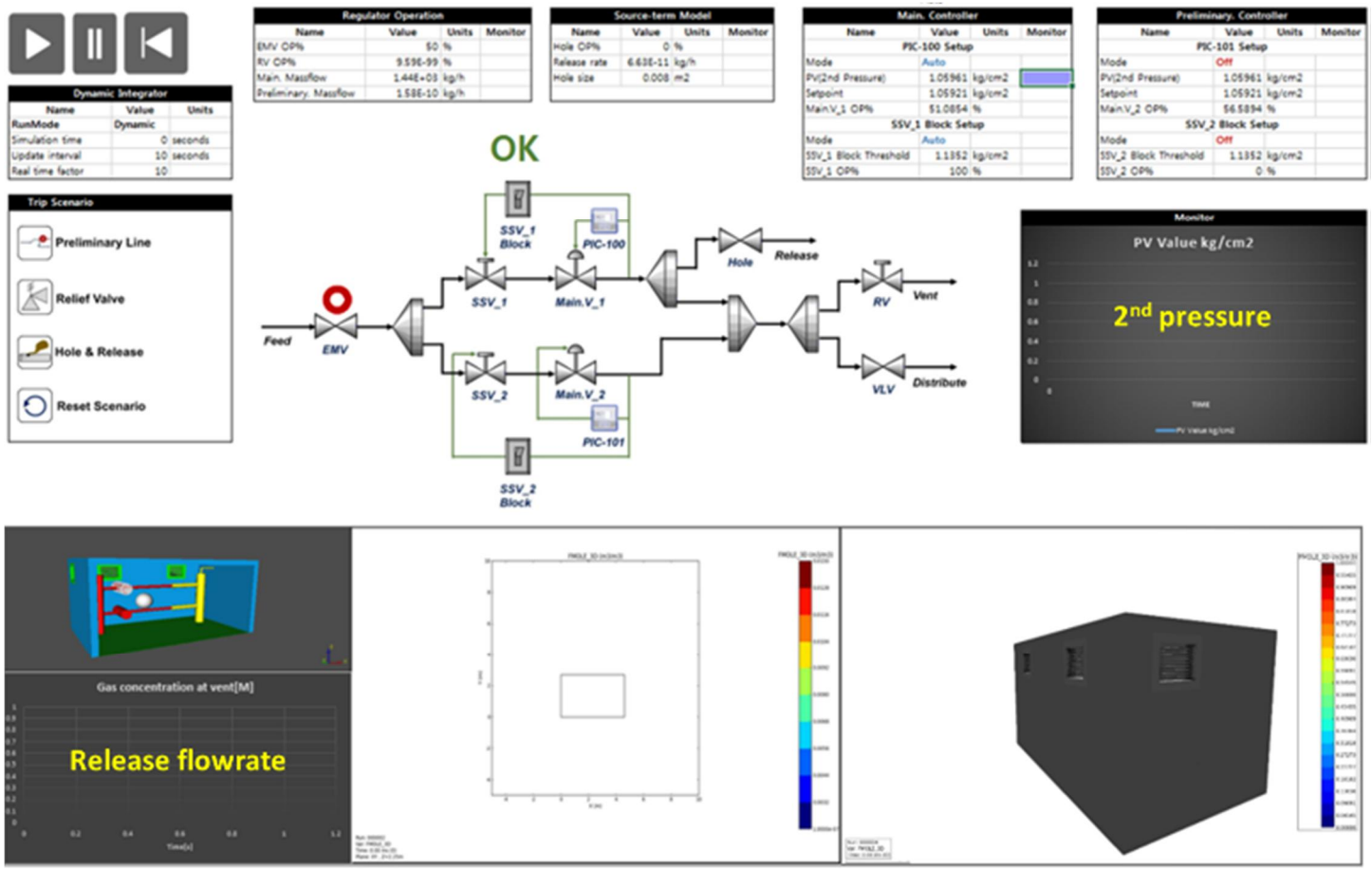

Figure 4-15. Demo version of interactive simulation module

The scenario propagation of worst case is shown in Figure 4-16. When the trainer clicks the 'Hole & Release' scenario button on the left, 2nd pressure starts to rise and the 2nd pressure keeps rising beyond the High alarm limit. When it reaches release pressure which was set up in advance, gas release begins through the valve named 'Hole'. If release occurs, the release rate is calculated in the source-term model and opening% of 'Hole' is adjusted automatically to meet the calculated release rate. In addition, corresponding dispersion simulation result which accepts the release rate as an input is displayed at the bottom from the data bank (Figure 4-16(a)). If the trainee clicks the EMV, inlet supply is shut off and only the released gas until that time would disperse outside (Figure 4-16(b)).

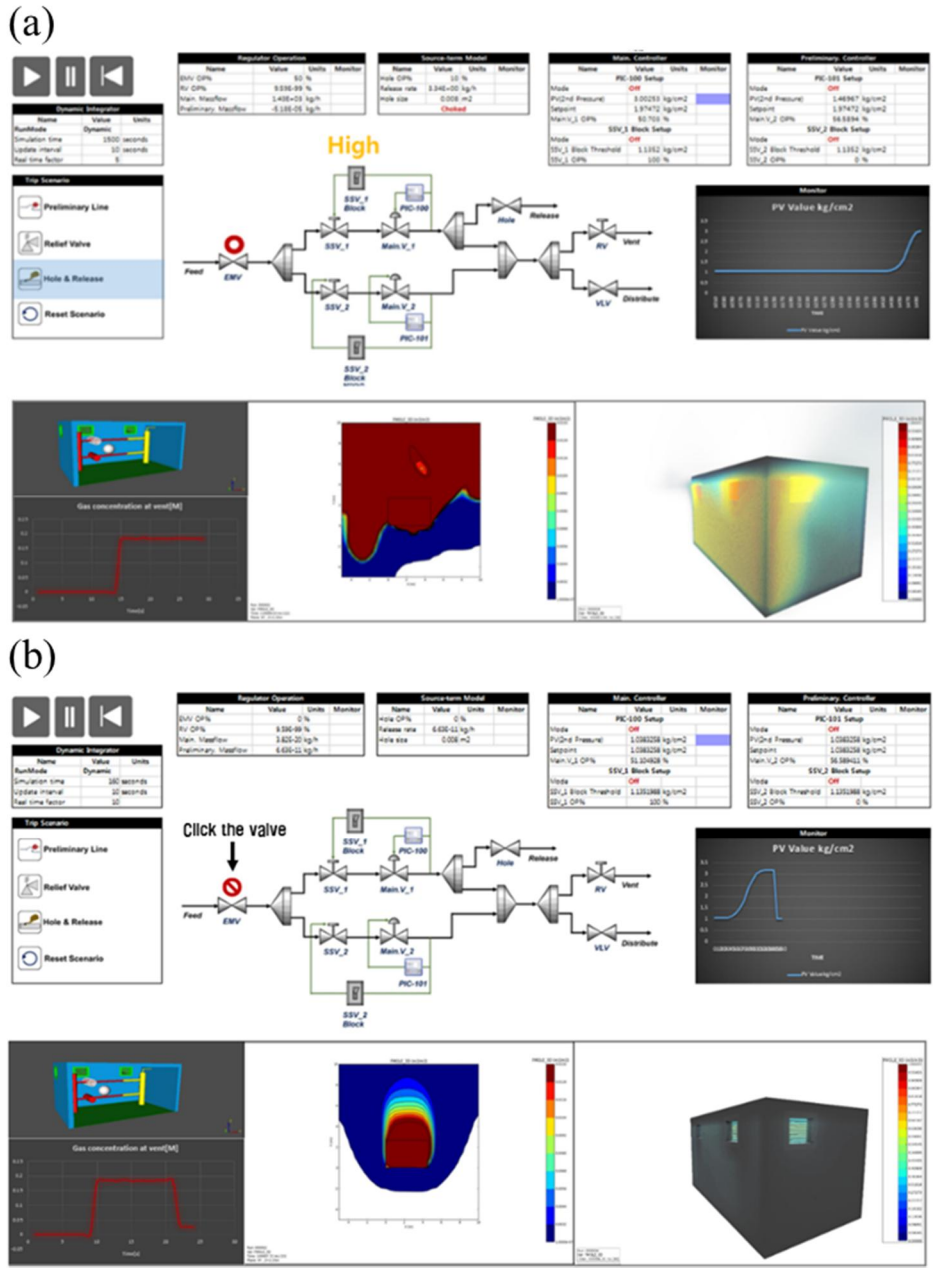

Figure 4-16. Worst case scenario propagation (a) when release starts and

(b) emergency shut down is completed

4.3.2. Prototype Test and Training Evaluation

By using data processing method in Figure 4-4, rating system was designed to evaluate the performance of the trainee. For instance, two training cases with lead time of 10 minutes (Operator 1) and 15 minutes (Operator 2) to take measures are simulated as in Figure 4-17, where the pressure accumulation at the equipment and associated release mass flowrate via the hole differs with each other.

The resultant dispersion outcomes to surrounding area and the explosion outcomes at the ignition point of highest flammability at 15min after the release starts are compared in Figure 4-18 and Figure 4-19 for each operator. As can be seen in the figure, stark difference can be seen in the two results. When this technique is applied to operator training system, it could help trainees to make a correct and prompt decision and accordingly to minimize accident damage.

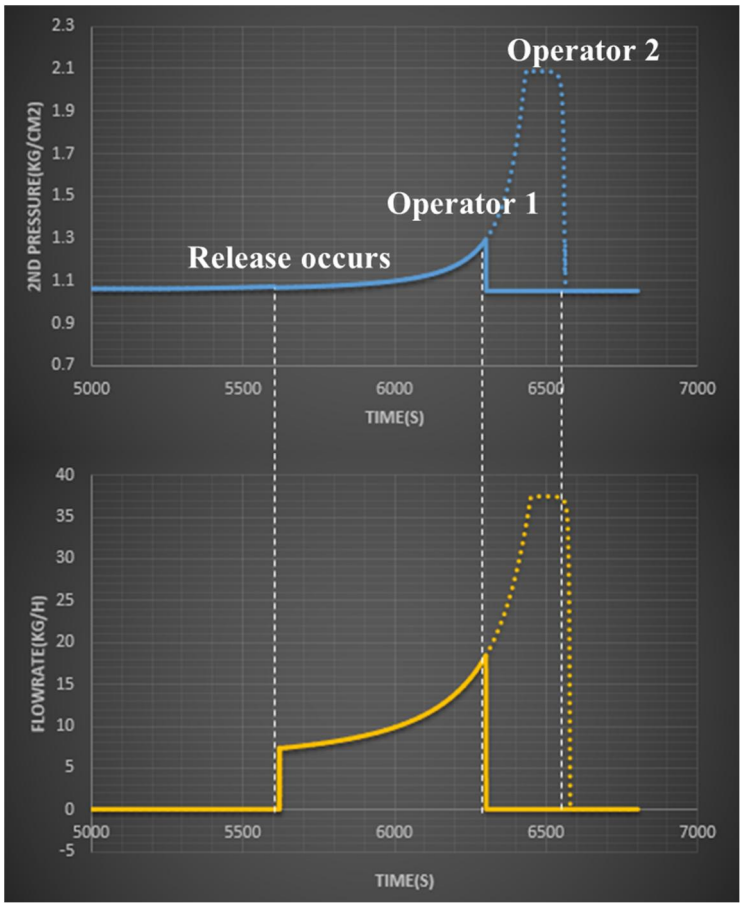

Figure 4-17. Pressure accumulation and release mass flowrate for two operators with different lead times to take measures

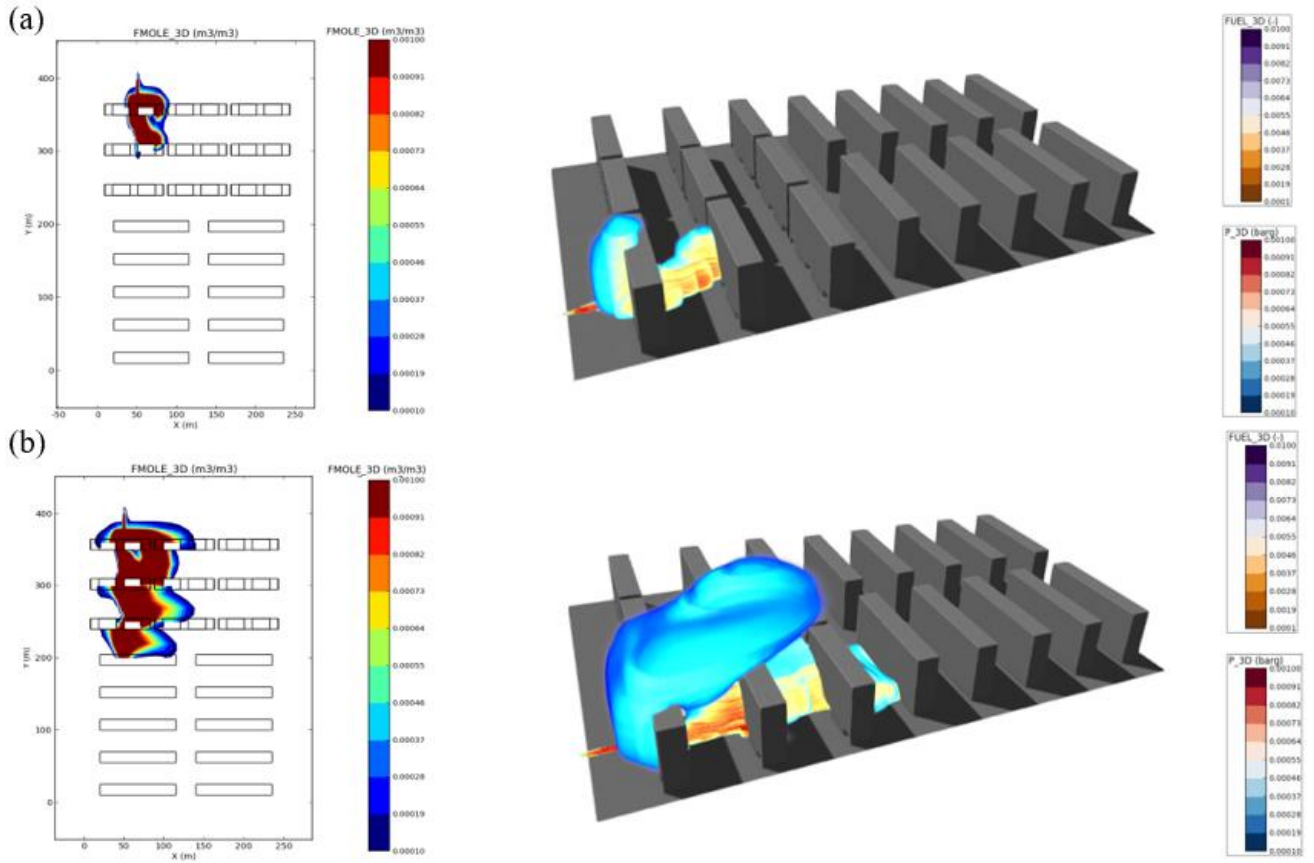

Figure 4-18. Gas concentration value from dispersion for two operators with different lead times to take measures (a) lead time of 10min (b) lead time of 15min

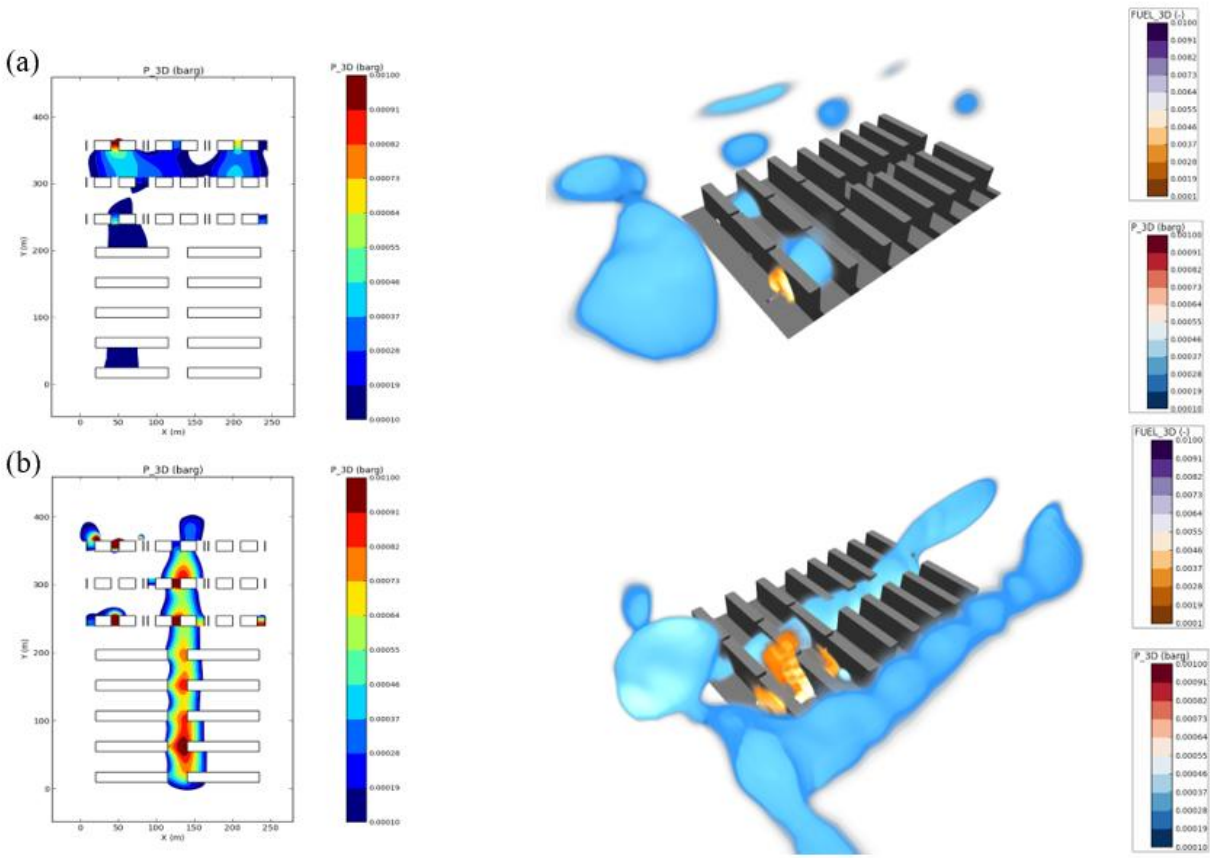

Figure 4-19. Overpressure value from gas explosion for two operators with different lead times to take measures (a) lead time of 10min (b) lead time of 15min

4.4. Concluding Remarks

In this study, development of plant interactive simulation model which will be used as an internal engine of operator training system targeting at pressure regulating station was done and the performance was rated. Developed model was designed to take correct and prompt measures depending on the process upsets and accident scenarios via OLE.

Representative scenario of 'Hole & Release' is studied as follows. When the instructor starts the scenario, 2nd pressure begins to rise due to a main valve malfunction. When it keeps rising with total failure of safety devices and reaches 1.1kg/cm2_g, gas release occurs near a pressure recorder via a hole of 10mm diameter.

The trainee who noticed this accident should shut-off the emergency shutdown valve manually. When this procedure is properly done, the training scenario terminates and the simulation results with respect to the lead time to take actions are used to rate the performance of the trainee. The model could be applied to a more complex process such as petrochemical plant in the future, and higher effectiveness of training is expected as operating procedure becomes more complex.

CHAPTER 5. Conclusion

This thesis developed new technologies for advanced process design and operation using superstructure and multi-modular approach with the recent need of natural gas industries in the context of new framework of process systems engineering. In the overall thesis, the optimal design of sustainable process, process intensification for sequential units, safety assessment, multi-objective optimization of economic feasibility and inherent safety, and multi-modular approach for interactive simulation of dynamic process and accident models for safer operation were discussed.

From modeling and technical perspectives, the contribution of the thesis is to solve a variety of problems in process systems engineering following the recent need of new technologies from oil and gas industries.

Chapter 2 addressed the problem occurring as two new trends emerged in the natural gas processing industries. One is the enlarged portion of unconventional natural gas sources like small-to-midsize reservoirs or shale gases recently, and the other is the switching of compressor drivers from steam turbines to highly efficient aero-derivative gas turbines or electric motors. The former requires sophisticated nitrogen recovery units in conventional LNG processes as the feed gases from unconventional sources are generally leaner containing higher amount of nitrogen. The latter makes the LNG processes completely recover the methane to product LNG almost not producing the fuel gas as the new drivers consume less or no fuel gas. Following these trends and associated needs of new technologies, the chapter aimed at designing new cryogenic nitrogen recovery processes integrated with LNG

production and NGL recovery through structural expansion and pinch-exergy integration. Consequently, each proposed solution improved the process efficiency by up 38.6% than that of the reference base case. Also, these solutions were compared with each other in terms of thermodynamic efficiency with respect to the nitrogen content in the feed gases so that the study could give reasonable guidelines to deciding the optimal solution based on the order of design priority at certain feed gases.

Chapter 3 tried to solve the problem of how to manage the plant risk fundamentally in the context of general procedures of process design. With the aim of designing a safer process in the context of these design procedures, Chapter 3 newly proposed two systematic approaches. One tried to reduce the risk through design modification of an existing GOSP plant based on the QRA results following the general design procedures. Meanwhile, the other integrated the conceptual design and hazard analysis by introducing inherent safety concept at the preliminary design stage, and decided an optimal process design through superstructure formulation and multi-objective optimization for minimizing both the TAC and the risk. This latter approach could largely lower the cost required for finalizing the design as it doesn't need to follow the general procedure where the recursive loop is recycled until the risk is reduced to an acceptable level. Despite the differences these two approaches have each other, however, they are essentially in the same context in that they share the same purpose of deciding a process design which is safer and/or even cheaper than the existing processes.

In Chapter 3.1, the risk potential in original design of GOSP was tried to be reduced by mitigating the flash fire and pool fire probabilities under the selected leak scenario. To do this, modification of the process design by altering the operating pressure of the three-phase separator from 12.0barg to 0.52barg was proposed. Modification resulted in a 27% decrease in the total societal risk from 1.41E-03/year to 1.02E-03/year with an additional capital cost of around $50,000, which dragged down the risk to the tolerable ALARP region.

In Chapter 3.2. applied the new methodologies for designing an optimal heat transfer structure and operating conditions of natural gas liquefaction processes considering the inherent safety, deciding that the SMR (single-stage mixed refrigerant process) structure with the TAC of 626.6MM$/yr and fatality frequency of 1.28E-03/yr has the priority over all possible solutions.

Chapter 4 addressed the problem incurred by the weak interactions between control room operators and field operators in operating a certain plant. Even though the real accident occurs in the plant site and the cooperation of operators is crucial for stably and safely operating a plant in unwanted situations, problems of information gap between each other has been hardly dealt with due to the different nature of each part. In this chapter, a new interactive operator training module covering the whole process from normal operation to accident situations was developed through multi-modular approach using advanced simulation and data processing technologies. This interactive simulation modeling delivers the online simulation results to the control room and field operators and induces them to take proper actions in case of a random accidental situation among pre-identified

scenarios in a chemical plant. Developed model integrates the real-time process dynamic simulation with the off-line database of 3D-CFD accident simulation results in a designed interface using OLE technology so that it could convey the online information of the accident to trainees which is not available in existing operator training systems. The model encompasses the whole process of data transfer till the end of the training at which trainees complete an emergency shutdown system in a programmed model. Consequently, the module could improve the effectiveness of operator training system through interactively linking the trainee actions with the model interface so that the associated accident situations would vary with respect to each trainee's competence facing an accident.

Nomenclature

ALARP	As low as reasonably practicable
BLEVE	Boiling liquid expanding vapor explosion
CAT	Catastrophic rupture
CFD	Computational fluid dynamics
CRDFFP	Continuous release with rainout delayed flash fire and pool fire effects
CRDFXP	Continuous release with rainout delayed flash fire and explosion effects
CRIHJP	Continuous release with rainout immediate horizontal jet fire and additional pool fire effects
CROP	Control room operator
C3MR	Propane precooled mixed refrigerant process
DMR	Dual mixed refrigerant process
ED	Exergy destruction
EE	Exergy efficiency
EIV	Emergency isolation valve
EOS	Equation of state
ESD	Emergency shutdown
ETA	Event tree analysis
F.F.	Fatality frequency
FOP	Field operator
GOSP	Gas oil separation plant
GSP	Gas subcooled process
GTU	Gas treatment unit
HAZID	Hazard identification
HAZOP	Hazard and operability
H&MB	Heat and material balance
HSE	Health and Safety Executive
ID	Inner diameter
IF	Isolation failure
IFCET	Inherent fire consequence estimation tool
IGPP	Integrated gas process plant
IR	Individual risk
IRA	Inherent risk assessment
iRET	Integrated risk estimation tool
IS	Isolation success
ISIM	Inherent safety index module
KOGAS	Korea gas corporation
LFL	Lower flammable limit
LMTD	Log mean temperature difference
LNG	Liquefied natural gas
LPG	Liquefied petroleum gas
MFC	Mixed fluid cascade
MILP	Mixed integer linear programming

MR	Mixed refrigerant
MSHE	Multi-stream heat exchanger
NGL	Natural gas liquid
NLL	Normal liquid level
NLP	Non-linear programming
NRU	Nitrogen recovery unit
NSGA-II	Non-dominated sorting genetic algorithm
OGP	Oil and gas producers
OLE	Object linking and embedding
OP	Output from the controller
OTS	Operator training system
PFD	Process flow diagram
P&ID	Piping and instrumentation diagram
Precooled	Precooled mixed refrigerant without a phase separator
PRI	Process route index
PSI	Process stream index
PV	Process variable
QRA	Quantitative risk assessment
SIS	Safety instrumented system
SMR	Single-stage mixed refrigerant process
SP	Set point
SQP	Sequential quadratic programming
SR	Societal risk
SSV	Slam shutoff valve
TAC	Total annual cost
TORCAT	Toxic release consequence analysis tool
2TISI	Two-tier inherent safety index
UFL	Upper flammable unit
VCE	Vapor cloud explosion
VLLE	Vapor-liquid-liquid equilibrium

Reference

CHAPTER 1

[1] Lee, Y., Lim, Y., & Lee, W. B. (2019). Integrated process design and optimization of nitrogen recovery in natural gas processing. *Industrial & Engineering Chemistry Research*.
[2] Lee, Y., Lee, S., Shin, S., Lee, G., Jeon, J., Lee, C. J., & Han, C. (2015). Risk-based process safety management through process design modification for gas treatment unit of gas oil Separation plant. *Industrial & Engineering Chemistry Research*, *54*(22), 6024-6034.
[3] Lee, Y., Ko, C., Lee, H., Jeon, K., Shin, S., & Han, C. (2017). Interactive plant simulation modeling for developing an operator training system in a natural gas pressure-regulating station. *Petroleum Science*, *14*(3), 529-538.

CHAPTER 2

[1] Christopher, M. O., Mark, J. R., Scott, R. T., & Gowri K. (2015). State-of-the-art nitrogen removal methods from Air Products for liquefaction plants. *LNG journal*.
[2] Chen, F., Okasinski, M., & Sabram, T. (2016). Novel nitrogen removal shemes for LNG plants with electric motor drive and varying feed composition. *Air Products and Chemicals, Inc*.
[3] Remeljej, C. W., & Hoadley, A. F. A. (2006). An exergy analysis of small-scale liquefied natural gas (LNG) liquefaction processes. *Energy*, *31*(12), 2005-2019.
[4] De Guido, G., Lange, S., & Pellegrini, L. A. (2015). Refrigeration cycles in low-temperature distillation processes for the purification of natural gas. *Journal of Natural Gas Science and Engineering*, *27*, 887-900.
[5] Mehrpooya, M., Vatani, A., & Mousavian, S. A. (2010). Introducing a novel integrated NGL recovery process configuration (with a self-refrigeration system (open–closed cycle)) with minimum energy requirement. *Chemical Engineering and Processing: Process Intensification*, *49*(4), 376-388.
[6] Vatani, A., Mehrpooya, M., & Tirandazi, B. (2013). A novel process configuration for co-production of NGL and LNG with low energy requirement. *Chemical engineering and processing: process intensification*, *63*, 16-24.
[7] He, T., & Ju, Y. (2014). Design and optimization of a novel mixed refrigerant cycle integrated with NGL recovery process for small-scale LNG plant. *Industrial & Engineering Chemistry Research*, *53*(13), 5545-5553.
[8] Mehrpooya, M., Hossieni, M., & Vatani, A. (2014). Novel LNG-based integrated process configuration alternatives for coproduction of LNG and NGL. *Industrial & Engineering Chemistry Research*, *53*(45), 17705-17721.
[9] Ansarinasab, H., & Mehrpooya, M. (2017). Evaluation of novel process configurations for coproduction of LNG and NGL using advanced exergoeconomic analysis. *Applied Thermal Engineering*, *115*, 885-898.
[10] Rufford, T. E., Smart, S., Watson, G. C., Graham, B. F., Boxall, J., Da Costa, J. D., & May, E. F. (2012). The removal of CO2 and N2 from natural gas: A review of

conventional and emerging process technologies. *Journal of Petroleum Science and Engineering*, *94*, 123-154.
[11] Kuo, J. C., Wang, K. H., & Chen, C. (2012). Pros and cons of different Nitrogen Removal Unit (NRU) technology. *Journal of Natural Gas Science and Engineering*, *7*, 52-59.
[12] Hamedi, H., Karimi, I. A., & Gundersen, T. (2018). Optimal cryogenic processes for nitrogen rejection from natural gas. *Computers & Chemical Engineering*, *112*, 101-111.
[13] Ghorbani, B., Hamedi, M. H., Amidpour, M., & Mehrpooya, M. (2016). Cascade refrigeration systems in integrated cryogenic natural gas process (natural gas liquids (NGL), liquefied natural gas (LNG) and nitrogen rejection unit (NRU)). *Energy*, *115*, 88-106.
[14] Ghorbani, B., Hamedi, M. H., & Amidpour, M. (2016). Development and optimization of an integrated process configuration for natural gas liquefaction (LNG) and natural gas liquids (NGL) recovery with a nitrogen rejection unit (NRU). *Journal of Natural Gas Science and Engineering*, *34*, 590-603.
[15] Ghorbani, B., Hamedi, M. H., Amidpour, M., & Shirmohammadi, R. (2017). Implementing absorption refrigeration cycle in lieu of DMR and C3MR cycles in the integrated NGL, LNG and NRU unit. *International Journal of Refrigeration*, *77*, 20-38.
[16] Ghorbani, B., Mehrpooya, M., Shirmohammadi, R., & Hamedi, M. H. (2018). A comprehensive approach toward utilizing mixed refrigerant and absorption refrigeration systems in an integrated cryogenic refrigeration process. *Journal of Cleaner Production*, *179*, 495-514.
[17] Mehrpooya, M., Sharifzadeh, M. M. M., & Ansarinasab, H. (2018). Investigation of a novel integrated process configuration for natural gas liquefaction and nitrogen removal by advanced exergoeconomic analysis. *Applied Thermal Engineering*, *128*, 1249-1262.
[18] Rosen, M. (2013). Exergy: energy, environment, and sustainable development/Ibrahim Dincer, Marc A. Rosen.
[19] Moran, M. J., Shapiro, H. N., Boettner, D. D., & Bailey, M. B. (2010). *Fundamentals of engineering thermodynamics*. John Wiley & Sons.
[20] Marmolejo-Correa, D., & Gundersen, T. (2012). A comparison of exergy efficiency definitions with focus on low temperature processes. *Energy*, *44*(1), 477-489.
[21] Hinderink, A. P., Kerkhof, F. P. J. M., Lie, A. B. K., Arons, J. D. S., & Van Der Kooi, H. J. (1996). Exergy analysis with a flowsheeting simulator—I. Theory; calculating exergies of material streams. *Chemical Engineering Science*, *51*(20), 4693-4700.
[22] Szargut, J., Morris, D. R., & Steward, F. R. (1987). Exergy analysis of thermal, chemical, and metallurgical processes.
[23] Kotas, T. J. (2013). *The exergy method of thermal plant analysis*. Elsevier.
[24] Bejan, A., Tsatsaronis, G., Moran, M., & Moran, M. J. (1996). *Thermal design and optimization*. John Wiley & Sons.
[25] Vatani, A., Mehrpooya, M., & Palizdar, A. (2014). Advanced exergetic analysis of five natural gas liquefaction processes. *Energy conversion and management*, *78*, 720-737.

[26] Tirandazi, B., Mehrpooya, M., Vatani, A., & Moosavian, S. A. (2011). Exergy analysis of C2+ recovery plants refrigeration cycles. *Chemical Engineering Research and Design*, *89*(6), 676-689.
[27] Smith, E. M. (2005). *Advances in thermal design of heat exchangers: a numerical approach: direct-sizing, step-wise rating, and transients*. Wiley.
[28] Kotas, T. J. (1995). The Exergy Method of Thermal Plant Analysis/Krieger Publishing Company. *Malabar, Florida*.

CHAPTER 3

[1] Freeman, R. A. (1990). CCPS guidelines for chemical process quantitative risk analysis. *Plant/Operations Progress*, *9*(4), 231-235.
[2] Rasmussen, N. C. (1975). *Reactor Safety Study: An Assessment of Accident Risks in U.S. Commercial Nuclear Power Plants*. [NUREG-75/014(WASH-1400)], Rockville, MD, USA
[3] Pasman, H., & Reniers, G. (2014). Past, present and future of Quantitative Risk Assessment (QRA) and the incentive it obtained from Land-Use Planning (LUP). *Journal of loss prevention in the process industries*, *28*, 2-9.
[4] Khan, F. I., Sadiq, R., & Husain, T. (2002). Risk-based process safety assessment and control measures design for offshore process facilities. *Journal of hazardous materials*, *94*(1), 1-36.
[5] Vinnem, J. E. (2013). *Offshore risk assessment: principles, modelling and applications of QRA studies*. Springer Science & Business Media.
[6] Khakzad, N., Khan, F., & Amyotte, P. (2011). Safety analysis in process facilities: Comparison of fault tree and Bayesian network approaches. *Reliability Engineering & System Safety*, *96*(8), 925-932.
[7] Jianwen, Z., Da, L., & Wenxing, F. (2014). An approach for estimating toxic releases of H2S-containing natural gas. *Journal of hazardous materials*, *264*, 350-362.
[8] Jung, S., Ng, D., Diaz-Ovalle, C., Vazquez-Roman, R., & Mannan, M. S. (2011). New approach to optimizing the facility siting and layout for fire and explosion scenarios. *Industrial & Engineering Chemistry Research*, *50*(7), 3928-3937.
[9] Yet-Pole, I., Shu, C. M., & Chong, C. H. (2009). Applications of 3D QRA technique to the fire/explosion simulation and hazard mitigation within a naphtha-cracking plant. *Journal of Loss Prevention in the Process Industries*, *22*(4), 506-515.
[10] Middha, P., Hansen, O. R., Grune, J., & Kotchourko, A. (2010). CFD calculations of gas leak dispersion and subsequent gas explosions: validation against ignited impinging hydrogen jet experiments. *Journal of hazardous materials*, *179*(1-3), 84-94.
[11] Di Domenico, J., Vaz Jr, C. A., & de Souza Jr, M. B. (2014). Quantitative risk assessment integrated with process simulator for a new technology of methanol production plant using recycled CO2. *Journal of hazardous materials*, *274*, 164-172.
[12] Nam, K., Chang, D., Chang, K., Rhee, T., & Lee, I. B. (2011). Methodology of life cycle cost with risk expenditure for offshore process at conceptual design stage. *Energy*, *36*(3), 1554-1563.
[13] Dinh, L. T., Pasman, H., Gao, X., & Mannan, M. S. (2012). Resilience engineering of industrial processes: principles and contributing factors. *Journal of*

Loss Prevention in the Process Industries, *25*(2), 233-241.
[14] Shariff, A. M., & Leong, C. T. (2009). Inherent risk assessment—a new concept to evaluate risk in preliminary design stage. *Process Safety and Environmental Protection*, *87*(6), 371-376.
[15] Gangadharan, P., Singh, R., Cheng, F., & Lou, H. H. (2013). Novel methodology for inherent safety assessment in the process design stage. *Industrial & Engineering Chemistry Research*, *52*(17), 5921-5933.
[16] Ordouei, M. H., Elkamel, A., & Al-Sharrah, G. (2014). New simple indices for risk assessment and hazards reduction at the conceptual design stage of a chemical process. *Chemical Engineering Science*, *119*, 218-229.
[17] Rathnayaka, S., Khan, F., & Amyotte, P. (2014). Risk-based process plant design considering inherent safety. *Safety science*, *70*, 438-464.
[18] Cetesb. Environmental Company of Sao Paulo State, Sao Paulo. (2003). Available at: http://www.ceresb.sp.gov.br (accessed 03.04.12).
[19] Health and Safety Executive (HSE). (2001). *Reducing Risks, Protecting People*. HSE's Decision-making Process.
[20] PETRONAS Carigali Iraq Holding BV. (2010). *Quantitative Risk Assessment (QRA) Study for the Garraf Final Development Plan (GFDP) Project*.
[21] International Association of Oil & Gas Producers (OGP). (2010). *Risk Assessment Data Directory.* Report No. 434.
[22] Health and Safety Executive (HSE). (2013). *Offshore Hydrocarbon Releases Statistics*
[23] EI. (2006). *EI Research Report: Ignition Probability Review, Model Development and Look-up Correlations*. Energy Institute. London.
[24] AIChE/CCPS. (2000). *Guideline for Chemical Process Quantitative Risk Analysis, Sec. Ed.* New York.
[25] Turton, R., Bailie, R. C., Whiting, W. B., & Shaeiwitz, J. A. (2008). *Analysis, synthesis and design of chemical processes*. Pearson Education.
[26] Mannan, S. (2013). *Lees' Process Safety Essentials: Hazard Identification, Assessment and Control*. Butterworth-Heinemann.
[27] Bernechea, E. J., & Arnaldos, J. (2014). Optimizing the design of storage facilities through the application of ISD and QRA. *Process Safety and Environmental Protection*, *92*(6), 598-615.
[28] Khan, F. I., & Amyotte, P. R. (2002). Inherent safety in offshore oil and gas activities: a review of the present status and future directions. *Journal of Loss Prevention in the Process Industries*, *15*(4), 279-289.
[29] Kletz, T. A. (1991). *Plant design for safety: a user-friendly approach*. New York: Hemisphere Publishing Corporation.
[30] Jafari, M. J., Mohammadi, H., Reniers, G., Pouyakian, M., Nourai, F., Torabi, S. A., & Miandashti, M. R. (2018). Exploring inherent process safety indicators and approaches for their estimation: A systematic review. *Journal of Loss Prevention in the Process Industries*.
[31] Leong, C. T., & Shariff, A. M. (2008). Inherent safety index module (ISIM) to assess inherent safety level during preliminary design stage. *Process Safety and Environmental Protection*, *86*(2), 113-119.
[32] Leong, C. T., & Shariff, A. M. (2009). Process route index (PRI) to assess level of explosiveness for inherent safety quantification. *Journal of Loss Prevention in*

the Process Industries, *22*(2), 216-221.
[33] Lawrence, D. (1996). *Quantifying inherent safety of chemical process routes* (Doctoral dissertation, © Duncan Lawrence).
[34] Heikkilä, A. M. (1999). *Inherent safety in process plant design: an index-based approach*. VTT Technical Research Centre of Finland.
[35] Palaniappan, C., Srinivasan, R., & Tan, R. (2004). Selection of inherently safer process routes: a case study. *Chemical Engineering and Processing: Process Intensification*, *43*(5), 641-647.
[36] Shariff, A. M., Leong, C. T., & Zaini, D. (2012). Using process stream index (PSI) to assess inherent safety level during preliminary design stage. *Safety science*, *50*(4), 1098-1103.
[37] Ortiz-Espinoza, A. P., Jiménez-Gutiérrez, A., & El-Halwagi, M. M. (2017). Including inherent safety in the design of chemical processes. *Industrial & Engineering Chemistry Research*, *56*(49), 14507-14517.
[38] Shariff, A. M., Rusli, R., Leong, C. T., Radhakrishnan, V. R., & Buang, A. (2006). Inherent safety tool for explosion consequences study. *Journal of Loss Prevention in the Process Industries*, *19*(5), 409-418.
[39] Shariff, A. M., & Zaini, D. (2010). Toxic release consequence analysis tool (TORCAT) for inherently safer design plant. *Journal of hazardous materials*, *182*(1-3), 394-402.
[40] Shariff, A. M., Wahab, N. A., & Rusli, R. (2016). Assessing the hazards from a BLEVE and minimizing its impacts using the inherent safety concept. *Journal of Loss Prevention in the Process Industries*, *41*, 303-314.
Protection, *104*, 254-267.
[41] Ruiz-Femenia, R., Fernández-Torres, M. J., Salcedo-Díaz, R., Gómez-Rico, M. F., & Caballero, J. A. (2017). Systematic tools for the conceptual design of inherently safer chemical processes. *Industrial & Engineering Chemistry Research*, *56*(25), 7301-7313.
[42] Vázquez, D., Ruiz-Femenia, R., Jiménez, L., & Caballero, J. A. (2018). Multiobjective Early Design of Complex Distillation Sequences Considering Economic and Inherent Safety Criteria. *Industrial & Engineering Chemistry Research*, *57*(20), 6992-7007.
[43] Eini, S., Abdolhamidzadeh, B., Reniers, G., & Rashtchian, D. (2015). Optimization procedure to select an inherently safer design scheme. *Process Safety and Environmental Protection*, *93*, 89-98.
[44] Eini, S., Shahhosseini, H. R., Javidi, M., Sharifzadeh, M., & Rashtchian, D. (2016). Inherently safe and economically optimal design using multi-objective optimization: the case of a refrigeration cycle. *Process Safety and Environmental*
[45] Crowl, D. A., Louvar, J. F. (1990) *Chemical process safety: Fundamentals with applications*. USA: Prentice Hall.
[46] Venkatarathnam, G., & Timmerhaus, K. D. (2008). *Cryogenic mixed refrigerant processes* (Vol. 100). New York: Springer.
[47] Wang, M., Khalilpour, R., & Abbas, A. (2014). Thermodynamic and economic optimization of LNG mixed refrigerant processes. *Energy Conversion and Management*, *88*, 947-961.
[48] Grodzevich, O., & Romanko, O. (2006). Normalization and other topics in multi-objective optimization.

[49] Roszkowska, E. (2011). Multi-criteria decision making models by applying the TOPSIS method to crisp and interval data. *Multiple Criteria Decision Making/University of Economics in Katowice*, *6*, 200-230.

CHAPTER 4

[1] European Chemical Industry Council (CEFIC). (2012). *THE CHEMICAL INDUSTRY IN EUROPE: TOWARDS SUSTAINABILITY*. report 2011/2012.
[2] Gupta, J. P. (2002). The Bhopal gas tragedy: could it have happened in a developed country?. *Journal of Loss Prevention in the process Industries*, *15*(1), 1-4.
[3] Holmstrom, D., Altamirano, F., Banks, J., Joseph, G., Kaszniak, M., Mackenzie, C., ... & Wallace, S. (2006). CSB investigation of the explosions and fire at the BP Texas City refinery on March 23, 2005. *Process safety progress*, *25*(4), 345-349.
[4] Kalantarnia, M., Khan, F., & Hawboldt, K. (2010). Modelling of BP Texas City refinery accident using dynamic risk assessment approach. *Process Safety and Environmental Protection*, *88*(3), 191-199.
[5] Antonovsky, A., Pollock, C., & Straker, L. (2014). Identification of the human factors contributing to maintenance failures in a petroleum operation. *Human factors*, *56*(2), 306-321.
[6] Meshkati, N. (1991). Human factors in large-scale technological systems' accidents: Three Mile Island, Bhopal, Chernobyl. *Industrial Crisis Quarterly*, *5*(2), 133-154.
[7] Aziz, H. A., Shariff, A. M., & Rusli, R. (2014). Operational Training Management System (OPTRAMS) for Safe Operation in Process Plant. *Advanced Materials Research*, *917*.
[8] Kletz, T. (1998). Process plants: A handbook for inherently safer designTaylor & Francis. *Bristol, PA*.
[9] Honeywell. (2005. *GUIDE TO THE NAPHTHA HYDRO DESULPHURIZATION STANDARD MODEL*. 2ND ed. Honeywell Process Solutions.
[10] Patle, D. S., Ahmad, Z., & Rangaiah, G. P. (2014). Operator training simulators in the chemical industry: review, issues, and future directions. *Reviews in Chemical Engineering*, *30*(2), 199-216.
[11] Ahmad, Z., Patle, D. S., & Rangaiah, G. P. (2016). Operator training simulator for biodiesel synthesis from waste cooking oil. *Process Safety and Environmental Protection*, *99*, 55-68.
[12] Dai, Y., Wang, H., Khan, F., & Zhao, J. (2016). Abnormal situation management for smart chemical process operation. *Current opinion in chemical engineering*, *14*, 49-55.
[13] Balaton, M. G., Nagy, L., & Szeifert, F. (2013). Operator training simulator process model implementation of a batch processing unit in a packaged simulation software. *Computers & Chemical Engineering*, *48*, 335-344.
[14] Cha, M., Han, S., Lee, J., & Choi, B. (2012). A virtual reality based fire training simulator integrated with fire dynamics data. *Fire Safety Journal*, *50*, 12-24.
[15] Cha, M., Huh, Y. C., & Mun, D. (2014). Framework of a Training Simulator for the Accident Response of Large-scale Facilities. *Korean Journal of Computational Design and Engineering*, *19*(4), 423-433.
[16] Schneider Electric. (2014*). TRAINEE GUIDEBOOK: EYESIM IMMERSIVE*

TRAINING SYSTEM GENERIC VIRTUAL CRUDE UNIT. Engineering Development Research Center(EDRC) of Seoul National University.
[17] Provost, G. T., Zitney, S. E., Turton, R. A., Erbes, M. R., & Stone, H. P. (2010, January). NETL Virtual Reality Dynamic Simulation Research and Training Center Promotes IGCC Technology With CO2 Capture. In *ASME 2010 Power Conference* (pp. 577-587). American Society of Mechanical Engineers.
[18] Kluge, A., Nazir, S., & Manca, D. (2014). Advanced applications in process control and training needs of field and control room operators. *IIE Transactions on Occupational Ergonomics and Human Factors*, *2*(3-4), 121-136.
[19] Liese, E., & Zitney, S. E. (2013, July). A Dynamic Process Model of a Natural Gas Combined Cycle: Model Development With Startup and Shutdown Simulations. In *ASME 2013 Power Conference* (pp. V002T08A004-V002T08A004). American Society of Mechanical Engineers.
[20] Kwon, H., Tak, K., Lee, I., Lee, J., & Moon, I. (2014). Web-based multi-dimensional education system for the simulated moving bed process. *Korean Journal of Chemical Engineering*, *31*(10), 1736-1745.
[21] Manca, D., Brambilla, S., & Colombo, S. (2013). Bridging between virtual reality and accident simulation for training of process-industry operators. *Advances in Engineering Software*, *55*, 1-9.
[22] Brambilla, S., & Manca, D. (2011). Recommended features of an industrial accident simulator for the training of operators. *Journal of loss prevention in the process industries*, *24*(4), 344-355.
[23] Nazir, S., & Manca, D. (2015). How a plant simulator can improve industrial safety. *Process Safety Progress*, *34*(3), 237-243.
[24] Nazir, S., Colombo, S., & Manca, D. (2013). Minimizing the risk in the process industry by using a plant simulator: a novel approach. *CHEMICAL ENGINEERING*, *32*.
[25] Colombo, S., & Golzio, L. (2016). The Plant Simulator as viable means to prevent and manage risk through competencies management: Experiment results. *Safety Science*, *84*, 46-56.
[26] Manca, D., Colombo, S., & Nazir, S. (2013, April). A plant simulator to enhance the process safety of industrial operators. In *European HSE Conference and Exhibition*. Society of Petroleum Engineers.
[27] Nazir, S., Sorensen, L. J., Øvergård, K. I., & Manca, D. (2015). Impact of training methods on Distributed Situation Awareness of industrial operators. *Safety science*, *73*, 136-145.
[28] Nazir, S., Colombo, S., & Manca, D. (2012). The role of situation awareness for the operators of process industry. *Chemical Engineering Transactions*, *26*.
[29] Lee, S. R., Sung, J.G., Kwon, J.R., & Lee, Y.S. (2010). Study on the Safety for Small-scale Governor Station. *Journal of the Korean Institute for Gas,* 1, 146-151.
[30] Emerson Process Management. (2016). *Types 1098-EGR and 1098H-EGR Pressure Reducing Regulators*. Bulletin 71.2:1098-EGR.

Abstract in Korean (국문초록)

본 논문은 공정시스템 분야의 최신기술 수요에 상응하는 최적 공정설계 및 운전기술 개발을 주목적으로 한다. 최근 셰일가스 등 변화하는 천연가스 자원으로부터 지속적인 부가가치 창출과 플랜트의 내재적 안전성을 제고할 수 있는 설계 및 운전을 도모하였다는 점에서 실제 산업에의 응용가치가 매우 높다.

첫 번째로 천연가스 가솔린회수 및 액화 통합공정에 질소회수공정을 추가하여, 저품질 천연가스로부터 지속적인 액화천연가스 생산이 가능한 공정을 설계하였다. 열교환망 및 분리공정 최적화를 위해 공정요소들의 엑서지를 최소화할 수 있는 초구조를 설계함으로써 기존의 연구가 찾지 못하였던 새로운 최적 구조 및 운전조건을 결정하였다. 나아가 서로 다른 천연가스 조성에 따라 각기 적용이 가능한 대안공정을 추가 설계·최적화함으로써 변화되는 천연가스 자원에 지속적인 가치창출을 위한 해답을 제시하고 있다.

두 번째로 공정의 예비설계단계에서 내재적 안전성의 개념을 도입하여, 경제성과 안전성의 균형을 유지하기 위한 새로운 다목적최적화 알고리즘을 개발하였다. 잠재적 위험도가 높은 천연가스 액화공정을 대상으로 액화사이클에 따른 초구조를 모사하여 두 가지 목적함수의 가중치에 따른 최적해를 결정함으로써 기존 최적화의 한계를 보완하였다.

마지막으로 플랜트 안전운전을 위해 공정이상에서부터 사고의 발생 및 전파과정을 실시간으로 구현할 수 있는 시뮬레이션 모듈을 개발하였다. 동적공정시뮬레이션 및 사고시뮬레이션의 두 가지 독립된 모듈을 객체연결매입 기법을 이용하여 연동함으로써 사고상황에서 운전원의 임의조치가 모듈에 실시간 반영되도록 하였다. 해당 모듈은 임의의 사고상황에서 제어실 및 현장 운전원의 적절한 대응을 효과적으로 유도할 수 있으며 나아가 플랜트 안전시스템설계에 객관화된 지표를 제시할 수 있었다.

본 논문은 위와 같이 실제 산업의 기술적 수요를 충족시키고 이를 발전시킴으로써 공정시스템 학술분야에 기여하였다.

주요어: 공정합성; 공정강화; 최적화; 내재적안전성; 다중모듈방식; 전산유체역학; 동적시뮬레이션; 위험성평가; 천연가스액화; 극저온;

학번: 2013-23169